Synthesis and characterisation of new copolymers for medical imaging visualization of medical device.

Mira Younis

Collège Doctoral du Languedoc-Roussillon

THÈSE

Pour obtenir le grade de Docteur

Délivré par **Université de Montpellier**

Préparée au sein de l'école doctorale Sciences Chimiques et Biologiques pour la Santé
Et de l'unité de recherche UMR CNRS 5247

Spécialité : Chimie et Physico-Chimie des matériaux

Présentée par **Mira YOUNIS**

Synthèses et caractérisation de nouveaux copolymères pour la visualisation de dispositifs médicaux en imagerie médicale

Soutenue le 17 décembre 2015 devant le jury composé de

Mme Valérie Langlois, Professeur, Université Paris 12	Président de la jurie
M. Bernard Martel, Professeur, Université Lille 1	Rapporteur
M. Jean Coudane, Professeur, Université de Montpellier	Directeur
M. John-Hanna EL-Nakat, Professeur, Université de Balamand	Directeur
M. Vincent Darcos, Ingénieur d'étude, Université de Montpellier	Co-encadrant
M. Youssef Bakkour, Professeur, Université de Balamand	Co-encadrant

UNIVERSITE MONTPELLIER

Acknowledgements

After three long years, involving lots of syntheses and characterizations, I would like to express my gratitude to people without whom this work would not have been accomplished. I hope that I have not forgotten anyone.

I would like to express my gratitude to Prof. Jean Coudane, my Ph.D. supervisor, who gave me the chance and opportunity to work within the group « Equipe Biopolymeres Artificiels ». Thank you for your guidance and comments throughout the thesis.

This thesis would not have been accomplished without the help and guidance of Dr. Vincent DARCOS. Thank you for your continuous follow-up and all your comments that enriched the thesis.

Dr. John Hanna El-NAKAT, my Lebanese supervisor, no words can express my gratitude. Thank you for believing in me and for giving me this opportunity.

Special thanks to Dr. Youssef BAKKOUR who suggested this opprtunity and helped me with the NMR spectra.

I would like to extend my gratitude to members of the Faculty of Sciences at the University of Balamand: Dean Jihad Attieh. Amal Aoun: I can not but say thank you for your on-going support that was all what I needed. Bilal El-Khoury: thank you for helping me with mounting up all set-ups. Salim Makhoul thank you for sharing our difficulties while abroad.

A big appreciation goes to Fanny COUMES for all her support during my times at Montpellier, it was a pleasure meeting you. Anita SCHULZ it was an honor meeting you, thank you for all your advice. I would also like to extend my gratitude to Assala, ready to help when needed. I would also like to thank Cedric Penigua for his help on the project, Salome for her help with cytocompatibility studies, Stephane for NMR analyses, and Sylvie for GPC. I would also like to thank Xavier and Benjamin for their help whenever needed.

A special thanks to my family Fouad, Raghida, Lara and Aida; thank you for being there and helping me achieve this.

To end this, I would like to thank my husband, Barbar Mitri who has been a source of encouragement and motivation during these three years. Thank you for giving me the moral support I needed.

TABLE OF CONTENTS

LIST OF FIGURES

LIST OF SCHEMES

List of Tables

GENERAL INTRODUCTION

Depuis l'aube de la civilisation, l'homme a cherché à trouver des matériaux pour remplacer ou améliorer certaines fonctions du corps. Le départ avait été avec les implants médicaux provenant de sources naturelles. Cependant, à partir de la deuxième partie du vingtième siècle, la vraie révolution a eu lieu avec l'introduction d'implants médicaux synthétiques. Les procédures chirurgicales impliquant des dispositifs médicaux implantés sont très populaires ces jours-ci, avec des millions de patients subissant ce type d'opération annuelle. Ces implants sont utilisés dans différentes parties du corps avec des applications dans diverss domaines (orthopédie, endoprothèses vasculaires, administration de médicaments, etc...) visant à l'amélioration de la qualité de vie du patient. Différents matériaux peuvent être utilisés pour la synthèse des dispositifs médicaux, tels que les matériaux polymères qui remplacent rapidement les autres classes de matériaux comme les métaux, les alliages et les céramiques. Les polymères synthétiques sont principalement utilisés et peuvent être classés en fonction de leur réactivité chimique comme:

- Matériaux polymères biodégradables utilisés pour des applications à court terme: ces matériaux possèdent l'avantage de dégradation dans le temps et donc une deuxième intervention de l'opération pour leur suppression est inutile.
- Matériaux polymères non biodégradables utilisés pour des applications à long terme: aussi connu comme polymères biostables. Ceux-ci offrent un soutien au fil du temps et continuent à avoir une performance ultime durant la vie d'un patient.

La visualisation de ces implants est une nécessité afin d'obtenir des informations concernant leur fixation dans le corps et le devenir post-opératoire. Par conséquent, des techniques de visualisation non invasives ont été développées telles que la radiographie, le scanner, l’échographie, l’imagerie par résonance magnétique (IRM). Parmi les différentes techniques d'imagerie que les cliniciens ont à leur disposition, l'IRM semble être l'outil idéal pour la localisation et la visualisation des implants médicaux. En effet, l'IRM est une technique non

invasive qui donne des images de haute résolution en relation avec la teneur en eau des tissus biologiques. Malheureusement, les implants médicaux polymères sont invisibles par l'IRM. Selon les praticiens de la santé, la visualisation est de très haute importance en raison des divers avantages offerts par cette technique. Avec l'aide d'autres techniques d'imagerie, l'IRM permet l'évaluation de la prothèse «fixation post-opération », l'intégration des tissus et le devenir post-opératoire.

Un des défis est alors de fixer un agent de contraste sur l'implant médical. A notre connaissance, il y a peu ou pas de systèmes satisfaisants pour la visualisation des implants médicaux par l'IRM. La raison principale est due à la difficulté de greffage d'un agent de contraste sur le matériau sans affecter ses propriétés. Des résultats très prometteurs et brevetés développés à l'IBMM ont permis de visualiser par IRM une prothèse utilisée en gynécologie et obstétrique. Dans cette approche, un agent de contraste à base de gadolinium sera fixé sur la prothèse pour la rendre visible. L'imagerie par fluorescnce attire également de plus en plus d'attention. Pour cette raison une étude préliminaire sur la synthèse de fluorophores organiques attachés à la chaîne polymère sera signalée. La synthèse de complexes d'europium fluorescents macromoléculaires sera décrite.

Since the dawn of civilization, man-kind has sought to find materials to replace or improve certain body functions. The start had been with medical implants from natural sources. However, starting from the second part of the 20th century, the real revolution occurred with the introduction of synthetic medical implants. Surgical procedures involving implanted medical devices are very popular these days, with millions of patients undergoing this type of operation yearly. These implants are used in different body parts with applications in different fields (orthopedics, cardiovascular stents, drug delivery, etc.) all aiming at the improvement of the patient's quality of life. Different materials can be utilized for the synthesis of medical devices as polymeric materials which are rapidly replacing other material classes as metals, alloys and ceramics. Synthetic polymers are mostly used and can be classified based on their chemical reactivity as:

- Biodegradable polymeric materials used for short-term applications: these materials possess the advantage of degradation over time and thus a second operation intervention for their removal is unnecessary.
- Non-biodegradable polymeric materials used for long-term applications: also known as biostable polymers. They offer support over time and continue to have ultimate performance during a patient's lifetime.

The visualization of these implants is a necessity in order to gain information concerning their fixation in the body and post-operation fate. Hence, non-invasive visualization techniques have been developed such as radiography, scanner, echography, magnetic resonance imaging (MRI). Among the different imaging techniques, clinicians have at their disposition, MRI seems to be the ideal tool for the localization and visualization of medical implants. In fact, MRI is a non-invasive technique resulting in high-resolution images related to the water content of biological tissues. Unfortunately, polymeric medical implants are invisible by MRI. According to health practitioners, such visualization is of very high importance due to the

various advantages offered by this technique. With the help of other imaging techniques, MRI allows the evaluation of prostheses' post-operation fixation, tissue integration and post-operation fate.

One of the challenges is to fix a contrast agent on the medical implant. Up to our knowledge, there is still a little or no satisfying systems for the visualization of medical implants by MRI. The main reason is due to the difficulty of grafting a contrast agent on the material without affecting its properties. Very promising and patented results developed at the IBMM have made it capable to visualize by MRI a prosthesis utilized in gynecology and obstetrics. In this approach, a gadolinium-based contrast agent is fixed on the prosthesis to make it visible.

Fluorescnce imaging is also attracting more attention. For these preliminary studies the synthesis of organic fluorophores attached to polymeric chain will be reported. The synthesis of fluorescent europium macromolecular complexes is also described.

CHAPTER 1
BIBLIOGRAPHY

1.1 Medical Devices Definition

According to ISO 13485 issued in 2003, a medical device is a manufactured product intended to cope with human disease, care for human injuries, meet human anatomical needs, maintain human physiological functions, support human life, or control human conception [1]. The European Commission in its Council Directive 93/42/EEC defined medical devices as articles intended to be used for a medical purpose as assigned by the manufacturer [2]. Due to the presence of a wide variety of these devices, their classification is based on their risk with a higher classification indicating higher risk.

1.2 Classification

The classification in EU and Canada groups these devices into four different classes, whereas the US groups them in three different classes [3]. Figure 1 represents the classification of medical devices based on their risk in each of the three mentioned countries.

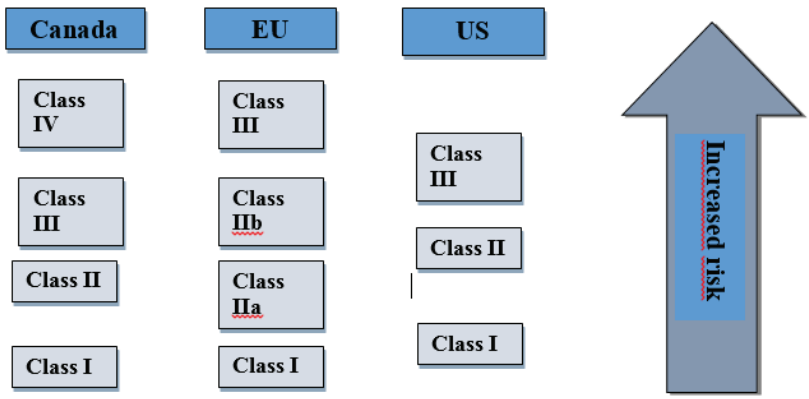

Figure 1: *Risk-based classification of medical devices in Canada, EU and US [3]*

For conciseness, we will focus on the European classification which has already stated, the European system classifies the devices into four classes, with the highest risk devices being in class III. There exist 18 rules for the classification of medical devices, with rules 1 to 12

classifying devices according to general criteria as invasiveness, duration of continuous contact, nature of tissue contact, and distinction between non-active and active devices. Rules 13 to 18 are special rules [4]. According to the directive 93/42/EEC, the duration of the contact of the medical device with the human body can be transient (intended use <60 min), short term (intended use ≤30 days) or long term (intended use >30days). Table 1 presents examples of product risk classification [5].

Class	Description	Examples	Risk
I	Non-invasive devices with no body interaction	Hospital beds, bed pans, sterile plasters	Low
IIb	Surgically invasive/active devices partially or totally implantable in the body May modify composition of body fluids	Infusion pumps, Ventilators, Surgical lasers	Medium
III	Support or sustain human life Prevent impairment of human health	Various implants: vascular and neurological, heart replacement valves, silicone gel-filled breast implants, and implanted cerebella stimulators	High

Table 1: *Details and examples of medical devices classification [6]*

In order to be precise, we will focus on implantable medical devices of the prosthesis type.

1.3 Medical implants and prosthetics

Surgical procedures involving implanted medical devices are becoming more and more popular, with millions of patients undergoing such procedures yearly. According to US FDA, medical implants are devices or tissues placed inside or on the surface of the body. These implants can serve one or several functions such as: medication delivery, body functions

monitoring, organ support, etc. In the case where the implants are intended to replace missing body parts, they belong to the prosthetic type [7].

1.3.1 Prosthetic biomaterials: definition and properties

An implanted prosthesis is fabricated from biomaterials which are defined according to the American National Institute of Health as any substance or combination of substances, other than drugs, synthetic or natural in origin, which can be used for any period of time, which augments or replaces partially or totally any tissue, organ or function of the body, in order to maintain or improve the quality of life of the individual [8]. Biomaterials should possess some important properties, so they can be used in the body without any rejection. The two most important properties which control the performance of the medical device are the biocompatibility and the biofunctionality.

1.3.1.1 Biocompatibility

According to Williams in 2008, biocompatibility refers to the ability of a biomaterial to perform its desired function with respect to a medical therapy, without eliciting any undesirable local or systemic effects in the recipient or beneficiary of that therapy, but generating the most appropriate beneficial cellular or tissue response in that specific situation [9]. Important components of biocompatibility are tissue response, cytotoxicity, genotoxicity, mutagenicity, carcinogenicity, and immunogenicity [10].

1.3.1.2 Biofunctionality

Biofunctionality refers to the material's ability to perform the function for which it has been designed during its entire duration of use, thus the ability of the material to satisfy its design

requirements while in service [11]. Other important requirements for biomaterials to be used in medical implants are: mechanical properties, corrosion, sterility etc. [11]

1.3.2 Types of Prosthetic Biomaterials

Biomaterials used in implants can be classified into two large groups: natural and synthetic. Synthetic biomaterials are further classified into: metallic, ceramic, and polymeric [12].

1.3.2.1 Natural Biomaterials

The advantages of this type of biomaterials are: biocompatibility, biodegradability, and remodeling. Natural biomaterials can be classified into several groups [12]:

- Protein-based: collagen, gelatin, silk
- Polysaccharide based: cellulose, chitin/chitosa, glucose
- Decellularized tissue derived

In fact, the most common type of prosthetic implants derived from natural biomaterials is the decellularized extracellular matrix of either animal (xenograph) or human origin (allograft) [13].

However, natural biopolymers have several disadvantages as: poor immunogenic response (where the body realized the biomaterial as foreign and tries to destroy it), high variability, and complex technological processing techniques [14].

1.3.2.2 Metallic Biomaterials

This type of biomaterials is still used extensively in surgical implants due to the high strength and resistance of metals. They are also relatively easy to fabricate [15]. Metallic prostheses for the hips, knees, and shoulders are very common. The three mostly used metals and alloys in these prostheses are: stainless steel, CoCr alloys and Ti alloys [16].

One example of titanium alloys is Nitinol which has experienced explosive growth since the end of last century. Nitinol first discovered in 1962, is a mixture of nickel and titanium. It is considered as a shape memory alloy with excellent biocompatibility, elasticity, and a wide range of biomedical applications: orthodontic wires, orthopedic implants, stents and catheters [17-18].

The major disadvantage of metallic implants is the risk of corrosion. Corrosion causes disintegration of the implant leading to its weakness, in addition to the harmful effects of the corrosion products on tissues and organs [19].

1.3.2.3 Ceramic biomaterials

The importance of this class of biomaterials is growing due to the advantages they offer including: high biocompatibility, resistance to corrosion, high resistance to compression, inertness, high fusion temperature in addition to low thermal and electrical conductivity [20]. Ceramics used for implants can be classified into 3 groups [21-23]:

- Non-absorbable or relatively inert ceramics: they conserve their physical and chemical properties once in the body. Examples include ceramics of alumina (Al_2O_3) and zirconia (ZrO_2). They are mostly used as structural-support implants such as bone plates and bone screws.
- Surface active or bioactive ceramics: they form bonds with adjacent tissues. An example of this type of ceramics is the bioglass which is mainly used in artificial bones and dental implants. They are also used as prosthetics for hard tissue [24].
- Bioresorbable or non-inert ceramics: as implied from their name, they are resorbed by the body and are then replaced by endogenous tissues. The time of resorption depends on the material used. Most of these ceramics are composed of calcium phosphate

derivatives. Hydroxyaptite (HAP) strongly represents the bone structure and is thus used in several dental and orthopedic implants.

1.3.2.4 Polymeric Biomaterials

This type of biomaterials is rapidly replacing other classes due to their flexibility, ease of production and low density [20]. This biomaterials enters into a wide variety of applications as facial prostheses, tracheal tubes, hip and knee joints, etc. [25]. Polymeric materials can be either of a natural source or a synthetic source. Natural polymers, as collagen, have several disadvantages, a poor immunogenic response, the possibility of bacterial and viral infection, and difficulty in reproduction, as previously described in the section of natural biomaterials. Synthetic polymers, on the other hand, can be easily produced and are highly versatile, which made them dominate different fields of medical implants [26].

There is a wide variety of synthetic polymers used as biomaterials, thus we will enter into further details in synthetic polymers used in prostheses.

1.4 Different classes of synthetic polymers used in prostheses

Synthetic polymeric materials have a wide range of applications ranging from medical disposable devices to prosthetic materials, implants, dental materials, etc. Polymers are considered as interesting materials for the conception of prostheses due to the wide variety of properties they offer. In fact, even the same polymer can present different properties based on a number of parameters:

- **Molecular weight**: polymer molecular weight is important because it determines many physical properties such as transition temperatures, mechanical properties as stiffness, strength, viscoelasticity, toughness and viscosity [27]. Molecular weight also affects the crystallinity of polymer, which usually decreases

with an increase of the molecular weight [28]. The degree of polymerization is also another mean of determining the length of the polymeric chain [29].

- **Stereoisomers**: Two polymers may have the same molecular formula and same structural formula, yet differing in their bond spatial arrangement. This results in stereoisomerism. Atactic, isotactic and syndiotactic stereoisomers are present.
    - Atactic polymer: in this case the side groups are positioned randomly on one or the other side of the polymer backbone.
    - Isotactic polymer: the side groups have the same configuration at successive, regularly spaced potions along the chain.
    - Syndiotactic polymer: side groups have a regular alteration in front and the back of the chain plane.

Stereoisomers have a strong impact on crystallinity. Atactic polymers are amorphous (non-crystalline) due to the random distribution of the side groups, which gives them a soft and flexible form. Isotactic polymers, due to their stereoregular structure, have strong intermolecular forces, and thus a stronger structure. Syndiotactic polymers have properties more similar to isotactic polymers rather than atactic ones due to stereoregularity. Thus, stereoregular polymer structures (isotactic and syndiotactic) are more crystalline than atactic polymers, due to their strong intermolecular forces [29].

Prosthetic implants can be either temporary or permanent depending on their application. For this, synthetic polymers constituting these implants can be differentiated into either biostable (for permanent applications) or biodegradable polymers (for temporary applications) [30]. In fact, the most common method for polymer degradation is the hydrolysis of the hydrolytically unstable backbone [31].

1.4.1 Synthetic Biostable Polymers

Biostable polymers are inert, cause minimal response in the surrounding tissue, and retain their properties for years [32]. Some examples of biostable polymers used in medical applications are listed below.

1.4.1.1 Polyethylene (PE)

There are various medical applications for polyethylene depending on the molecular weight. Polyethylene can be classified into 3 classes: low density, high density (HDPE) and ultrahigh molecular weight (UHMWPE). The most attention has been given to the last two classes due to their chemical inertness, and biostability. An example of the use of polyethylene is in the anterior cruciate ligament prosthesis [33]. One of the first commercial knee ligament prostheses tested for approval by the FDA in the 1970s was made from UHMWPE [34].

1.4.1.2 Polypropylene (PP)

Polypropylene is a very rigid plastic that has found its way into several applications in prosthetics. It is one of the most biostable and biocompatible polymers widely used. PP has excellent stiffness and strength as compared to polyethylene [33]. Meshes made of polypropylene have been widely used as prosthetic material for hernia repair during the last twenty years due to their stability, strength, inertness and handling qualities. These meshes are composed of monofilament fibers having different sizes of pores. Depending on the manufacturer, meshes differ in the pore size, thickness, pliability, etc. [35].

1.4.1.3 Poly(tetrafluoroethylene) (PTFE)

PTFE is composed of polymer chains of carbon saturated with fluorine. PTFE is biostable and has minimum interaction with blood components due to its electronegativity. PTFE is used

extensively in cardiovascular prosthetic implants and is known as extended poly(tetrafluoroethylene) or ePTFE [36].

1.4.1.4 Poly(methyl methacrylate) (PMMA)

PMMA is the most common of manufactured acrylic compounds with two unique properties: optical clarity and weather resistance [29]. Other advantages of PMMA include bioinertness and non-degradability [33]. PMMA has been the primary material used in prosthetic eyes for the past 60 years [37]. PMMA has also found its way into bone prosthetics [38].

1.4.1.5 Poly(dimethyl siloxane) (PDMS)

PDMS is a silicone elastomer which is biostable, non-toxic, biocompatible, blood compatible, elastic, transparent, durable and bio-inert. Its bio-inertness makes it very attractive to biomedical applications since it inhibits microbial growth [33]. It is mainly used in facial prostheses [39].

1.4.1.6 Poly(urethanes) (PU)

Poly(urethanes) are biocompatible, blood compatible, fatigue resistant, durable and elastic [33]. They are the most commonly used materials for the production of artificial heart valves, veins and arteries [40].

1.4.1.7 Poly(sulfone) (PSU)

This type of polymers has several properties as: high thermal stability, high toughness and strength, fire and stress crack resistance, and transparency [29]. One of the applications of polysulfones is in artificial heart components [25].

1.4.2 Synthetic Biodegradable Polymers

For many applications, biodegradable polymers are favored over biostable ones due to issues of biocompatibility related to long-term non-degradable polymers [25, 41].Synthetic polymers used in medical applications can degrade by one of the following mechanisms: hydrolysis, oxidation, enzymatic degradation, and physical degradation [25]. Examples of some biodegradable polymers used in medical prostheses are listed below.

1.4.2.1 Aliphatic Polyesters

Due to the favorable characteristics of biocompatibility and biodegradability of polyesters, they are considered one of the most important classes of biodegradable polymers [42]. Examples of aliphatic polyesters are poly(ε-caprolactone), poly(hydroxybutyrate), polylactide. For example, polylactide is used in fracture fixation [43].

1.4.2.2 Polyorthoesters

Materials made of polyorthoesters are hydrophobic with hydrolytic linkages. These materials are sensitive to acids, but stable to bases which allows controlling their degradation rates by adding acid or base excipients [31]. Polyorthoesters have been used as controlled release of drug devices since the early 1970s [44].

1.4.2.3 Polyanhydrides

Polyanhydrides are considered to be biocompatible, and their degradation in vivo yields non-toxic diacids which are then eliminated from the body as metabolites [45]. Their degradation times can be adjusted from days to weeks [31]. Polyanhydrides have been used as drug delivery system and in the design of the device Gliadel used for the treatment of brain cancer [45].

1.4.2.4 Polycarbonate

Polycarbonate is considered as a type of polymer with properties as: heat and resistance, clarity, stability [29]. For more than 20 years, it has been used in cardiac surgery products as blood oxygenators due to its glass-like clarity allowing visual evaluation of the blood flow [46].

1.4.2.5 Polyamides

Nylon is the generic name given to a group of polymers belonging to the class of polyamides. Nylon is known for its mechanical properties, mainly stress resistance. It is also known for its flexibility [47]. Biodegradable nylon and other polyamides have found applications in sutures, coatings and medical device packaging [48].

1.5 Medical imaging surface modalities

Imaging modality is defined as a method used to acquire data about tissues in animals or humans. The imaging technique can be used to detect several centimeters below the surface or just a few mm deep [49]. The obtained information is then transformed into images elucidating the anatomy of organs, size and localization or existence of certain pathologies. These imaging modalities allow physicians to make accurate diagnosis. In addition to the visualization of organs, the visualization of prosthetic implants is a necessity in order to obtain post-operation information (such as fixation of the implant, inflammation) and to follow-up the fate of absorbable implants. There are several non-invasive medical imaging modalities currently employed in medicine. For the sake of conciseness, only few imaging modalities will be discussed in details.

1.5.1 X-ray and computed tomography (CT):

X-ray imaging is a low cost imaging technique that has been used for over a century for medical imaging following X-rays discovery by Roentgen in 1895. In the early 70's, X-ray computed tomography (CT) was developed to produce cross-sectional images of the body. This method has proved to be a very essential technique in medical diagnosis and treatment techniques. Conventional X-ray, computed tomography (CT), and mammography are medical imaging techniques depending on X-rays. Conventional X-ray produces 2-D image as compared to 3-D image produced by CT. X-ray imaging depends on the absorption of X-ray beams. Once the beam passes through the patient, some of the rays scatter from the original beam while others are attenuated when absorbed by the tissues. The absorption depends on the organ, and this difference in absorption results in an emerging beam having different intensities. However, in the case where the organs have similar densities, distinction by radiography is difficult. In this case contrast agents as barium sulfate and iodine are used [50]. The main disadvantage of radiography is the presence of ionizing radiation [51].

1.5.2 Ultrasound

Ultrasound modality, also known as sonography, has been used to image the body for more than 50 years and is also one of the most widely used imaging techniques nowadays. In this technique, ultrasound waves are transmitted from a transducer (probe) to a body part. Upon the reflection of waves from this part, an ultrasound image is produced. Ultrasound images have several advantages mainly safety due to the absence of ionizing radiation, unlike X-rays. It is also inexpensive when compared to other imaging techniques [52]. Yet, the difficulty to produce a whole-body scan and the difficulty to examine certain organs (as lungs and brain) are one of the drawbacks of this technique. In addition, the resolution offered by this technique is lower compared to other imaging techniques, in the case where the organ is large or the object is far from the transducer [53].

1.5.3 Magnetic Resonance Imaging (MRI)

MRI has become an important diagnostic tool during the last few decades with nearly 60 million scans performed yearly worldwide [54]. The use of MRI as a diagnostic tool is growing rapidly in both the number of installed instruments and the number of performed scans [55]. The main advantages of MRI are its excellent contrast resolution and the absence of ionizing radiation [56,57]. This technique depends on the application of strong magnetic field and radiowaves to nuclei possessing a spin to obtain cross-sectional images of organs in the body [57]. Due to the increased popularity of this technique, its high resolution and absence of ionizing radiation, it will be discussed in details in the following section. However, before going into further details of MRI it is worth mentioning that other other imaging techniques are present as optical imaging and radionuclide imaging.

1.6 Magnetic Resonance Imaging

1.6.1 Brief History

MRI is based on the physics of nuclear magnetic resonance (NMR) which was discovered by Bloch and Purcell and obtained the Nobel Prize in Physics in 1952 for this [58]. They discovered that certain nuclei once placed in a magnetic field and pulsed with proper radiowaves, emitted radiosignals with frequencies characteristic for each element. In the late 1960s, Damadian discovered that NMR parameters of normal cells are different than those of malignant ones [56] and in the mid 1970s the first NMR image was produced by Lauterbur [59]. Since then, this technology has evolved rapidly. The technique was called later MRI rather than NMRI (nuclear magnetic resonance imaging) because the word “nuclear” was not publically accepted.

1.6.2 Principle [56, 60, 61, 62]

Magnetic resonance depends on the interactions between an applied magnetic field and a nucleus with a spin. The nuclear spin or the intrinsic spin angular momentum is one of the properties of nuclei and is directly related to the atomic composition. This spin *(I)* is quantized to certain values depending on the atomic number and atomic weight. A nucleus possesses:

- No spin if it has even atomic number and even atomic weight
- Half-integral values of I (1/2, 3/2…) if it has even atomic number and odd atomic weight
- Integral value of I (1, 2…) if it has odd atomic number and even atomic weight.

Examples of nuclei mostly examined by NMR include: ^{1}H, ^{13}C, ^{17}O, ^{31}P, ^{15}N, ^{29}Si, ^{19}F.

However, most MRIs choose the hydrogen nuclei for probing the body for several reasons: I=1/2, it is the most abundant isotope of hydrogen, and has the largest response to an applied magnetic field (very high gyromagnetic ratio). In addition to all what is mentioned, water and fat are the main constituents of the body's tissues and both contain hydrogen atoms.

Thus, a positively charged nucleus possesses in addition to the spin a magnetic moment which is parallel to the axis of rotation. A tissue contains several hydrogen atoms, each having a spin vector with defined magnitude, yet randomly directed thus producing no net magnetization (sum of vectors=0) (Figure 2).

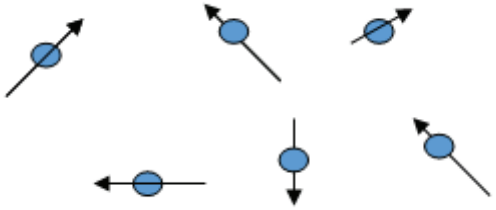

Figure 2: *Random orientation of protons of hydrogen resulting in zero net magnetization*

If this tissue is subjected to external magnetic field B_o, protons of hydrogen precess (rotate) either parallel (lower energy state) or antiparallel (high energy state) to the magnetic field, with more protons in the lower state than in the higher one thus resulting in net magnetization M_0 as revealed in Figure 3

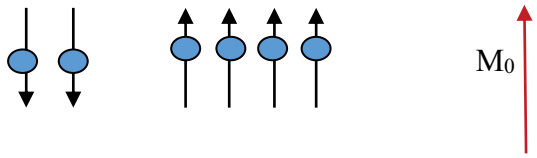

Figure 3: *Production of the net magnetization in presence of an external magnetic field*

In fact, this precession occurs at a frequency known as the Larmor frequency directly proportional to the magnetic field and the gyromagnetic ratio specific to each nucleus (γ) as shown in Equation 1:

$$\omega_0 = \gamma B_0 \qquad \textbf{(Equation 1)}$$

Once net magnetization is produced, a pulse of the specific frequency (Larmor frequency) will be applied. Only protons spinning at the same frequency will absorb this energy and then reemit the energy at the same frequency (that is, all nuclei of hydrogen will emit at the same frequency).

Upon exposing the tissue to the correct ω_0, the radiofrequency energy is absorbed (by the lower energy state protons) and M_0 is flipped away from the equilibrium position.

After excitation, the excited nuclei will return back to their lower energy state (emitting energy at ω_0) and M_0 will return to its equilibrium state along the direction of B_0 by a process called relaxation which can be either longitudinal or transversal. These relaxation processes determine the shape of the MR image.

For the process of relaxation to be understood, an x, y, z frame of rotation should be pictured with the Z-axis having the same direction as M_0 and the X and Y axis at right angles as shown in Fig. 4. Thus the Z-axis is the equilibrium state.

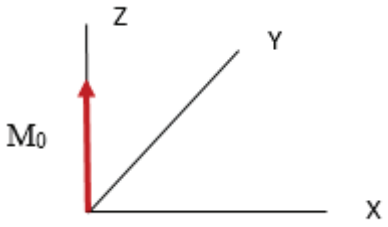

Figure 4: *X,Y,Z axis of rotation*

- **Longitudinal Relaxation or T1 Relaxation [56,60]**

This is also called the spin lattice relaxation. Following an excitation, M_0 flips from the z-axis. The time needed for M_0 to return to 63% of its original value along the z-axis is called T1 relaxation as shown in figure 5.

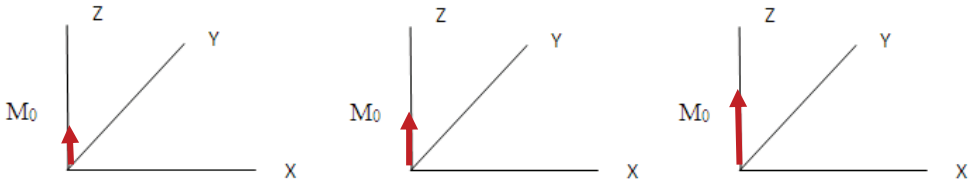

Figure 5: *Gradual increase of M_0 along the Z-axis following an excitation*

Equation 2 represents the return of the magnetization to its value along the Z-axis:

$$M_{(z)} = M_0(1-e^{-t/T1}) \quad \textbf{(Equation 2)}$$

Where T1 represents the spin-lattice relaxation and M_0 is the net magnetization.

➢ **Transverse relaxation or T2 relaxation [60,63]**

This is also called spin-spin relaxation. It is the time needed for the transverse component of M to decay to 37% of its initial value after the excitation. After the radiofrequency pulse, M_0 is rotating in the X-Y plane around the Z-axis. Spin-spin relaxation refers to the energy transfer from one excited proton to the nearby proton. Unlike T1 in which the energy is transferred to the surrounding, here the energy is transferred as spin excitation. These interactions cause loss in phase coherence hence a decrease in the magnitude of transverse magnetization and hence loss of signal intensity. Once each xy component is balanced by an opposite one, the dephasing process is then complete and the magnetization vector aligns with the applied field again.

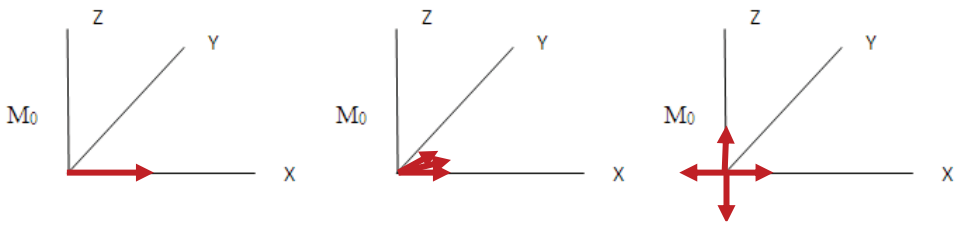

Figure 6: *Transverse relaxation T2*

T1 and T2 are two independent processes that happen simultaneously. The molecular structure and chemical composition of tissues influence the values of T1 and T2 with a general rule that T2 can never exceed T1. Depending on the tissue's nature (solid or liquid) these values can change. Longer T1 values, in the order of seconds, are observed in solids due to interatomic bonds resulting in rigidity, thus fewer collisions. However, in the case of liquid (which is the case of most tissues in the body) T1 values are in the order of milliseconds, since molecules tend to collide frequently. T2 values, and as noted before, depend on field non-homogeneities. Solids exhibit shorter T2 because interactions increase the decay process

(more spin-spin interactions). Liquids on the other hand have more molecular motion thus increasing T2. In general various diseases increase the H_2O content, thus an increase in T2 is observed [61].

Figure 7 represents the effect of water mobility on T1 and T2 [64], and Table 2 represents T1 and T2 values in different tissues [65].

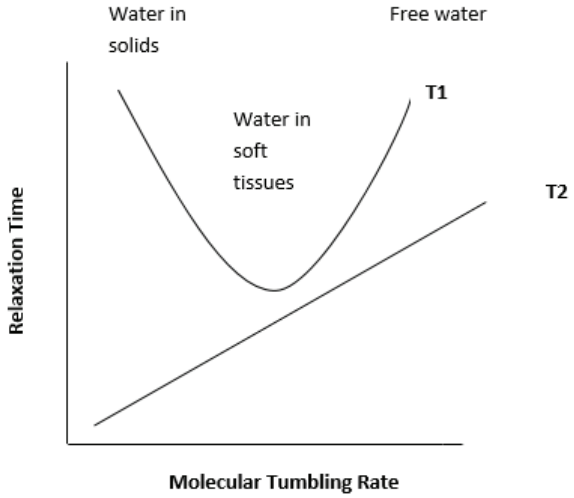

Figure 7: *Effect of water mobility on T1 and T2*

Tissue Type	**T1(ms)**	**T2(ms)**
Liver	812	42
Muscle	1412	50
Kidney	1194	56
Blood	1932	275
Adipose	423	154

Table 2: *Relaxation times in water molecules present in different types of tissue at 3T*

Over the years much effort has been made in order to enhance the image contrast between some naturally low contrast organs or between a healthy and an affected part by the use of a contrast agent. To enhance the differentiation between tissues in MRI, contrast agents (CAs) are used to shorten the relaxation parameters (T1 and T2) of surrounding water molecules.

Currently almost 30% of MRI exams include the use of contrast agents and the number is expected to increase with the production of new agents [66].

1.6.3 MRI Contrast Agents

Contrast agents are products that allow increasing the image contrast in order to differentiate between healthy and pathological areas [67]. Iodine and sulfate were among the first contrast agents used in radiography. These radiographic contrast agents attenuate more X-rays than soft tissues in the body, thus enhancing the contrast [68].

However, the mechanism by which MR contrast agents enhance image contrast is different than that of radiographic contrast agents. MR contrast agents are indirect agents in the sense that they are not directly visualized in the image, but enhance the contrast by altering the relaxation times (T1 or T2) [60, 69]. In addition the dose of MR contrast agents needed is lower than that of radiographic contrast agents, thus lowering the probability of adverse reactions [60]. MR contrast agents can be classified as T1 or T2 agents based on their effect of shortening T1 or T2 relaxation times. Paramagnetic contrast agents as Mn^{2+} and Gd^{3+} are considered as T1 agents while superparamagnetic contrast agents (as iron oxides) are considered as T2 agents [70]. It is important to note that the concentration of the contrast agent has a direct effect on the signal intensity. Depending on the concentration, the signal reaches a maximum before it starts decreasing. For example, low concentrations of paramagnetic contrast agents enhance signal intensity by decreasing T1. However, by increasing the concentration, the agent will have more effect on T2 thus resulting in a decrease in signal intensity [60, 71]. One of the problems of T2 contrast agents is the increase in magnetic susceptibility leading to artifacts at high field strengths [60,72]. Iron oxides are rarely used with less than 10% of contrast agents. For this, most clinically used contrast agents are T1 contrast agents or paramagnetic contrast agents which will be discussed in

details. Note that T1 contrast agents are also called positive contrast agents, while T2 contrast agents are called negative contrast agents.

1.6.3.1 T1 Contrast Agents or Paramagnetic Contrast Agents

1.6.3.1.1 Effect of Contrast Agents on T1[60, 72]

T1 relaxation depends on excited protons giving their energy to the surrounding tissue. In the case where a paramagnetic ion is used, the energy transfer occurs from the excited protons to the free unpaired electrons of the ion. The most efficient energy transfer occurs when the protons are in the coordination sphere of the metal complex that is the innermost layer of atoms surrounding the metal ion. This is called the inner sphere relaxation, one of the two mechanisms due to the paramagnetic ion. At this point, water molecule enters into the coordination sphere, exchanges its energy with the electron of the metal ion and is rapidly replaced by another water molecule. This is represented as the residence time of the water molecule in the coordination sphere $\tau_{m.}$ The process of exchange of energy is represented in Figure 8. The energy exchange from the protons to the electrons results in a shorter relaxation time T1 thus brighter image contrast.

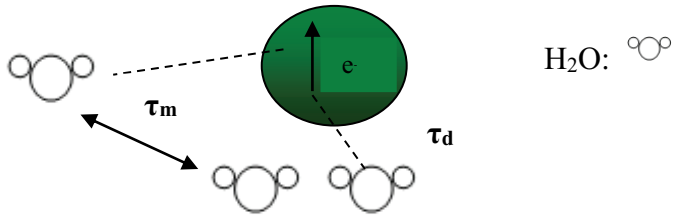

Figure 8: *Inner and outersphere paramagnetic relaxation processes*

In fact, paramagnetic agents decrease T1 thus resulting in an increase in relaxation rate (R1=1/T1) hence improvement in image contrast. τ_m and τ_D are two factors related to the paramagnetic ions influencing relaxivity. Other factors include:

- q: number of coordinated water molecules (upon increasing q from 1 to 2, relaxivity increases by 30%)

- r: proton metal distance

1.6.3.1.2 Paramagnetic Ions Used in MRI

Different forms of positive contrast agents are available, all of which are composed of paramagnetic ions having one or more unpaired electrons attached to a chelating complex. Most paramagnetic ions used are lanthanide ions, which are well known for their magnetic properties [73]. The most commonly used lanthanide ion in MRI contrast agents is Gd^{3+} which will be discussed in details. Mn^{2+} is the second mostly used lanthanide in positive contrast agents. Mn^{2+} was the first contrast agent used and was introduced by Lauterbur in 1978. Due to the presence of 5 unpaired electrons, Mn^{2+} has strong paramagnetic effects resulting in a decrease in T1 and enhanced image contrast. In most cases, Mn^{2+} is chelated in order to decrease its toxicity with Mn-DPDP (manganese dipyridoxaldiphosphate) and FDA approved this contrast agent for liver imaging [70,74]. Other paramagnetic ions are rarely used in MRI.

1.7 Gadolinium: Element of Choice for MRI

Gd^{3+} is the most commonly used lanthanide as a positive contrast agent with a large number of MRIs employing Gd (III) complexes, in order to enhance image contrast. The strongest emphasis is placed on these complexes, although complexes of other paramagnetic ions, especially Mn(II) and Fe(III), have been developed and approved. Yet, complexes of the latter two ions become weakly chelated and dissociate spontaneously in *in vivo* conditions. For example, MnDPDP (Fig. 9) is a weak chelate which dissociates *in vivo* to give free manganese ion, which is then taken by hepatocytes [75].

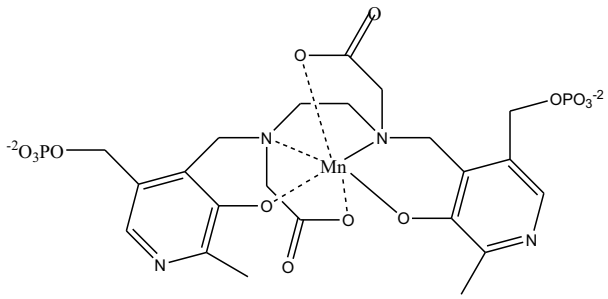

Figure 9 : *Chemical Structure of MnDPDP*

1.7.1 Gadolinium Characteristics

Lanthanides, especially Gadolinium, have found their way into medical diagnosis during the last few decades. Gd is a soft silvery atom first discovered in 1880 by Jean Charles Galissard de Marignac and was named in honor of Johan Gadolin. Gd has no known biological role and is completely absent from the human body. With an atomic number of 64, Gd has the electronic configuration of [Xe] $4f^7$ $5d^1$ $6s^2$ with 8 unpaired electrons. It has 7 isotopes, Gd-158 being the most abundant, and possessing an average molecular weight of 157.25 g/mol [76].

The most common oxidation state of Gd is 3, with Gd^{3+} having 7 unpaired electrons. The 7 unpaired electrons yield a high magnetic moment. Yet, this is not the only reason for choosing Gd^{3+} since other lanthanide ions as Dysprosium (III) and Holmium (III) possess even higher magnetic moment. However, Gd3+ has a symmetric ground state leading to a longer electronic relaxation time thus allowing water protons to feel the effects of Gd^{3+} [66,77].

Due to its paramagnetic effect (presence of 7 unpaired electrons) Gd^{3+} can influence both T1 and T2. However, since T1 is much longer than T2, Gd^{3+} affects more dominantly T1 at moderate doses and yields brighter images contrast [78].

However, Gd^{3+} cannot be used in its free form because free Gd^{3+} is toxic at the doses needed for MRI, this is why it is given under the form of stable complexes that keep the metal intact until excretion [79]. Gd^{3+} has an ionic radius of 0.99 Å very close to that of Ca^{2+} which is the

reason of free Gd^{3+} toxicity: Gd^{3+} will thus compete (and with higher affinity, due to the trivalent charge) with Ca^{2+} in systems that need Ca^{2+} for proper functioning leading to disruption in biological systems [66,80]. For this, proper ligands should be chosen in order to form Gd-complexes that remain intact. The choice of stable complexes along with the dose of Gd^{3+} has gained more importance because of nephrogenic systemic fibrosis (NSF). The main cause of NSF is transmetallation between Gd^{3+} released from the chelate and endogeneous metals salts as Zn^{++} , Cu^{++}, and Ca^{++}. NSF mainly occurs in patients with severe renal failure. These patients take longer time to clear Gd-complexes, which increases the risk of transmetallation between Gd^{3+} and endogeneous ions thus releasing free Gd^{3+} [81]. Free Gd3+ can precipitate as a salt and is deposited in target tissue especially in patients with NSF. There is also evidence that Gd^{3+}can kill macrophages [82,83].Patients with NSF end up having stiffness in joints, muscle weakness, leg restlessness.

For this, the complexation is necessary in order to eliminate any risks associated with free Gd^{3+} and prevent the precipitation of gadolinium salts. Thus, the rate of dissociation of Gd-complex determines its toxicity. Therefore, the choice of the complex is detrimental for the stability and biophysical properties.

1.7.2 Gadolinium Complexes

The chelation of Gd^{3+} in complexes is essential in order to eliminate tissue interaction with free Gd and decrease toxicity. The LD_{50} of free Gd^{3+} can be up to 50 times higher than chelated Gd [79,82]. Physicochemical properties of the Gd-complex depend on the nature of the chelate used, which can be cyclic or linear, ionic or non-ionic. These features determine the stability of the complex [84]. In general, Gd-MRI contrast agents can be classified as linear or macrocyclic chelates.

An example of an approved and clinically used ionic linear chelate for Gd^{3+} is diethylenetriamine penta-acetic acid (DTPA) forming Gd-DTPA known commercially as Magnevist®. An example of ionic cyclic chelate for Gd^{3+} is tetraazacyclododecane tetra-acetic acid (DOTA) forming Gd-DOTA commercially known as Dotarem® [84]. Figure10 represents the structures of some Gd(III) chelates developed for clinical use as MRI contrast agents.

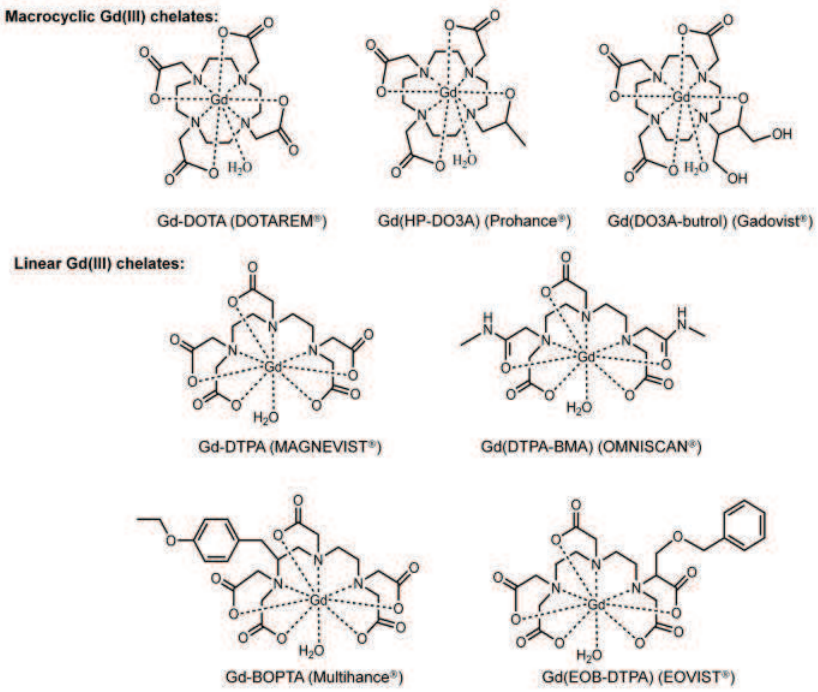

Figure 10: *Clinically used Gd-based MRI contrast agents [85]*

As it can be concluded, linear chelates (usually derivatives of DTPA) are open cycles where the DTPA chelates acts as pliers for Gd3+. On the other hand, macrocyclic chelates (derivatives of DOTA) offer strong rigid ring able to cage Gd3+ ion. Thus, the structure of the chelate affects the stability of the complex [84]. The structure of the complex (depending on the nature of the chelate) also affects its biodistribution, which can be in the extracellular fluid, intracellular fluid or liver [86]. By modifying the chemical structure of the complex (for

example attaching macromolecules), the rate and path of excretion are affected [87]. The majority of Gd complexes utilize either DTPA or DOTA as chelates.

1.8 Mechanism of Gd^{3+} Complexation

Lanthanides tend to have high coordination numbers in an aqueous medium due to their larger sizes. In all clinically used Gd(III) MRI contrast agents, Gd^{3+} has a coordination number of 9 with 8 binding sites with a ligand (chelate) and the ninth coordination site occupied by a water molecule [66]. Figure 11, represents Gd^{3+} complexation with DTPA and DOTA.

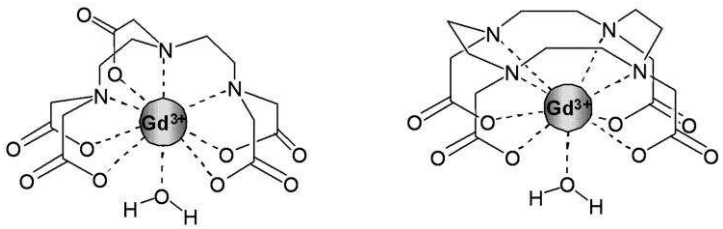

Figure 11*: Complexation of Gd with DTPA and DOTA*

The ligands used for chelation are donor atoms. For example, DTPA offers octadentate ligands for Gd^{3+} with 3 nitrogen donor atoms and 5 carboxylate oxygen donor atoms. DOTA also offers octadentate ligands with 4 nitrogen donor atoms and 4 carboxylate oxygen atoms. In both cases, the ninth coordination site is occupied by a water molecule [80]. In general, complexes derived from DTPA follow the same coordination as DTPA, while those derived from DOTA follow the same coordination as DOTA.

The rate at which the metal-ligand complex is formed depends on many factors as pH, temperature, concentration of reactants, and whether the ligand is linear or cyclic. Linear Gd-complexes are formed much faster than the corresponding macrocyclic complexes [80].

1.8.1 Gd Complex Stability

Stability of Gd-complexes is of utmost importance because it is directly related to toxicity. The Gd-complex should remain intact in the body until its excretion in order to avoid the toxic effects of free Gd^{3+}. In this sense, two stability constants should be discussed: the thermodynamic stability constant (K_{st}) and the conditional stability constant (K_{eff}). K_{eff} is the measure of the stability of the complex at physiological pH of 7.4 which is in fact more precise. Different complexes have different basicities, K_{st} is a theoretical measure of stability under very basic conditions (taking into account that all ligands are deprotonated). However, at physiological pH, some protonation must occur and hence the measure of K_{eff} is a more precise measure of the stability constant [66, 80, 84]. Table 3 represents K_{st}, K_{eff}, and the type of molecular structure of different clinically used Gd complexes.

Commercial Name	**Scientific Name**	**Formula**	**LogK_{st}**	**Logk_{eff}**	**Molecular Structure**
Magnevist®	Gadopentate dimeglumine	Gd-DTPA	22.1	18.1	Linear Ionic
Dotarem®	Gadoterate meglumine	Gd-DOTA	25.8	18.8	Macrocyclic Ionic
ProHance®	Gadoteridol	Gd-HP-DO3A	23.8	17.1	Macrocyclic non-ionic
Omniscan®	Gadodiamide	Gd-DTPA-BMA	16.9	14.9	Linear non-ionic
MultiHance®	Gadobenate dimeglumine	BOPTA	22.6	18.4	Linear ionic
Gadovist®	Gadobutrol	Gd-BT-DO3A	21.8	14.7	Macrocyclic non-ionic
OptiMARK®	Gadoversetamide	Gd-DTPA-BMEA	16.6	15	Linear non-ionic

Table 3: *Stability constants and molecular structures of clinically used Gd-complexes [88]*

1.8.2 Transmetallation

This is the process in which other metal ions replace Gd^{3+} inside the complex with the highest probability being the replacement of Gd^{3+} by Zn^{2+}. The transmetallation process is represented by the following reactionreaction [89]:

$$GdL^{n} + [M]^{x+} \leftrightarrow Gd^{3+} + [ML]^{-}$$

Where M can be Fe^{3+}, Ca^{2+}, Cu^{2+} and Zn^{2+}….

The order of affinity of complexation agents to some cations is: $Fe^{3+}>Cu^{2+}>Zn^{2+}$

The highest attention is given to Zn^{2+} rather than the other two cations because iron in the serum is regulated by transferrin and Cu^{2+} is present in fairly low concentrations. Free Gd^{3+} is then precipitated as gadolinium phosphate in soft tissues of the body [80]. The transmetallation process is represented in Fig. 12 [84].

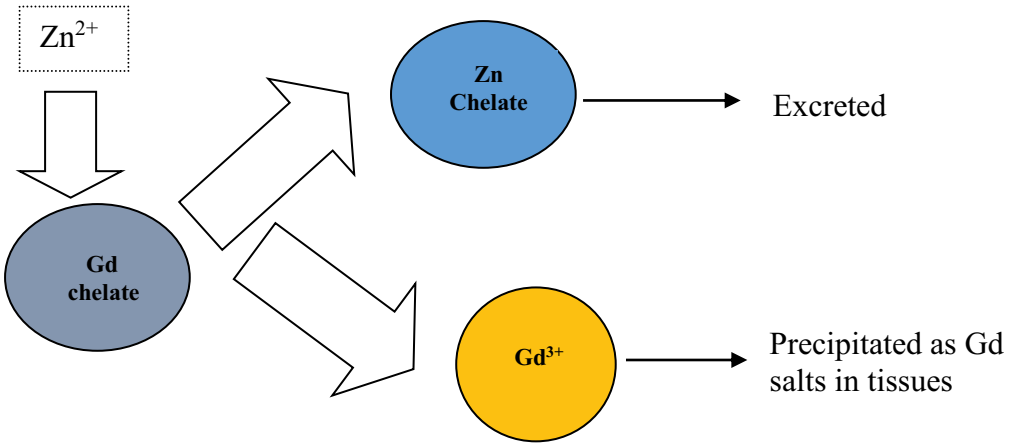

Figure 12: *Mechanism of the transmetallation process*

Table 2 reveals that almost all complexes have relatively high stability constants, with macrocyclic complexes having the highest stability. In general, macrocyclic chelates are more stable than the corresponding linear ones [84], however this is not always necessarily true. In some cases, DTPA derivatives are more stable than the corresponding macrocyclic ones [80].

Most utilized Gd-based contrast agents are not organ specific and are extracellular fluid agents. Most chelates used for gadolinium are hydrophilic, thus MRI contrast agents are hydrophilic, which limits their cell penetration [66, 86]. In general, most MRI contrast agents are administered intravenously with a terminal half-life of around 1.5 hours for extracellular agents [86].

1.9 Macromolecular Contrast Agents

Almost all clinically accepted Gd complexes with cyclic or linear chelates are low molecular weight complexes. Their small size causes their rapid renal clearance. Modifying the chemical properties of Gd-chelates (by attaching macromolecules for example) affects their pharmacokinetics and clearance rate, thus extending their residency time in the body [87].

The use of macromolecules as polymers and dendrimers causes an increase in the image contrast and resolution due to their larger sizes which retards the complex rotational moment, causing a decrease in T1 (increase in relaxivity R1=1/T1) and thus increased contrast [90,91]. Polymeric based macromolecular Gd contrast agents are being studied and evaluated as potential MRI contrast agents. In this case, biocompatible polymers are attached to Gd complexes. The polymers used can be either biodegradable or non-biodegradable. Depending on the position of the Gd-chelate in the polymeric chain, macromolecular contrast agents can be classified into four groups represented in Fig.13 where Gd is an abbreviation for Gd-chelate.

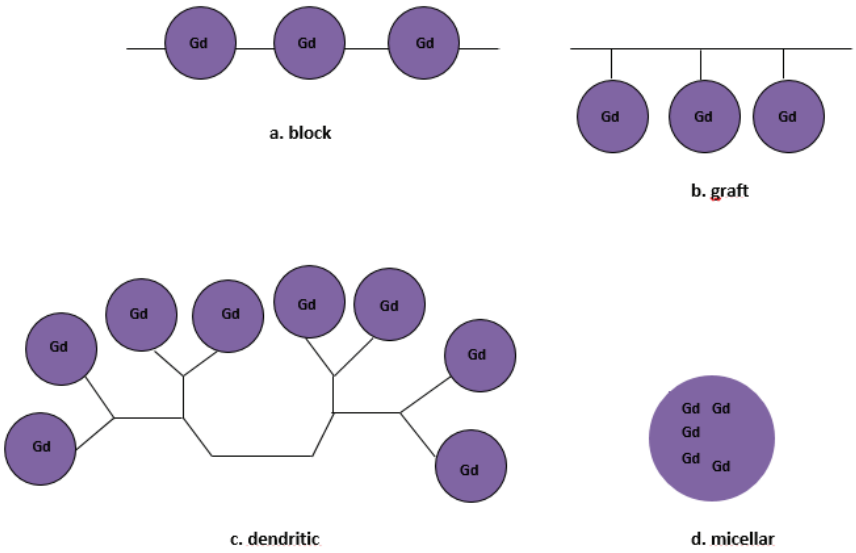

Figure 13: *Different structures of macromolecular contrast agents [91]*

In the case of block (a), in graft and dendritic macromolecular contrast agents (b and c), Gd with DTPA chelates is attached to polymers by the interaction of functional groups of DTPA chelates with functional group in polymers [91]. Graft macromolecular contrast agent is the structure of the contrast agent synthesized in our case and will be discussed in details in later sections. In the case of micellar contrast agents (d), Gd-chelates are either in the shell or in the core of the micellar structure. The size and structure of the micelle is designed according to the application. The methods used for their synthesis is mainly emulsion polymerization [91].

1.9.1 Micellar MRI Contrast Agents

Doiron et al. demonstrated the possibility of incorporating Gd-DTPA complex in microspheres of the copolymers PLA-PEG [92]. The system works on the idea of trapping a hydrophilic complex (Gd-DTPA) with high Gd content into a polymeric particulate system. However, due to the high hydrophilicity of the chelate, 90% of the complex was released after 1 hour, and 100% after 5 hours. This is similar to results obtained by Chen et al., in which Gd-

DTPA in PLA-PEG nanoparticles allowed an MRI visualization time of 4.5 hours [93]. Fig. 14 schematizes the preparation of gadolinium conjugated with PLA-PEG nanoparticles in which a Gd-DTPA is chelated to the shell layer of the micellar structure.

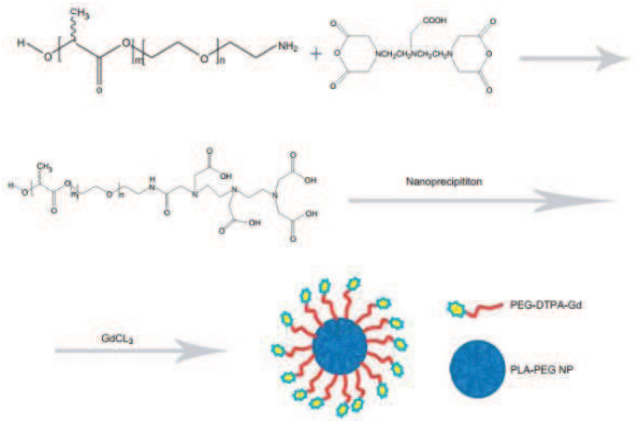

Figure 14: *Gadolinium conjugated to PLA-PEG nanoparticles [93]*

Thus, the incorporation of a hydrophilic complex of gadolinium in a hydrophobic polymer matrix only allows short-term visualization due to the rapid release of the complex.

1.9.2 Graft macromolecular contrast agents

In this case, the chelate is grafted on the linear polymeric chain carrier in order to avoid its release. The polymer used can be natural or synthetic. The molar mass and the structure of the polymer used determine the pharmacokinetics of the macromolecular contrast agents [91]. Modifications on Gd complexes have been made to conjugate polymers, to improve the contrast and to increase the contrast agent retention time in the body. Polymers can be either biodegradable or biostable depending on the needed duration of visualization. Schuhmann-Gampierri et al. covalently linked poly(lysine) to Gd-DTPA and evaluated its pharmacokinetics as compared to Gd-DTPA. This polymeric contrast agent had three times higher relaxivity than Gd-DTPA and increased half-blood distribution [94]. Zheng-Rang et al. synthesized a biodegradable polysulfide GdIII contrast agent. These macromolecular contrast

agents degraded in the body into small and excretable Gd complexes. These agents prolonged contrast enhancement in blood pool with a minimal Gd(III) retention [95].

In some cases, the chelate is modified in order to be attached to the macromolecular contrast agent. For example, Blanquer et al. obtained a PCL grafted with Gd-DTPA by modifying DTPA dianhydride to give Bn_2-DTPA-PCl. This compound was further reacted with anionic PCL, treated and purified to yield DTPA-PCL which was then complexed with Gd^{3+} to yield the Gd-DTPA-PCL as macromolecular contrast agent [96]. Fig. 15 represents the PCL grafted with Gd-DTPA

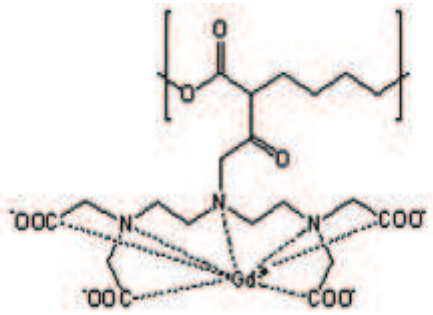

.

Figure 15: *PCL grafted with Gd-DTPA [96]*

Another method to graft contrast agents to macromolecules is Huisgen click chemistry reaction between a polymer bearing a pendant alkyne group and a Gd-DTPA complex with an azide group. This reaction leads to the formation of a triazole unit which is stable to metabolic degradation [97].

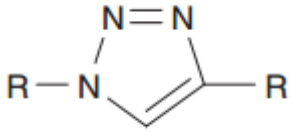

Figure 16: *Triazole moiety [97]*

1.9.3 Block MRI Contrast agents

In this type of macromolecular contrast agents Gd^{3+} chelates are inserted onto DTPA bis-amide or DTPA diester copolymers. They are synthesized by condensation of DTPA dianhydride with monomers having a diol or a diamine, followed by complexation with gadolinium [91]. Figure 17 represents some examples of block copolymers MRI contrast agents.

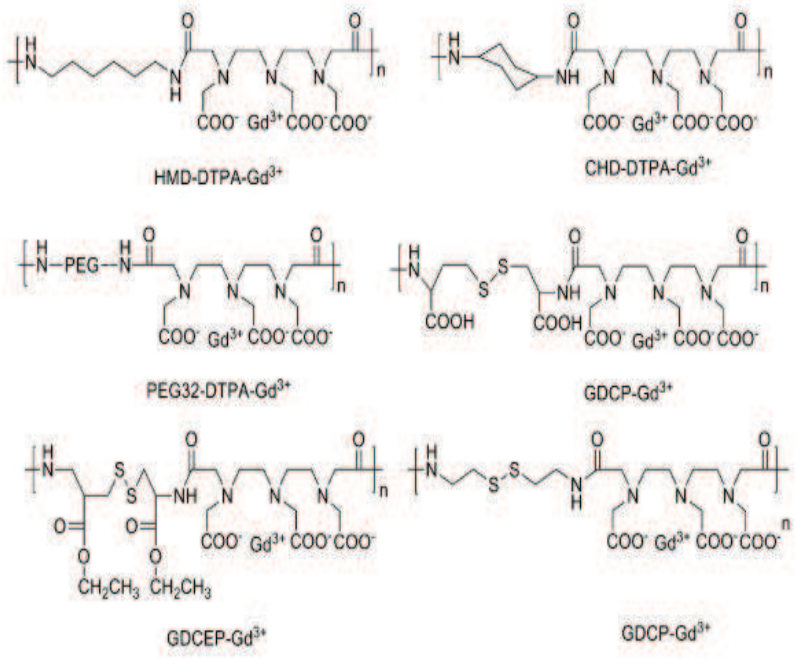

Figure 17: *Some examples of block copolymers as MRI contrast agents [91]*

1.9.4 Dendritic MRI contrast agents

These compounds have a precise spherical and highly branched structure. There are various types of dendrimers with various types, chemical structures and functional groups. Examples of dendrimers used for conjugation to contrast agents include poly(propyleneimine), poly(amidoamine), and poly(L-lysine). All these dendrimers have amino groups on their surface, enabling their conjugation with DTPA and DOTA chelates. However, it is important to take into consideration the issue of biocompatibility especially for *in vivo* applications [91]. Figure 18 represents a poly(lysine) dendrimer.

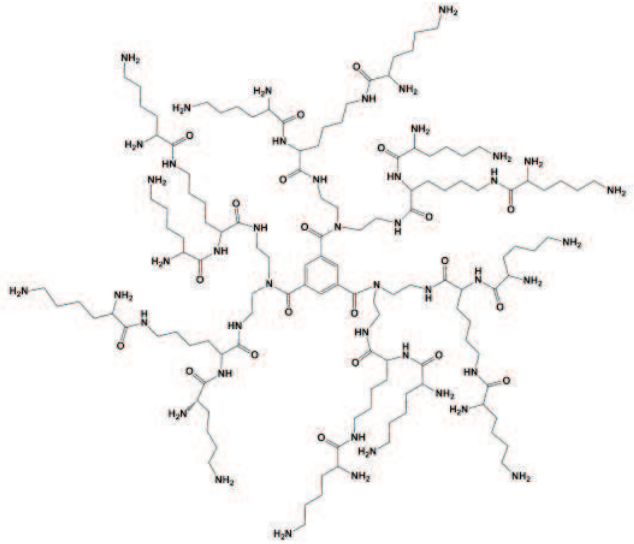

Figure 18: *Poly(L-lysine) dendrimer with aromatic core [91]*

In fact, medical imaging techniques are not only used to visualize and detect pathologies and changes in the body. The visualization of prosthetic implants is of high importance to obtain informations concerning their post-operation fate, localization in the body, and to monitor any changes in these materials.

1.10 Techniques for the visualization of prosthetic implants

The following part will discuss the imaging techniques used to visualize prosthetic implants depending on their type.

1.10.1 Visualization of Metallic Implants

Metallic medical implants have the capacity of absorbing more X-rays than soft tissues, thus the follow-up of metallic implants can be performed by X-ray pictures [98]. For example, the follow-up of a metallic stent was performed using CT scans and X-rays [99]. Unfortunately, the MRI visualization of metallic implants produces distorted images due to the large

difference in magnetic properties between tissues and metallic implants [100]. This geometric distortion is called the susceptibility artifact. These artifacts decrease the usefulness of the MR technique in the visualization of metallic implants. In general, ferromagnetic metallic implants produce high magnetic field inhomogeneities in their neighborhood thus resulting in signal loss represented as a dark region in the area surrounding the implant [101]. However, implants of titanium alloys which are non-ferromagnetic produce much less severe artifacts than stainless steel implants which are ferromagnetic (Fig. 19) [102]. For example, nitinol (nickel and titanium alloy) produces smaller artifacts than stainless steel on MR images [103].

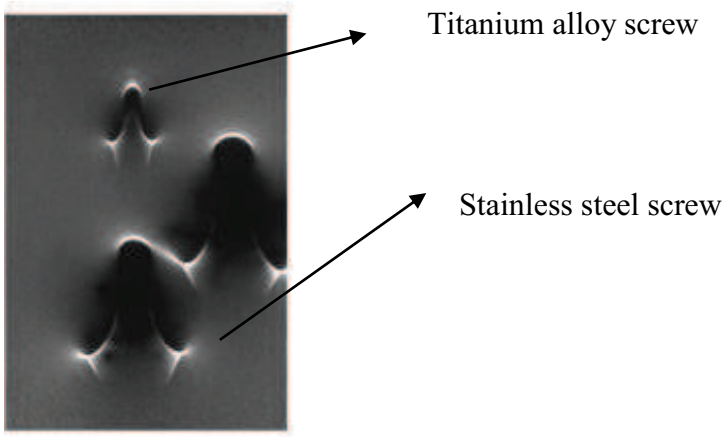

Figure 19: *MR images of titanium alloy and stainless steel screws [102]*

1.10.2 Visualization of Ceramic Implants

Many ceramic implants are composed of calcium phosphate due to its similar chemical and structural properties to the mineral portion of bones and teeth [104]. Therefore, calcium phosphate ceramics absorb X-rays in a coefficient similar to that of bones and thus are visible on radiographs since the mineral content of the bone determines its radiographic appearance [105]. Zirconia ceramics also absorb X-rays strongly, and are thus visible and can be localized on radiographs [106]. In some cases, opacifier materials such as barium and strontium are added in order to enhance the contrast of calcium phosphate cements on CT scans [107].

The visualization of zirconia dental implants is possible by MRI because these implants produce high hyposignal intensity that creates clear images without distortion and artifacts [108] as shown in Figure 20.

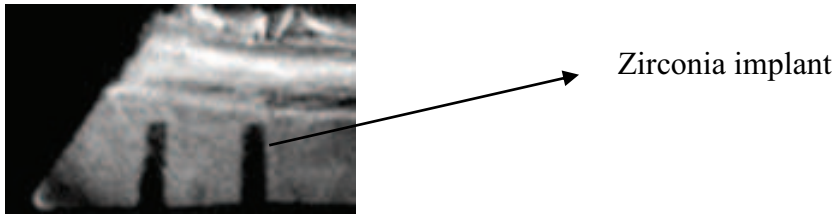

Figure20: *MRI visualization of zirconia implant [108]*

1.10.3 Visualization of polymeric implants

In general polymeric biomaterials are not visible by classical ways of visualization. To be visible by X-ray, the polymeric biomaterial has to be radio-opaque to attenuate the radiation and be visible on the radiograph. Most polymeric biomaterials are radiotransparent and thus the addition of opacifiers is a necessity in order to render them radio-opaque. For example, poly(methyl methacrylate) is radiotransparent, but can be visualized by X-ray through the addition of opacifiers such as $BaSO_4$, ZrO_2, and iodine [109,110]. Nottelet et al. bound iodine to PCL by anionic modification of PCL. The obtained polymer turned out to be opaque enough to be visualized by X-ray [111]. However, opacifiers pose some disadvantages as: the need for high concentrations of radio-opaque fillers and the problems of the leakage of metals into body fluids.

Unfortunately, polymeric meshes which are extensively used in hernia repair and vaginal prolapses are invisible by MRI because their structure is very thin and the T2 relaxation time of the polymer is very short [112]. Thus these meshes remain invisible by MRI after their implantation. Their visualization by MRI is a necessity in order to follow-up any complications associated to the mesh as: seromas, bacterial infections, chronic pain,

adhesions, and mesh shrinkage [113]. The visualization of these implants by MRI rather than by other imaging techniques, is due to MRI's non-invasiveness and the high-resolution images produced, which is related to the water content of biological tissues.

The radiological visibility of the meshes is determined by several properties such as: density, structure and thickness of the material [114]. ePTFE meshes are clearly visible by MRI, allowing accurate assessment of the mesh and its fixation. This can be explained by the microporous and hydrophobic structure of ePTFE which inhibits collagen tissue infiltration [115]. ePTFE visibility increases with an increase of the thickness of the mesh. On the other hand PP and polyester meshes, unlike ePTFE, have a density similar to that of adjacent muscles, thus resulting in poor or even total invisibility by MRI [114,116].

PP meshes have been widely used in hernia repair during the last twenty years due to their stability, strength and inertness [35,117]. Despite their popularity, the visualization of PP meshes by MRI is of high necessity as stated above, in order to follow-up the fate of the mesh and any post-operation complications. One of the advantages of MRI vs CT is the absence of ionizing radiation. This gives rise to the question of how to render this polymeric mesh visible by MRI.

Several attempts have been done in order to render these meshes visible and thus to improve patient's safety. This is done by the incorporation of contrast agents on the meshes. One method involves the incorporation of ferro particles on the surface of the mesh. Kraemer *et al*. showed that loading superparamagnetic iron oxide particles on surgical meshes resulted in rendering these meshes visible by MRI. These meshes appeared as a hypointense signal (dark) as compared to the bright contrast of the surrounding abdominal tissues [112,113,118].

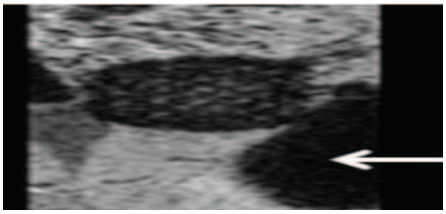

Figure 21: *Coronal view of surgical mesh loaded with superparamagnetic iron oxide particles [113]*

In order to obtain a positive contrast in MRI, gadolinium contrast agents are used. In the literature one can find some publications for rendering PP meshes visible by MRI using polymeric contrast agents. Guillaume *et al*. [119] reported a method of binding Gd-DTPA to poly(methyl acrylate). Coating PP mesh with this contrast agent resulted in an MRI visualization at 7T and a stability of at least 6 months. Blanquer *et al*. reported the synthesis of PCL-GdDTPA by grafting Gd-DTPA to biodegradable PCL. By coating this contrast agent on a mesh, MRI visualization of at least one year was possible [96]. EL Habnouni *et al*. described the synthesis of a macromolecular contrast agent using the principle of azide-alkyne Huisgen 1,3-dipolar cycloaddtion between an azide containing contrast agent and propargylated PCLs. In this case, the propargyl ratio on PCL has been controlled, thus allowing the control of Gd^{3+} grafted onto the contrast agent. These macromolecular contrast agents were stable for more than 90 days and were found to be biocompatible. Films of these PCL macromolecular contrast agents are MRI visible [120]. Porsio et al. synthesized MRI visible nanoparticles from the macromolecular contrast agent synthesized by El Habnouni also using the principle of Huisgen cycloaddition. These nanoprticles allowed MRI visualization with amounts of Gd^{3+} as low as 0.1% by weight [121].

Huisgen 1,3-dipolar cycloaddition is one of the most popular forms of click reaction combining together an alkyne function with an azide group. The concept of click chemistry

has been gaining much attention recently with various medical applications, such as the synthesis of macromolecular contrast agents for MRI as discussed earlier.

1.11 Why click reaction?

The term “click chemistry” was first described by Sharpless et al. as an approach to develop modular and selective blocks that can be applied on small scales as well as on large scales. This reaction is: modular, wide in scope, high yields generation, readily available starting materials, simple reaction conditions, and removal of by-products by non-chromatographic techniques [122]. The most typical “click reaction” is the Huisgen 1,3-dipolar cycloaddition reaction, also termed the [3+2] azide-alkyne cycloaddition yielding a triazole, a five-member heterocycle ring. The reaction was first discovered in 1963 by Huisgen without gaining attention because it needed high temperatures and pressures and yielded 1,4 and 1,5 triazoles which is unfavorable for biomedical applications [97,123]. In 2001, Tornøe and Meldal introduced the use of Cu(I) catalyst allowing the reaction to take place at mild conditions and also allowed the regioselective synthesis of 1,3 triazoles [124]. The idea of the introduction of Cu as a catalyst had been realized independently by the Sharpless and the Meldal laboratories. This CuAAC is the abbreviation that will be used for copper catalyzed Huisgen 1,3-dipolar cycloaddition and the general mechanism is represented in Fig. 22.

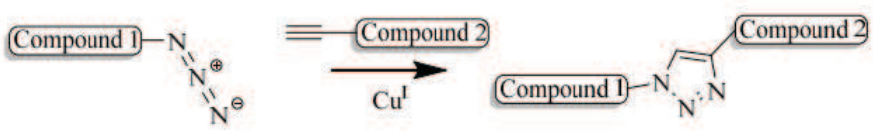

Figure 22: *General mechanism for CuAAc reaction [125]*

The mild reaction conditions needed and the high yield obtained from this reaction had made it gain popularity in the biomedical field. In addition, the triazole moiety formed during this reaction is stable to metabolic degradation [97].

The objective of this work is to synthesize a stable MRI macromolecular contrast agent intended for long-term visualization. For this, a high molecular weight polymer bearing an alkyne group will be synthesized. Thus poly(methyl methacrylate-*co*-propargyl methacrylate), PMMA-*co*-PPMA, will be prepared by free radical polymerization of methyl methacrylate and propargyl methacrylate. A monofunctional Gd-DTPA ligand bearing an azide group will be grafted on the polymeric backbone in order to obtain the stable azide moiety by CuAAC as shown in Scheme 1. This also allows the control of the amount of Gd^{3+} incorporated in the contrast agent.

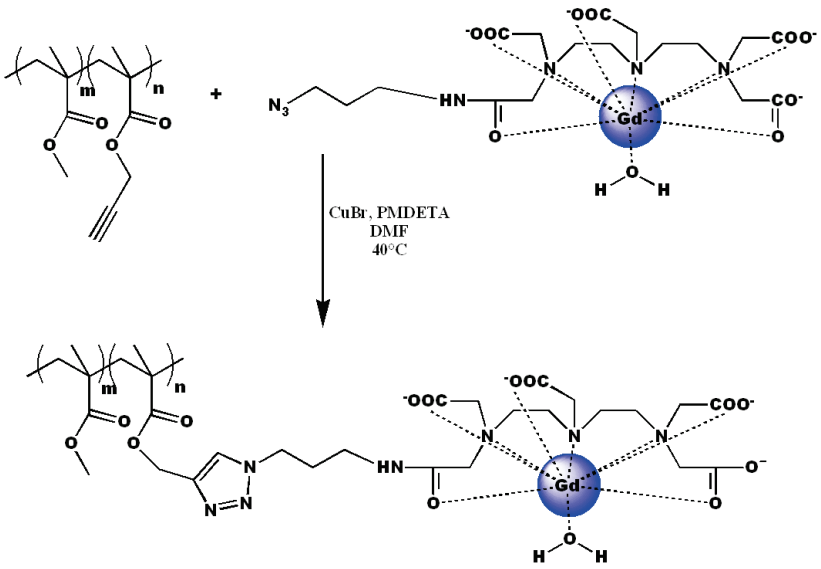

Scheme 1**:** *Grafting of azido-functionalized Gd-DTPA on polymeric backbone by CuAAC*

The novelty of this work resides in the synthesis of monofunctional azido functionalized Gd-DTPA ligand, the MRI contrast agent, which will be grafted on the polymeric backbone. This azido functionalized DTPA ligand can either contain amide functional group or an ester one depending on whether the reaction of DTPA bisanhydride is reacted with an azido-amine or

an azido-alcohol. In the literature most of the obtained ligands are bifunctional (bearing either two amide or two ester groups). Many publications describe the synthesis of DTPA bis-amides which is relatively easy and does not require tedious purification steps [126-128]. However, when one comes to monoamide DTPA ligands, there are no references. Despite the difficulty of the synthesis of monoamide DTPA ligands, they are ligands of choice for several reasons. Monoamide-DTPA micelles have been found to show higher relaxivities than the corresponding bis-amide ones [129] and the chelating potency of DTPA monoamides is better than the one of corresponding bis-amides [130].

The main efforts reside in the synthesis of monoamide Gd-DTPA ligands. However, the synthesis of mono-ester Gd-DTPA ligands will be also reported although it is known that the stability of the ester group is less than that of the amide group.

Once, the polymeric monoamide Gd-DTPA contrast agent is obtained, it will be assessed for its ability to render a polypropylene mesh MRI visible. The obtained polymeric contrast agent will be placed on a commercial PP mesh using the airbrushing technique, and the visualization of the coated mesh will be assessed on a 7T MRI instrument. The airbrushing technique is a versatile method allowing the preparation of homogenous and regular film without altering the mesh shape and mesh mechanical properties [119].

Since the polymeric contrast agent is intended for use in long-term visualization and is intended to be used in biomedical applications, cytocompatibility and stability tests will be performed

1.12 Fluorescence

Although MRI is a highly sensitive and non-invasive imaging technique, fluorescence spectroscopy is another promising diagnostic technique with fast and rapid diagnostic ability. The central part of fluorescence spectroscopy is attributed to fluorophores. A fluorophore

absorbs energy at specific wavelength and re-emit energy at a different but specific wavelength [131]. CuAAC being a versatile and regioselective reaction that only requires mild reaction conditions will be employed in order to synthesize different types of fluorophores. Clickable fluorodyes will be synthesized using the reaction between an azide-bearing fluorophore and the alkyne group of PMMA-co-PMA. The select fluorophores are anthracene, rhodamine B isothiocyanate (RITC), fluorescein isothiocyanate, and Europium. All fluorophores will be modified to contain an azide group which will eventually undergo fluorogenic click reactions.

The main characteristics of the fluorophores are the following:

- Anthracene: Anthracene is used to determine fluorescence in quantum yield. 1-amino anthacene has been identified as a fluorescent general anesthetic [132]. However, once an azide group is introduced next to the anthryl group, an electron is tranferred to the excited anthracene through a photoinduced electron transfer (PET) and this quenches the fluorescnce of the anthracene. However, the formation of a triazole moiety through CuAAC reaction decreases the electron donating effect of nitrogen which ends the PET effect and restores the fluorescence of anthracene. This is called a fluorogenic CuAAC reaction, which is a reaction between non-fluorescent alkyne and non-fluorescent azide to yield a highly fluorescent triazole complex (Fig. 23) [133]

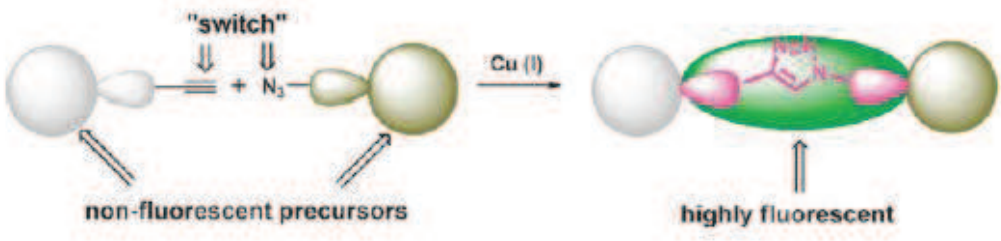

Figure 23: *Fluorogenic CuAAC [133]*

For this reason, azido anthracene will undergo CuAAC reaction with PMMA-co-PMA to obtain the triazole unit and quench the PET effect.

- Rhodamine B isothiocyanate (RITC): Rhodamine dyes are widely used as fluorescent dyes due to their high photostability and high fluorescent quantum yields. Also, for biological applications fluorescent dyes absorbing in the near infra red region are preferred because that region is mostly noninvasive with a minimal unwanted background signal [134]. RITC will be modified to contain an azide group, and then clicked to PMMA-co-PMA to form the stable triazole moiety. The obtained fluorescent polymer will be tested for fluorescence.

- Fluorescein isothiocyanate (FITC): FITC is a chemical dye widely used in immunochemistry and for labeling proteins [135].

- Europium salts: Europium complexes are gaining attention as fluorescent markers because they have large Stocke shift and long life emission. The ligand absorbs the radiation and transfers it to Eu through internal energy emission process, resulting in Europium emission [136]. In our case, europium will be chelated in azido DTPA mono-amide in the same way as Gd3+, and the obtained complex will be clicked to PMMA-co-PMA. The obtained product will be tested for fluorescence.

The fluorescence part is in fact a perspective for this thesis. It is a building block for further work to be carried out inclusing stability of the fluorophores in the formed complexes. The europium complex reveals that the synthesized complex can serve as an MRI contrast agent when Gd is used and as a fluorophore when europium is used.

1.13 Conclusion

The use of polymers in prosthetic implants is increasing, especially in the field of reinforcement medical implants as meshes. At the same time, the follow-up of these implants is a necessity with MRI being the most favored one in localizing and visualizing prothetic

implants. Long-term visualization of these implants is highly favored because it allows clinicians to localize the implanted prosthesis throughout its lifetime in the body.

For this, the grafting of the contrast agent will be done on a non-biodegradable polymer, PMMA. For this the contrast agent will be grafted on the backbone of PMMA using CuAAC, in which a stable triazole moiety will be formed.

This work involves three chapters:

The first chapter describes the synthesis of azido functionalized DTPA ligands and the synthesis of the non-biodegradable propargylated PMMA.

The second chapter describes the MRI visualization of polypropylene meshes after being coated with the synthesized polymeric contrast agent. Since the polymeric contrast agent is intended to be used in biomedical application, stability and cytotoxicity results are also presented in this chapter.

The third chapter describes the synthesis of polymeric fluorophores. Preliminary fluorescent results are presented.

References:

[1]: ISO 13485 2003 Standard for medical devices- definitions. Updated December 20, 2004. http://www.praxiom.com/iso-13485-definitions.htm

[2]: Medical devices: Guidance document. European Commission, DG Enterprise, Directorate G. Unit 4- Pressure Equipment, medical devices, metrology. MEDDEV 2.1/1, April 1994

[3]: Medical device regulations, classification and submissions. November 5, 2012. http://www.marsdd.com

[4]: Basic information about the European Directive 93/42/EEC on Medical Devices. MDC, medical device certification.

[5]: European Commission DG Health and Consumer. Directorate B, Unit B2. Cosmetics and medical devices. MEDDEV 2.4/1. Rev-9. June 2010

[6]: French-Mowat, E.; Burnett, J. How are medical devices regulated in the European Union? *Journal of the Royal Society of Medicine* **2012**, 105, S22-S28.

[7]: US Food and Drug Administration. Protecting and Promoting your health. Implants and prosthetics.
http://www.fda.gov/MedicalDevices/ProductsandMedicalProcedures/ImplantsandProsthetics/

[8]: Bergmann, C.; Stumpf, A. Dental Ceramics. *Springer-Verlag Berlin Heidelberg* **2013**

[9]: Williams, DF. On the mechanisms of biocompatibility. *Biomaterials* **2008**, 29, 2941-2953

[10]: Sikalidis, C. Advances in Ceramics: Electric and magnetic ceramics, Bioceramics, ceramics and the environment. *Intech Rijeka Croatia* **2011,** 359-378

[11]: Patel, N.; Gohil, P.A Review on Biomaterials: Scope, Applications, and Human Anatomy Significance. *International Journal of Engineering Technology and Advanced Engineering* **2012,** 2, 91-101

[12]: Ha, T.; Quan,T. Naturally derived biomaterials: Preparation and Application. *Tissue Engineering and Rgenerative Medicine CRC Press, Boca Raton,* **2013,** 247-272

[13]: http://www.oulu.fi/spareparts/ebook_topics_in_t_e_vol3/abstracts/coburn_01.pdf

[14]: Ali, S. ; AlMaatouq, M. ; Mohamed, A.Classifications, surface characterization and standardization of nanobiomaterials. *International Journal of Engineering Technology and* **2013**, 2, 187-199

[15]: Narayan, R. Biomedical Materials.*Springer, New York* **2009,** 41

[16]: Hermawan, H.; Ramdan, D.; Djuansjah, J. Metals for biomedical applications. *Biomedical Engineering –From Theory to Applications* **2011**, 411-430

[17]: Kuo, CL.; Wang, MC.; Shia, AS. Superiority of Nitinol Piston over conventional prostheses in Stapes surgery: First comparative Results in the Chinese population in Taiwan. *Journal of the Chinese Medical Association* 2010, 73, 241-247.

[18]: Duerig, T.; Pelton, A.; Stockel, D. An overview of nitinol medical applications. *Materials Science and Engineering: A* **1999,** 273-275, 149-160.

[19]: Oldani, C.; Dominguez, A. Titanium as a biomaterial for implants. *Recent Advances in Arthoplasty* **2012,** 149-161

[20]: Saenz, A.; Rivera-Munoz, E.; Brostow, W.; Castano, V. Ceramic Biomaterials: an introductory overview. *Journal of Materials Education* **1999,** 21, 297-306

[21]: Bergmann, CP.; Stumpf, A. Biomaterials.*Dental Ceramics* **2013,** 9-13

[22]: Hench, L. Bioceramics: from concept to clinic. *Journal of the American Ceramic Society* **1991,** 74, 1487-1510

[23]: Simon, J.P.; Fabry, G. An overview of implant materials. *Acta Orthopaedica Belgica* **1991,** 57, 1-5

[24]: Thamaraiselvi, T.V.; Rajeswari, S. Biological Evaluation of Bioceramic materials- A Review. *Trends in Biomaterials and Artificial Organs* **2004**, 18, 9-17

[25]: Domb, AJ. ; Khan, W. Implantable medical devices. *Focal Controlled Drug Delivery, Controlled Release Society* **2014**

[26]: Venkatraman, S.; Boey, F.; Lao, L.L. Implanted Cardiovascular polymers: Natural, synthetic and bio-inspired. *Progress in Polymer Science* 2008**,** 33, 853-874

[27]: Polymer Molecular Weight

http://www.ias.ac.in/initiat/sci_ed/resources/chemistry/MolWeight.pdf

[28]: How Plastics are made? Ch. 1 International Association of Plastic Distributors. http://www.modernplastics.com/pdf/IAPD_plastics_intro1.pdf

[29]: McKeen, L. Plastics used in medical devices. *Handbook of Polymer Applications in Medicine and Medical Devices, Elsevier,* **2013**

[30]: ternberg, K. Current requirements for polymeric biomaterials in otolaryngology. *Current Topics in Otorhinolaryngology-Head and Neck Surgery* **2011**, 8

[31]: Middleton, JC. ; Tipton, AJ. Synthetic biodegradable polymers as orthopedic devices. *Biomaterials* **2000,** 21, 2335-2346

[32]: Dumitriu, S. Bioabsorbable polymers for medical applications with an emphasis on orthopedics surgery. *Polymeric biomaterials: revised and expanded. Dekker,* **2001**

[33]: Kumbar, S.; Laurencin, C.; Deng, M. Natural and synthetic biomedical polymers. *Elsevier,* **2014**

[34]: Salamone, J. Polymeric materials encyclopedia. *CRC Press, Boca Raton,* **1996**

[35]: Doctor, H.G. Evaluation of various prosthetic materials and newer meshes for hernia repair. *Journal of Minimal Access Surgery* **2006**, 2, 110-116

[36]: Clinical applications of cardiovascular patches http://www.diss.fu-berlin.de/diss/servlets/MCRFileNodeServlet/FUDISS_derivate_000000001760/03_1.pdf;jsessionid=A132BAB150DE3C81852D8429407FB8D5?hosts=

[37]: Hughes, MO. Incorporating Gold into ocular prosthetics. *Journal of Opthalmic Prosthetics* **2010,** 31-43

[38]: Varma, V.; Varma, A .K; Manglandan, TS. ; Bal, A.; Kumar, H. Use of poly (methyl methacrylate) as prosthetics replacement of destroyed foot bones. *The Journal of Diabetic Foot Complications* **2012**, 4, 71-82

[39]: Maxilloacid prosthetic rehabilitation of acquired defects.

http://famona.tripod.com/ent/cummings/cumm080.pdf

[40]: Burke, A.; Hasirci, N. Polyurethanes in biomedical applications. *Biomaterials* **2004**, 553, 83-101

[41]: Suggs, LJ. ; Moore, SA. ; Mikos, AG. Synthetic biodegradable polymers for medical applications. *Physical properties of polymers handbook Springer, New York* **2006**

[42]: Bikiaris, D.; Karavelidis, V.; Karavas, E. Novel Biodegradable Polyesters. Synthesis and Application as Drug Carriers for the Preparation of Raloxifene HCl Loaded Nanoparticles. *Molecules* **2009***, 14,* 2410-2430

[43]: Ikada, Y.; Tsuji, H. Biodegradable polyesters for medical and ecological applications. *Macromolecular Rapid Communications* **2009,** 21, 117-132

[44]: Einmahl, S.; Capancioni, S.; Schwach-Abdellaoui, K.; Gurny, R. Therapeutic Applications of Viscous and Injectable poly(ortho esters). *Advanced Drug Delivery Reviews* **2002,** 53, 45-73

[45]: Kumar, N.; Langer, RS. ; Domb, AJ. Polyanhydrides: an overview. *Advanced Drug Delivery Reviews* **2002,** 54, 889–910

[46]: Medical Applications of Polycarbonate

http://www.mddionline.com/article/medical-applications-polycarbonate

[47]: Kohli, S.; Bhatia, S. Polyamides in dentistry. *International Journal of Scientific Study* **2013**, 1, 20-25

[48]: Bezwada, RS. From Biostable to biodegradable polymers for biomedical applications. *Polymeric materials: Science and Engineering* **2009**, 101, 1044-1045

[49]: Gleich, B. Priniples and Applications of Magnetic Particle Imaging. *Springer Fachmedein, Wiesbaden* **2013**

[50]: X-ray contrast media made clear.

http://hsc.uwe.ac.uk/idis2/contrast_agents/CM%20Zip/ContrastMedia_Schering.pdf

[51]: Understanding Medical Radiation. Types of Medical Imaging.

https://www.medicalradiation.com/types-of-medical-imaging/

[52]: U.S> Food and Drug Administration. Radiation-Emitting Products. Ultrasound Imaging.

http://www.fda.gov/Radiation-EmittingProducts/RadiationEmittingProductsandProcedures/MedicalImaging/ucm115357.htm#benefitsrisks

[53]: Moestue, SA. ; Gribbestad, IS. ; Hansen, R. Intravascular Targets for Molecular Contrast – Enhanced Ultrasound Imaging. *International Journal of Molecular Sciences* 2012, 13, 6679-6697

[54]: Sutton, R. ; Kanal, E. ; Wilkoff, BL. ; Bello, D. ; Luechinger, R. ; Jenniskens, I. ; Hull, M. ; Sommer, T. eSafety of magnetic resonance imaging of patients with a new Medtronic EnRhythm MRI SureScan pacing system: clinical study design. *Trials* **2008**, 9:68.

[55]: Chung, M.: Dahabre, IJ. ; Hadar, N. Ratichek, SJ. ; Gaylor, JM. ; Trikalinos, TA. ; Lau, J. Emerging MRI Technologies for Imaging Muscoskeletal Disorders Under Loading Stress. *Comparative Effectiveness Technical Briefs* **2011,** No. 7.

[56]: MRI Physics. E. Blink http://www.mri-physics.net/bin/mri-physics-en-rev1.3.pdf

[57]: U.S. Food and Drug Administration. Radiation-Emitting Products. MRI (Magnetic Resonance Imaging)

http://www.fda.gov/Radiation-EmittingProducts/RadiationEmittingProductsandProcedures/MedicalImaging/ucm200086.htm#rb

[58]: The Nobel Prize in Physics 1952. Felix Bloch, E.M. Purcell http://www.nobelprize.org/nobel_prizes/physics/laureates/1952/

[59]: Lauterbur, pC. Image formation by induced local interactions: Examples employing nuclear magnetic resonance. *Nature* **1973**, 242, 190-191

[60]: Brown, MA. ; Semelka, R.C. MRI Basic Principles and Applications. *Wiley-Liss, Nw Jersy,* **2003**

[61]: Hendee, W.; Morgan, CJ. Magnetic Resonance Imaging – Part I. Physical Principles. Medical Progress. *The Western Journal of Medicine,* **1984**, 141, 491-500

[62]: Hans, L. Introduction to Magnetic Resonance Imaging Techniques. *Danish Research Centre for Magnetic Resonance (DRCMR) Copenhagen University Hospital Hvidovre*. Revised August **2009**, 1-48

[63]: Relaxation in NMR spectroscopy. Copyright Hans J. Reich 2010. University of Wisconsin http://www.chem.wisc.edu/areas/reich/nmr/08-tech-01-relax.htm

[64]: Revise MRI.com. Shorter T1 in tissues. http://www.revisemri.com/questions/misc/shorter_t1_tissues

[65]: Yankeelov, T.; Pickens, D.; Price, R. Quantitaive MRI in Cancer. *CRC Press,* **2011**

[66]: Caravan, P.; Ellison, JJ. ; McMurry, TJ. ; Lauffer, RB. Gadolinium (III) Chelates as MRI contrast agents: structure, dynamics and applications. *Chemicals Reviews* **1999**, 99, 2293-2352

[67]: Perez-Mayoral, E.; Soler-Padros, J.; Negri, V.; Cerdan, S.; Ballesteros, P. Synthetic Approaches to Heterocyclic Ligands for Gd-Based MRI Contrast Agents. *Molecules* **2007**, 12, 1771-1795

[68]: Thomsen, HS. ; Aspelin, P. *Contrast Media*, **2006,** Springer-Verlag Berlin.

[69]: Scherzinger, AL. Basic Principles of Magnetic Resonance Imaging- An update. *Western Journal of Medicine* **1985**, 143, 782-792

[70]: Stijker, GJ. ; Mulder, WJ. ; Van Tilborg, GA. Nicolay, K.MRI Contrast Agents: Current Status and Future Perspectives. *Anticancer Agents in Medicinal Chemistry* **2007**, 7, 291-305

[71]: Krause, W. Formulations of Extracelluar MRI Contrast Agents Based on Gd. *Contrast Agents I: Magnetic resonance Imaging* 2002**,** Springer, Berlin.

[72]: Burtea, C.; Laurent, S.; Vander Elst, L.; Muller, RN. Contrast agents: magnetic resonance. *Handbook of experimental pharmacology* **2008,** 185, 135-165.

[73]: Wang, BW. ; Jiang, S.; Wang, XT. ; Gao, S. Magnetic Molecular Materials with Paramagnetic Lanthanide Ions. *Science in China Series B: Chemistry* **2009**, 52, 1739-1758

[74]: Karabulut, N. ; Elmas, N. Contrast agents used in MR imaging of the liver. *Diagnostic and Interventional Radiology* **2006**, 12, 22-30

[75]: Gallez, B. ; Bacic, G. ; Swartz, HM. Evidence for the dissociation of the hepatobiliary MRI Contrast Agent Mn-DPDP. *Magnetic Resonance in Medicine* **1996,**35, 14-19.

[76]: Royal Society of Chemistry. Periodic Table: Gadolinium http://www.rsc.org/periodic-table/element/64/gadolinium

[77]: Hermann, P.; Kotek, J.; Kublicek, V.; Lukes, I. Gadolinium (III) complexes as MRI contrast agents: ligand design and properties of the complexes. *Dalton Transactions* **2008,** 3027-3047

[78]: Ni, Y. MR Contrast Agents for Cardiac Imaging. *Clinical Cardiac MRI, Springer-Verlag Berlin* **2012,** 31-51.

[79]: Bianchi, A. ; Calabi, L. ; Corana, F. ; Fontana, S. ; Losi, P. ; Maiocchi,A. ; Paleari, L. ; Valtancoli, B. Thermodynamic and structural properties of Gd(III) complexes with

polyamino-polycarboxylic ligands: basic compounds for the development of MRI Contrast agents. *Coordination Chemistry Reviews* **2000,** 204,309–393

[80]: Sherry, AD. ; Caravan, P. ; Lenkinski, RE. Primer on Gadolinium Chemistry. *Journal of Magnetic Resonance Imaging* **2009,** 30, 1240–1248

[81]: Broome, DR. Nephrogenic systemic fibrosis associated with gadolinium based contrast agents: A summary of the medical literature reporting. *European Journal of Radiology* **2008,** 66, 230–234

[82]: Ersoy, H.; Rybiciki, FJ. Biochemical Safety Profiles of Gadolinium-Based Extracellular Contrast Agents and Nephrogenic Systemic Fibrosis. *Journal of Magnetic Resonance Imaging* **2007**, 26, 1190-1197

[83]: Abraham, JL. ; Chandra, S. ; Thakral, C. ; Abraham, JM. SIMS imaging of gadolinium isotopes in tissue from Nephrogenic Systemic Fibrosis patients: Release of free Gd from magnetic resonance imaging (MRI) contrast agents. J.L. *Applied Surface Science* **2008,** 255, 1181–1184

[84]: Morkos, SK. Extracellular gadolinium contrast agents: Differences in stability. *European Journal of Radiology* **2008,** 66, 175–179

[85]: Zhou, Z.; Lu, ZR. Gadolinium-Based Contrast Agents for MR Cancer Imaging. *Wiley Interdiscplinary Reviews. Nanomedicine and Nanobiotechnology* 2013**,** 5, 1–18.

[86]: Aime, S.; Caravan, P. Biodistribution of gadolinium-based contrast agents, including gadolinium deposition. *Journal of Magnetic Resonance Imaging* **2009**, 30, 1259–1267.

[87]: Huang, CH.; Tsourkas, A. Gd-based macromolecules and nanoparticles as magnetic resonance contrast agents for molecular imaging. *Current Topics in Medicinal Chemistry* **2013**, 13, 411–421

[88]: Runge, VM. Conventional Contrast Agents (Gadolinium Chelates). *Proceedings of the International Society of Magnetic Resonance in Medicine* **2011**, 19

[89]: Idee, JM. ; Port, M. ; Robic, C. ; Medina, C. ; Sabatou, M. ; Corot, C. Role of thermodynamic and kinetic parameters in Gadolinium Chelate stability.*Journal of Magnetic Resonance Imaging* **2009**, 30, 1249–1258

[90]: Bryson, JM. ; Reineke, JW. ; Reineke, TM. Macromolecular imaging agents containing lanthanides; can conceptual promise lead to clinical potential? *Macromolecules* **2012,** 45, 8939-8952

[91]: Tang, J.; Sheng, Y. ; Hu, H. ; Shen, Y. Macromolecular MRI contrast agents: Structures, properties and applications. *Progress in Polymer Science* **2013,** 38, 462-502

[92]: Doiron, AL. ; Chu, K. ; Ali, A. ; Brannon-Peppas, L. Preparation and initial characterization of biodegradable polymers containing Gadolinium-DTPA contrast agent for enhanced MRI. *Proceedings of the National Academy of Science of the United Staes of America* **2008**, 105, 17232–17237

[93]: Chen, Z. ; Yu, D. ; Liu, C. ; Yang, X. ; Zhang, N. ; Ma, C. ; Song, J. ; Lu, Z. Gadolinium-conjugated PLA-PEG nanoparticles as liver targeted molecular MRI contrast agent. *Journal of drug targeting* **2011**, 19, 657-665.

[94]: Schuhmann-Giampieri, G. ; Schmitt-Willich, H. ; Frenzel, T. ; Press, WR. ; Weinmann, HJ. In vivo and in vitro evaluation of Gd-DTPA-polylysine as a macromolecular contrast agent for magnetic resonance imaging. *Investigative Radiology* **1991**, 11, 969-974.

[95]: Lu, ZR. ; Mohs, AM. ; Zong, Y. Feng, Y. Polydisulfide Gd(III) chelates as biodegradable macromolecular magnetic resonance imaging contrast agents.*International Journal of Nanomedicine* **2006**,1, 31–40

[96]: Blanquer, S. ; Guillaume, O. ; Letouzey, V. ; Lemaire, L. ; Franconi, F. ; Paniagua, C. ; Coudane, J. ; Garric, X. New magnetic-resonance-imaging-visible poly(ε-caprolactone)based polyester for biomedical applications. *Acta Biomateriala* **2012**, 8(3), 1339-1347

[97]: Nwe, K.; Brechbiel, MW. Growing applications of "Click Chemistry" for Bioconjugation in Contemporary Biomedical Research. K. *Cancer Biotherapy and radiopharmaceuticals* **2009**, 24, 289-302

[98]: Chen, H.; Rogalski, MM. ; Anker, JN. Advances in functional X-ray imaging techniques and contrast agents. *Physical Chemistry Chemical Physics* **2012**, 14, 13469–13486

[99]: Nagata, T. ; Makutani, S. ; Uchida, H. ; Kichikawa, K. ; Maeda, M. ; Yoshioka, T. ; Anai, H. ; Sakaqushi, H. ; Yoshimura, H. Follow-up Results of 71 Patients Undergoing Metallic Stent Placement for the Treatment of a Malignant Obstruction of the Superior Vena Cava. T. *Cardiovascular and Interventional Radiology* **2007**, 30, 959–967

[100]: Viano, AM. ; Gronemeyer, SA. ; Halilolglu, M.; Hoffer, FA. Improved MR imaging for patients with metallic implants. A.M. *Magnetic Resonance Imaging* **2000,** 18, 287–295

[101]: Stradiotti, P.; Curti, A.; Castellazzi, G.; Zerbi, A. Metal-related artifacts in instrumented spine. Techniques for reducing artifacts in CT and MRI: state of the art. *European Spine Journal* **2009**, 18 (Suppl 1), S102–S108

[102]: Lee, MJ. ; Kim, S.; Lee, SA. ; Song, HT; Huh, YM. ; Kim, DH. ; Han, SH. ; Suh, JS. Overcoming Artifacts from Metallic Orthopedic Implants at HighField-Strength MR Imaging and Multidetector CT. *RadioGraphics* **2007,** 27, 791–803

[103]: Buecker, A.; Spuentrup, E.; Ruebben, A.; Gunther, RW. Artifact-Free In-Stent Lumen Visualization by Standard Magnetic Resonance Angiography Using a New Metallic Magnetic Resonance Imaging Stent. *Circulation* **2002**, 105, 1772-1775.

[104]: Predoi, D.; Vatasescu-BBalcan, RA. ; Pasuk, I.; Costache, M. Calcium phosphate ceramics for biomedical applications. *Journal of Optoelectronics and Advanced Materials* **2008,** 10, 2151 – 2155

[105]: Caroll, Q. Patient Status and Contrast agent. *Practical Radiographic Imaging*, Springfield, Illinois **2007,** 148

[106]: Riedel, R.; Chen, IW. *Ceramics Science and Technology, Synthesis and Processing*. *John Wiley & Sons*. **2011**, 370

[107]: Ventura, M. ; Sun, Y. ; Rusu, V. ; Laverman, P. ; Borm, P. ; Heerschap, A. ; Oosterwijk,E. ; Boerman, OC. ; Jansen, JA. ; Walboomers, XF. Dual Contrast Agent for Computed Tomography and Magnetic Resonance Hard Tissue Imaging.*Tissue Engineering*: *Part C* 2013, 19, 405-416

[108]: Duttenhoefer, F.; Mertens, ME. ; Vizkeletey, J.; Gremse, F. ; Stadelmann, VA. ; Sauerbier, S. Magnetic resonance imaging in zirconia-based dental implantology. *Clinical Oral Implants Research* **2015**, 26, 195-1202

[109] : Lewis G. Properties of acrylic bone cement: state of the art review. *Journal of Biomedical Materials Reseach* **1997**, 38, 155–182.

[110]: Aldenhoff, Y. ; Kruft, M. ; Pijipers, A. ; van der Veen, F. ; Bulstra, S. ; Kuijer, R. ; Koole, L. Stability of radiopaque iodine-containing biomaterials. *Biomaterials* **2002**, 23, 881–886.

[111]: Nottelet, B.; Coudane, J. ; Vert, M. Synthesis of an X-ray opaque biodegradable copolyester by chemical modification of poly (e-caprolactone). *Biomaterials* **2006,** 27, 4948–4954

[112]: Kraemer, NA. ; Otto, J. ; Hodenius, M. ; Slabu, I. ; Baumann, M. ; Klinge, U. ; Muellen, A. ; Obolenski, B. ; Guenther, RW. ; Krombach, GA. Development and Positive Contrast Imaging of an MR-Visible Mesh-Implant for repair of abdominal hernia. *Proceedings of the International Society of Magnetic Resonance Medicine* **2009**, 17, 663

[113]: Kuehnert, N.; Kraemer, NA. ; Otto, J.; Donker, HC. ; Slabu, I. ; Baumann, M. ; Kuhl, CK. ; Klinge, U. In vivo MRI visualization of mesh shrinkage using surgical implants loaded with superparamagnetic iron oxides. *Surgical Endoscopy* **2012,** 26, 1468–1475

[114]: Racik, S.; LeBlanc, KA. The Radiologic Appearance of Prosthetic Materials Used in Hernia Repair and a Recommended Classification. *American Journal of Roentgenology* **2013,** 201, 1180-1183

[115]: Kirchhoff, S.; Ladurner, R.; Kirchoff, C.; Mussack, T.; Reiser, MF. ; Lienemann, A. Detection of recurrent hernia and intraabdominal adhesions following incisional hernia repair: a functional cine MRI-study. *Abdominal Imaging* **2010**, 35, 224–231

[116]: Fischer, T.; Ladurner, R.; Gangkofer, A.; Mussack, T.; Reiser, M.; Lienemann, A. Functional cine MRI of the abdomen for the assessment of implanted synthetic mesh in patients after incisional hernia repair: initial results. *European Radiology* **2007**, 17, 3123–3129

[117]: Brown, CN. ; Finch, JG. Which mesh for hernia repair? *Annals of the Royal College of Surgeons of England* **2010,** 92:272-278

[118]: Kraemer, NA. ; Donker, HC. ; Otto, J. ; Hodenius, M. ; Senegas, J. ; Slabu, I. ; Klinge, U. ; Baumann, M. ; Mullen, A. ; Obolenski, B. ; Gunther, RW. ; Krombach, GA. A Concept for Magnetic Resonance Visualization of Surgical Textile Implants. *Investigative Radiology* 2010**,** 45, 477-483

[119]: Guillaume, O. ; Blanquer, S. ; Letouzey, V. ; Cornille, A. ; Huberlant, S. ; Lemaire, L. ; Franconi, F. ; de Tayrac, R. ; Coudane, J. ; Garric, X. Permanent Polymer Coating for in vivo MRI Visualization of Tissue Reinforcement Prostheses. O. Guillaume et al. *Macromolecular Bioscience* **2012**, 12, 1364–1374

[120]: El-Habnouni, S. ; Nottelet, B. ; Darcos, V. ; Porsio, B. ; Lemaire, L. ; Franconi, F. ; Garric, X. ; Coudane, J. MRI-Visible Poly(ε-caprolactone) with Controlled Contrast Agent Ratios for Enhanced Visualization in Temporary Imaging Applications. *Biomacromolecules* **2013**, 14, 3626−3634

[121]: Porsio, B. ; Lemaire, L. ; El Habnouni, S. ; Darcos, V. ; Franconi, F. ; Garric, X. ; Coudane, J. ; Nottelet, B. MRI-visible nanoparticles from hydrophobic gadolinium poly(ε-caprolactone) conjugates. *Polymer* **2015,** 56, 135-140

[122]: Kolb, HC. ; Finn, MG.; Sharplees, KB. Click Chemistry: Diverse Chemical Function from a Few Good Reactions *Angewandte Chemie International Edition* **2001**, 40, 2004-2021

[123]: Huisgen, R. 1,3-dipolar cycloadditions. Past and Future. *Angewandte Chemie International Edition* **1963**, 2, 565-598

[124]: Meldel, M.; Tornoe, CW. Cu catalyzed azide-alkyne cycloadditin. *Chemical Reviews* **2008**, 108, 2952-3015

[125]: Fuaad, AA. ; Azmi, F.; Skwarczynski, M.; Toth, I. Peptide Conjugation via CuAAC 'Click' Chemistry. *Molecules* **2013**, 18, 13148-13174

[126]: Baia, P.; Andre, JP. ; Geraldes, C.; Martins, JA. ; Merbach, AE. ; Toth, E. Lanthanide (III) Chelates of DTPA Bis(amide) Glycoconjugates: Potential Imaging Agents Targeted at the Asyaloglycoprotein Receptor. *European Journal of Inorganic Chemistry* **2005**, 2110–2119

[127]: Cheng, TH. ; Lin, KT. ; Ou, MH. ; Shih, HL. ; Liu, G. ; Wang, Y. Water-exchange and Relaxometric Studies of Gd(III) Complexes with DTPA-bis(amide) Ligands. *Journal of the Chinese Chemical Society*, **2001**, 48, 1099-1105

[128]: Botteman, F. ; Nicolle, GM. ; Elst, LV. ; Laurent, S. ; Merbach, A.E. ; Muller, RN. Synthesis, Variable Temperature and Pressure ^{17}O NMR Study of Bis(alkylamide) Derivatives of $[(Gd\text{-}DTPA)(H2O)]^{2-}$An Assessment of the Substitution Effect on Water Exchange Kinetics. *European Journal of Inorganic Chemistry* **2002**, 2686-2693

[129]: Parac-Vogt, TN.; Kimpe, K. ; Laurent, S. ; Pierart, C. ; Elst, LV. ; Muller, RN. ; Binnemans, K. Gadolinium DTPA-Monoamide Complexes Incorporated into Mixed Micelles as Possible MRI Contrast Agents. *European Journal of Inorganic Chemistry* **2004**, 3538-3543

[130]: Ardestani, M.S.; Arabzadeh, AJ. ; Heidari, Z. ; Hosseinzadeh, A. ; Ebrahimi, H. ; Hashemi, E. ; Mosaybenia, M. ; Shafee-Alavidgeh, M. ; Alavi, A. ; Babaei, MS. ; Rahmim, A. ; Ebrahimi, SES, Amanlou, M. Novel and facile methods for the synthesis of DTPA-mono-amide: a new completely revised strategy in radiopharmaceutical chemistry. *Journal of Radioanalytical and Nuclear Chemistry* **2010**, 283, 447–455

[131]: Sauer, M.; Hofkens, J.; Enderlein, J. Handbook of fluorescence spectroscopy and Imaging. *WILEY-VCH Weinheim*, **2011**

[132]: Butts, CA.; Xi, J. ; Barringan, G. ; Saad, AA. ; Venkatachalan, SP.; Pearce, RA. ; Klein, ML.; Eckenhoff, RG. ; Dmochowski, IJ. Identification of a fluorescent general anesthatic, 1-amino anthacene. *Proceedings of the National Academy of Sciences* **2009**, 106, 6501-6506

[133]: Le Droumaguet, C.; Wang, C. ; Wang, Q. Fluorogenic click reaction. *Chemical Society Reviews* 2010, 39, 1233-1239

[134]: Kolmakov, K. ; Belov, VN. ; Bierwagen, J. ; Ringemann, C. ; Muller, V. ; Eggeling, C. ; Hell, SW. Red-emitting Rhodamine dyes for fluorescence microscopy and nanoscopy. *Chemistry* **2010**, 16, 158 – 166

[135]: Rath, NC.; Huff, GR.; Balog, JM.; Huff, WE. Fluorescein isothiocyanate staining and characterization of avian heterophils. Vetrinary Immunology and Immunopathology **1998**, 64, 83-95

[136]: Evangelista, RA.; Pollak, A.; Allore, B.; Tepleton, EF.; Morton, RC.; Diamandis, EP. A new europium chelate for protein labelling and time-resolved fluorometric applications. R. Clinical Biochemistry **1988**, 21, 173-178

CHAPTER 2
SYNTHESIS of MRI VISIBLE PMMA

This chapter details all chemical strategies used throughout the thesis in order to obtain poly(methyl methacrylate) (PMMA) based contrast agent in order to render a polypropylene (PP) mesh visible by MRI. Thus the ultimate aim is to synthesize a polymeric contrast agent able to induce a sufficient hyper signal in MRI to visualize the mesh. For this the contrast agent will be grafted through a triazole moiety on a PMMA backbone to obtain a stable polymeric contrast agent for long-term visualization by MRI of a polypropylene mesh.

As a first step, two types of azido functionalized diethylene triamine pentaacetic acid (DTPA) ligands will be synthesized (one with an amide group and the second with an ester group). The synthesized ligands will then be complexed with gadolinium (Gd^{3+}). PMMA bearing pendant propragyl units will be also prepared via free radical polymerization and microwave assisted polymerization. Taking advantage from the alkyne group of the polymer and the azide group of the Gd-DTPA complex, copper (I)-catalyzed azide alkyne cycloaddition (CuAAC) will be employed to obtain PMMA MRI contrast agent.

Due to the higher stability of the amide bond, azido functionalized monoamide DTPA ligand clicked on PMMA will be tested for its suitability to render a polypropylene mesh visible by MRI. For this, a commercial polypropylene mesh will be coated with this contrast agent and assessed for MRI visualization at 7T field strength. The contrast agent will be also tested for cytocompatibility and stability in order to study the feasibility of its application in the biomedical field. The effect of the amount of Gd^{3+} present in the polymeric contrast agent on the visibility of the mesh will be monitored. Also, the link between the increase of the amount of grafted Gd^{3+} on the stability and cytocompatibility of the contrast agent will be followed. Scheme 2 shows the synthesis of MRI visible PMMA from azido-functionalized monoamide DTPA ligand.

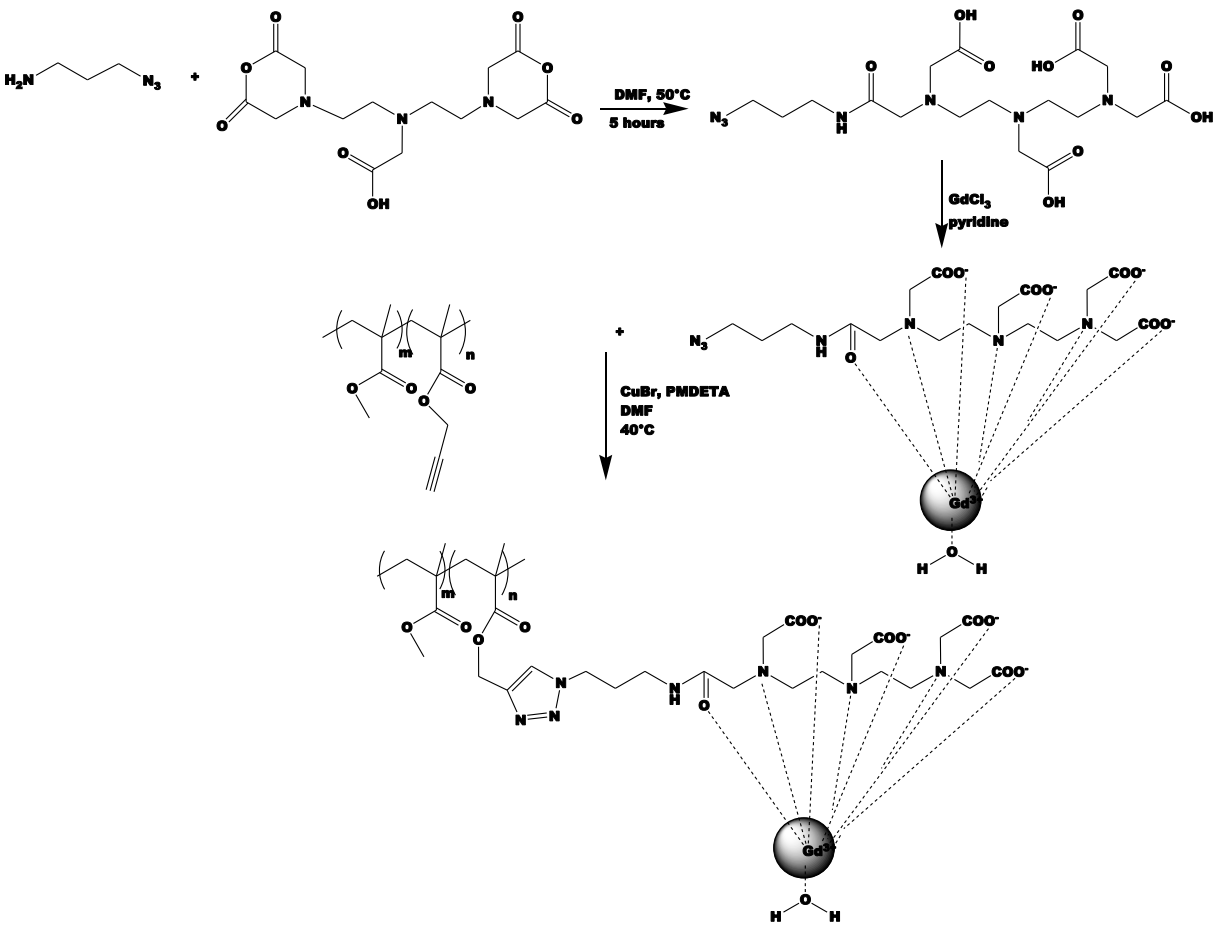

Scheme 2: *Synthesis of MRI-visible PMMA*

2.1 Synthesis of azido functionalized DTPA ligands

The synthesis of azido functionalized ligands is done through the reaction between DTPA bis-anhydride and an organic azide. Depending on whether the azide contains an amine or an alcohol, an azido functionalized amide based or ester based DTPA ligand will be obtained respectively. Most azides are explosive substances, which under the slightest input of external energy (heat, pressure) decompose and release nitrogen. For example, heavy metal azides are used in the explosives technology [1].

There are various ways to synthesize organic azides. In our case, the synthesis of organic azido molecules (3-azido propanol and 3-azido propylamine) is done by nucleophilic substitution reaction between sodium azide and a halogenated precursor (3-chloro propanol or

3-chloropropylamine). The following rule should be applied [2] to obtain non-explosive organic azides, N_C, N_O and N_N standing for the numbers of Carbon, oxygen and nitrogen atoms in the molecule:

$$(N_C+N_O)/N_N \geq 3$$

By looking at the structure of 3-azido propanol (Fig. 24) and 3-azido propylamine (Fig. 25), both azides are potentially explosive and extreme care must be taken during their synthesis and use.

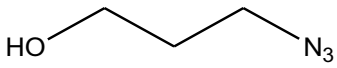

Figure 24: *Structure of 3-azido propanol*

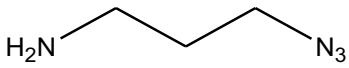

Figure 25: *Structure of 3-azido propylamine*

2.1.1 Synthesis of azido functionalized monoester DTPA ligand

Macromolecular contrast agents containing ester groups can be found in literature. One example is GdDTPA cysteine diethyl ester copolymer (GdCEP) which is a biodegradable polydisulfide Gd(III) complex. The synthesis of this agent is done through copolymerization of DTPA bisanhydride with diethyl ester followed by complexation with $GdCl_3$ to obtain GdCEP in a yield of 11%. This contrast agent resulted in strong contrast enhancement in tumor cells [3].

Quay *et al.* describe in their US patent the modification of DTPA bis-anhydride through the reaction of DTPA bis-anhydride with alcohol [4] to obtain ester groups. The synthesis of Gd-DTPA bis(benzyl ester) and Gd-DTPA bis(methyl ester) is reported in literature by the

reaction of the appropriate alcohol and DTPA bis anhydride [5,6]. The general structure of DTPA bis-ester is represented in Fig. 26.

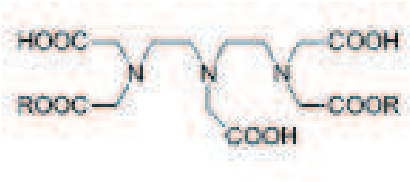

Figure 26: *General structure of DTPA bis-ester*

The formation of DTPA ligands containing several ester groups can be found in literature. However, no mono-ester Gd-DTPA ligand is described. Our aim is not only to synthesize a mono-ester DTPA ligand, but also an azido functionalized one. The formation of this group is done through the reaction between the anhydride group of DTPA bis-anhydride and the alcohol group of 3-azido propanol. Since only one ester group is desired, the 3-azido propanol should be used either in equimolar or less than equimolar quantaties as that of DTPA bis-anhydride.

As a first step, 3-azido propanol (1) was synthesized by the reaction of 3-chloropropanol with sodium azide (Fig. 27).

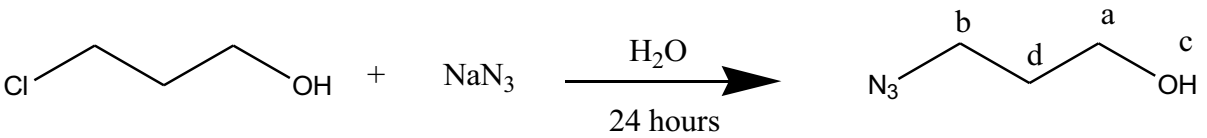

Figure 27: *Synthesis of 3-azido propanol*

^{1}H NMR in $CDCl_3$ (Fig. 28) revealed the purity of compound 1.

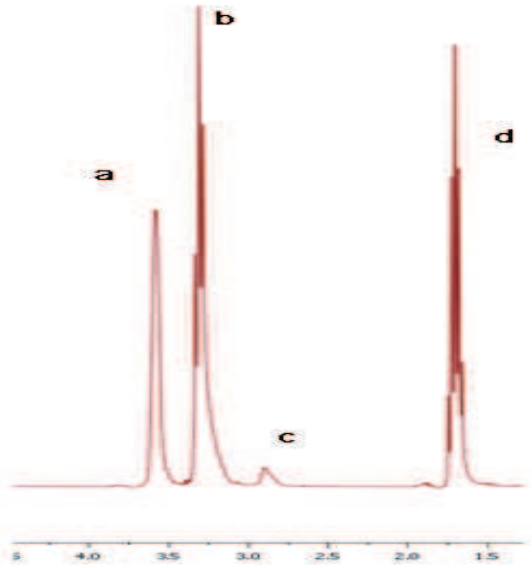

Figure 28: *^{1}H NMR of 3-azido propanol*

The esterification reaction between equimolar ratios of DTPA bis-anhydride and (1) in DMF yielded a mixture of azido functionalized mono-ester DTPA ligands (2) and azido functionalized bis-ester DTPA ligand (3) (Scheme 3).

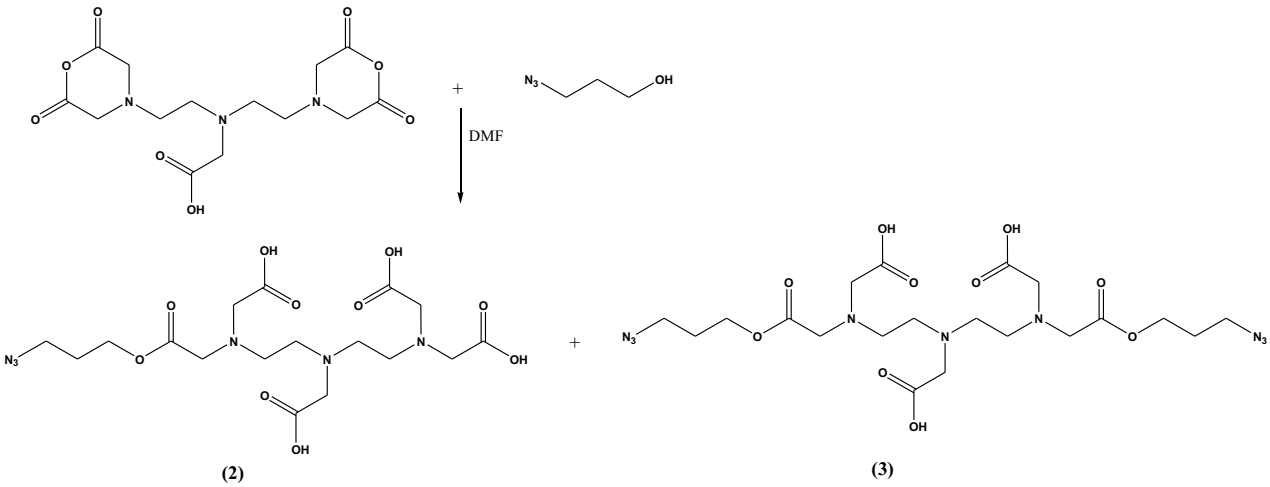

Scheme 3: *Synthesis of ester based DTPA ligands*

Therefore, a preparative HPLC step was needed to separate the two compounds. The purification step yielded 750mg of compound (2) starting from 2g of the mixture of (2) and (3). Hence, azido functionalized mono-ester DTPA ligand was obtained with a yield of 38%.

The ^{1}H NMR spectrum of compound 2 in D_2O is shown in Fig. 29.

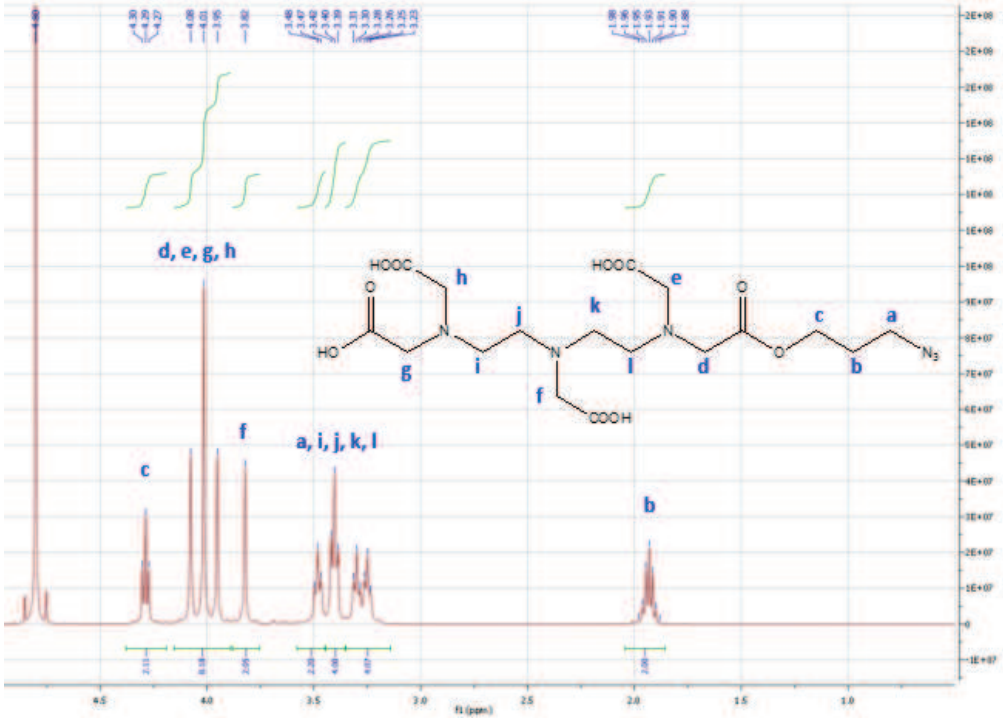

Figure 29: *^{1}H NMR of azido functionalized mono-ester DTPA*

The purity of the compound was further assessed by $^{1}H,^{1}H$ COSY NMR (Fig .30).

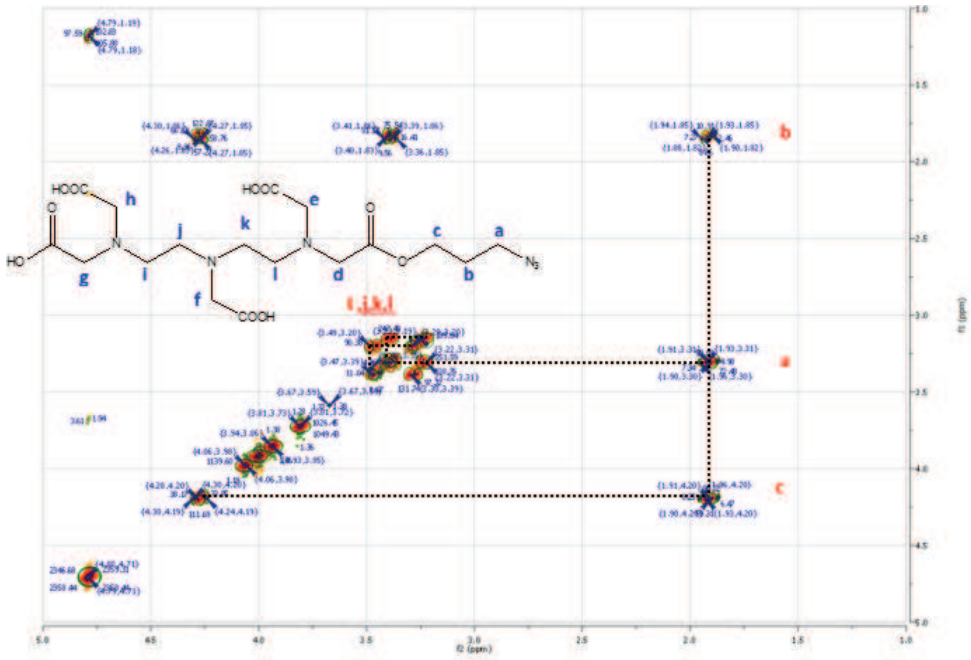

Figure 30: *$^{1}H,^{1}H$ COSY NMR of azido functionalized mono-ester DTPA*

LC-MS analysis of the compound was also performed. The theoretical molar mass of compound (2) is 476.44 g/mol while that of compound (3) is 559.24 g/mol. LC-MS spectrum (Fig. 31) of the pure product (2) obtained after HPLC revealed a single peak at 477.2 g/mol corresponding to $[M+H]^{+}$ experimental as compared to 477.44 theoretical.

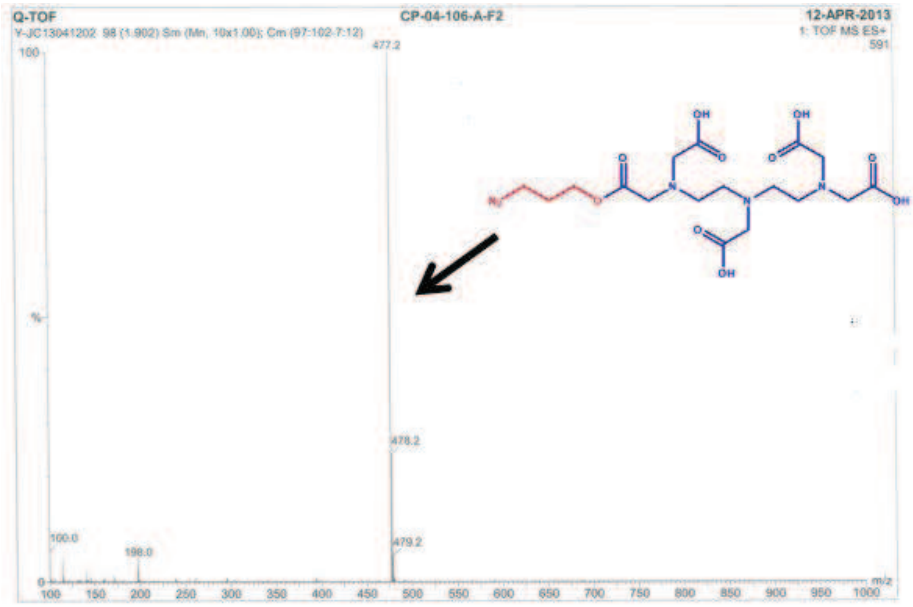

Figure 31: *LC-MS of azido functionalized mono-ester DTPA*

2.1.2 Synthesis of azido functionalized monoamide DTPA ligand

Many publications are describing the synthesis of DTPA ligands containing an amide moiety. The synthesis of bis-amide DTPA ligands is relatively easy and only requires the use of an excess amine as compared to that of DTPA bis-anhydride, without the need for tedious purification steps. Several publications describe the synthesis of bis-amide DTPA ligands, in which the synthesis is ensured only by the use of an excess of amine [7, 8]. The synthesis of alkyne functionalized DTPA bis-amide in a quantitative yield is also reported [9]. Moreover, azido functionalized bis(amide) DTPA ligands have also been synthesized [10]. Both of these ligands have been grafted on macromolecular architectures via CuAAC.

Concerning the synthesis of mono-amide DTPA ligands, only few publications are available. The main reason resides in the fact that these compounds are obtained in low yields with multi-step reactions. For example, a mono-maleimide of DTPA has been synthesized via multi-step reactions with a final low yield [11]. The reaction of DTPA bis-anhydride with equimolar or less proportion of amine results in the formation of a mixture of DTPA mono-amide and DTPA bis-amide [12, 13, 14]. Yet, despite the challenging synthesis, the formation of mono-amide DTPA ligands is interesting. The chelating power of DTPA in DTPA mono-amide is higher than in the corresponding bis-amide [12]. Another study revealed that micelles containing gadolinium mono-amide DTPA complexes showed higher relaxivity than micelles with bis-amide DTPA complexes, due to a more efficient exchange of coordinated water molecule [15]. In addition, the dissociation rate of linear bis-amide Gd-DTPA chelates is higher than the one of other chelates due to insufficient thermodynamic and kinetic stabilities [16].The aim was to find a simple and versatile method for the synthesis of an azido functionalized mono-amide DTPA ligand under mild reaction conditions. As a first step, 3-azido propylamine (4) was synthesized by the reaction between 3-chloropropylamine and NaN_3 (figure 32).

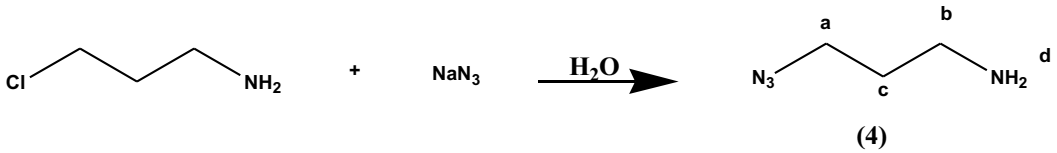

(4)

Figure 32: *Synthesis of 3-azido propylamine*

After distillation, a pure compound (4) was obtained and ^{1}H NMR spectrum (Fig. 33) in $CDCl_3$ is represented.

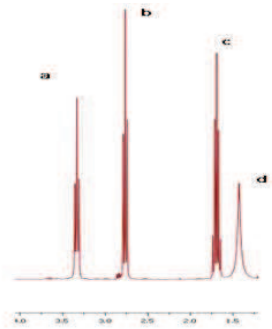

Figure 33: *^{1}H NMR of 3-azido propylamine*

The reaction of DTPA bis-anhydride with 3-azido propylamine yielded a mixture of azido functionalized mono-amide DTPA ligand (5) and bis-amide DTPA ligand (6) (Scheme 4).

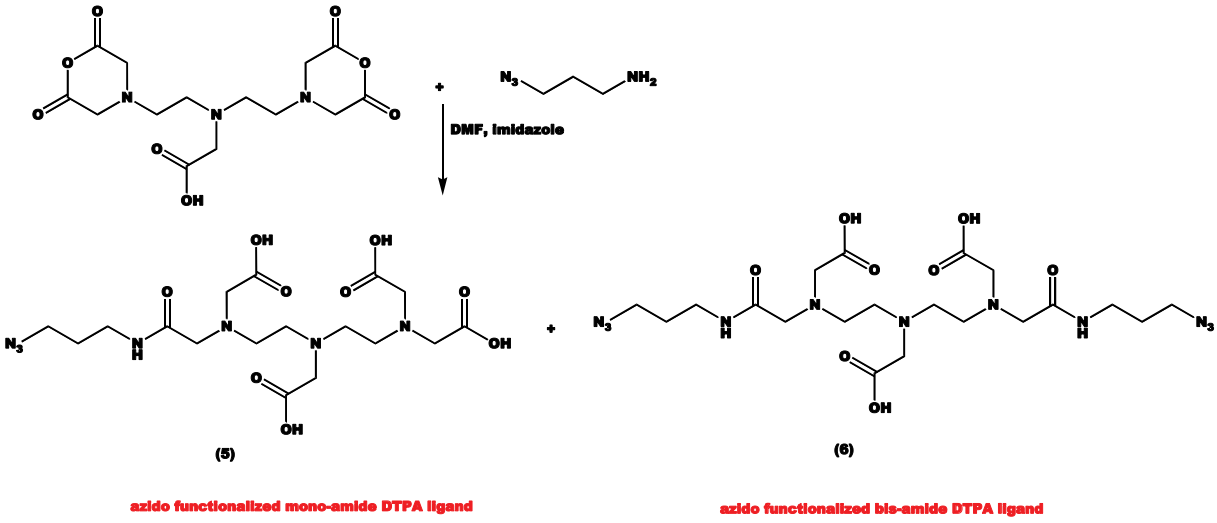

Scheme 4: *Synthesis of amide based DTPA ligands*

Several experimental conditions were tested in order to obtain compound (5). The reaction between DTPA bis-anhydride and 3-azidopropylamine always yielded a mixture of compounds (5) and (6), with compound (5) always in very low yields. The reaction of 1 equivalent of DTPA bis-anhydride with 0.5 equivalent of 3-azido propylamine in DMF followed by hydrolysis, yielded a mixture of compounds (5) and (6). By HPLC, compound (5) was achieved with only a 7 % yield. To obtain a higher selectivity towards the formation of compound (5), according to a modified protocol [17], equimolar amounts of DTPA bis-anhydride and 3-azidopropylamine were used. However, in this case a solubilizer, imidazole, was used. Imidazole is used for its good promotion ability to homogenize the reaction mixture in dry media, due to the low melting point of imidazolium salt [18]. By preparative HPLC separation, pure compound (5) was achieved as a white solid with a 30% yield.

^{1}H NMR (in D_2O) (Fig. 34) and ^{1}H,^{1}H COSY NMR (Fig. 35) of pure compound (5) are presented hereby.

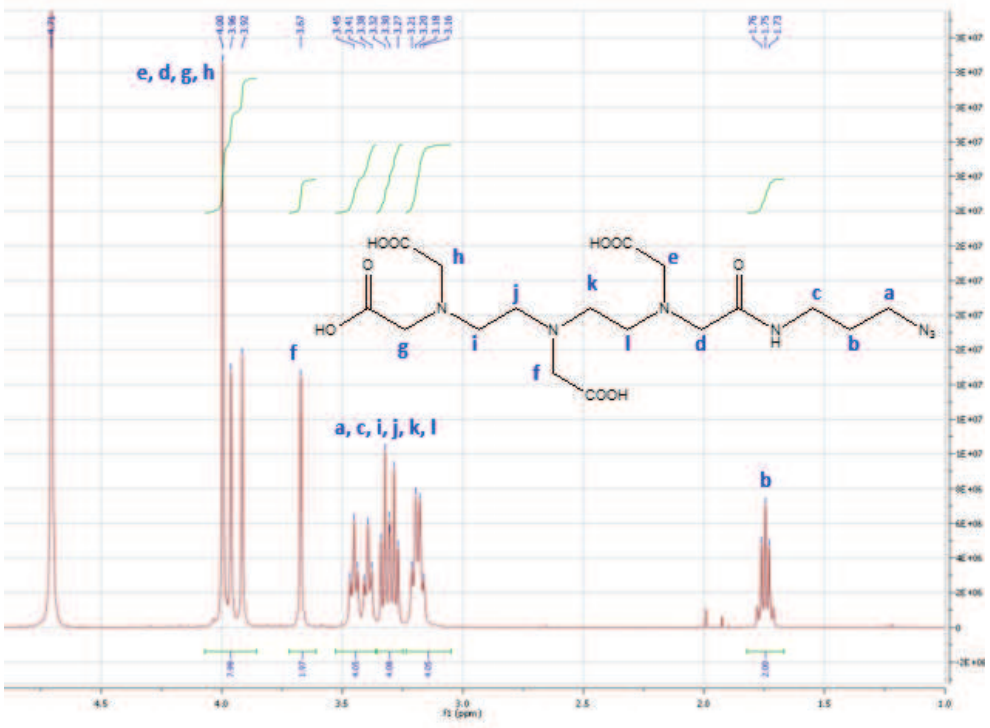

Figure 34: *^{1}H NMR of azido functionalized mono-amide DTPA*

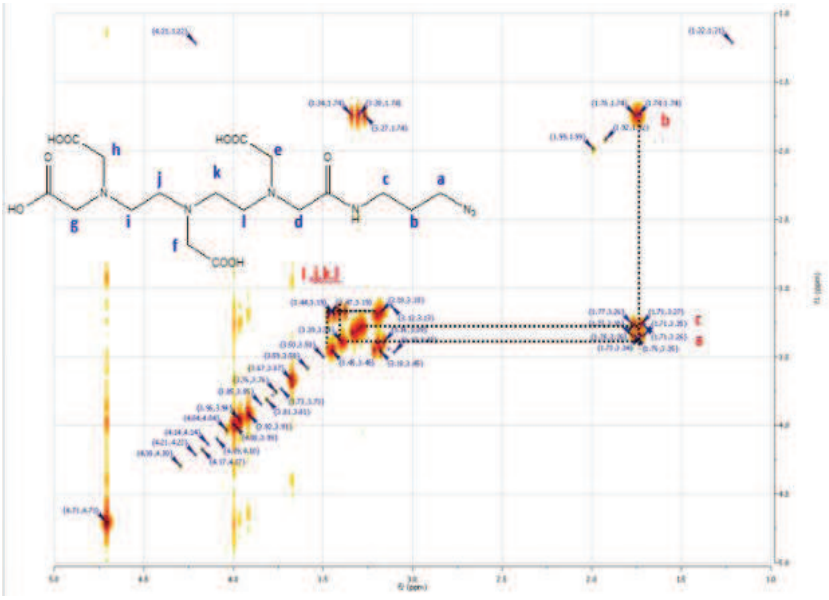

Figure 35: *$^{1}H,^{1}H$ COSY NMR of azido functionalized mono-amide DTPA*

After HPLC separation, the LC-MS spectrum (Fig. 36) revealed the presence of pure compound (5) with a unique peak at 476.2 g/mol corresponding to $[M+H^{+}]^{+}$ as compared to 476.45 theoretical.

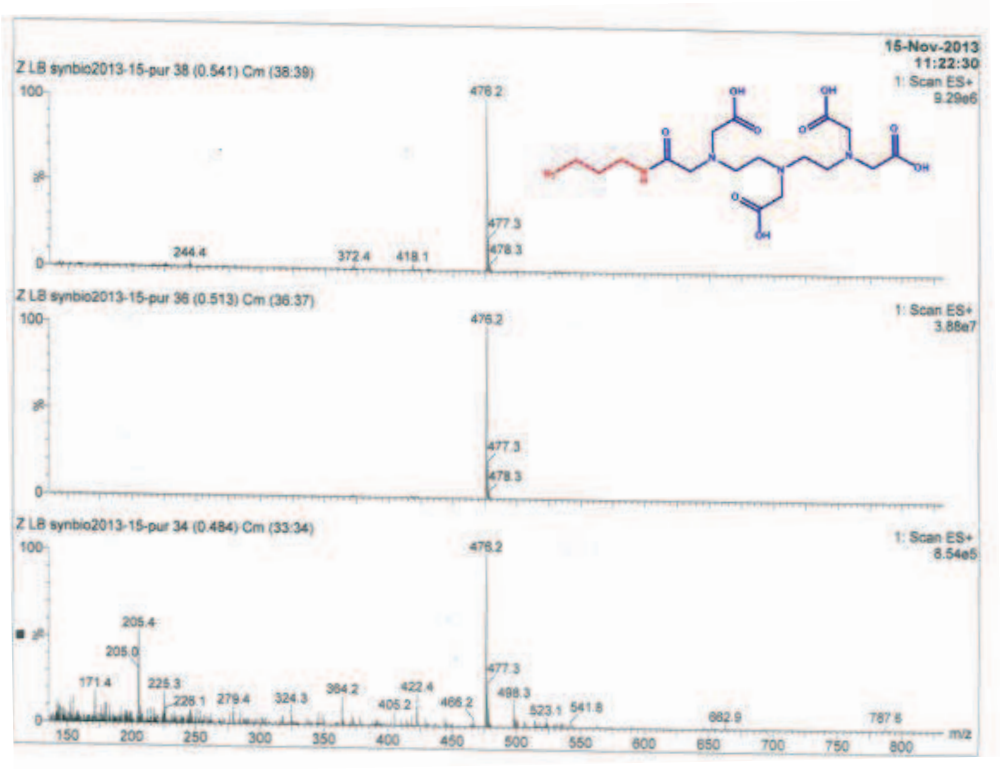

Figure 36: *LC-MS of azido functionalized mono-amide DTPA*

2.2 Synthesis of gadolinium complexes

In order to obtain the gadolinium complexes, compounds (2) and (5) were reacted with $GdCl_3$ in pyridine to obtain azido functionalized monoester Gd-DTPA (7) and azido functionalized mono-amide Gd-DTPA respectively (8) as represented in Scheme 5 and 6 respectively.

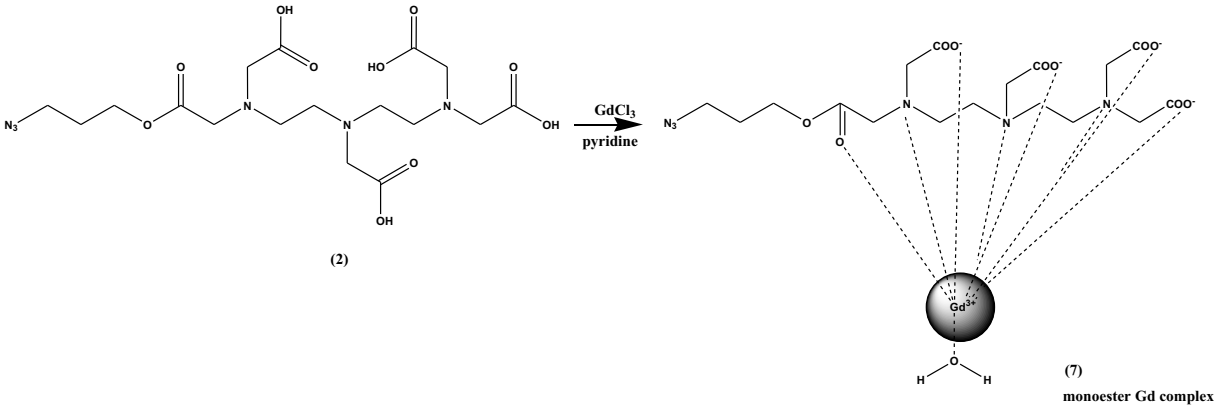

Scheme 5: *Synthesis of azido functionalized mono-ester Gd-DTPA*

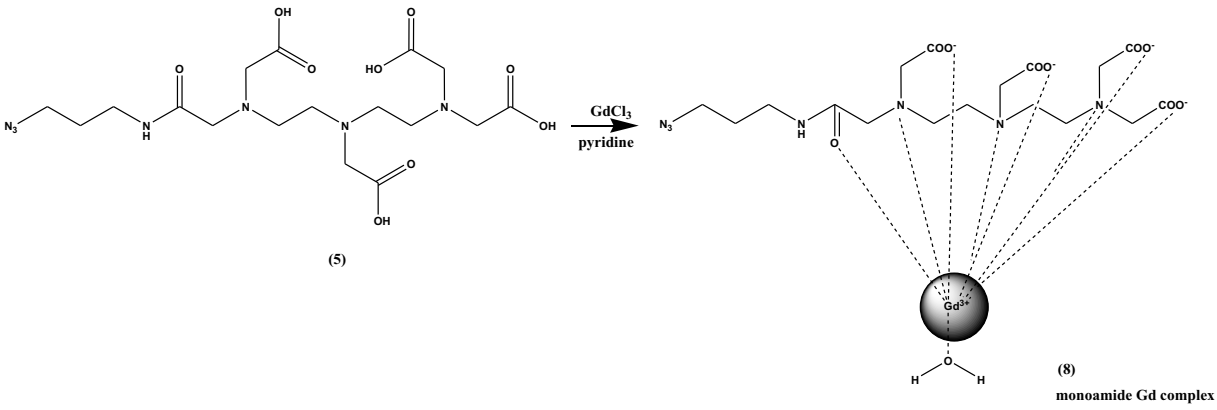

Scheme 6: *Synthesis of azido functionalized mono-amide Gd-DTPA*

Due to the toxicity of free Gd^{3+}, extreme care must be taken to ensure the complete incoroporation of Gd^{3+} in compounds (7) and (8). To ensure the absence of free uncomplexed Gd^{3+}, a methyl thymol blue (MTB) test was performed [19].

2.2.1 MTB test

MTB is a colored indicator used to measure the amount of metal salts. In our case MTB acts as an indicator for the presence of Gd^{3+} according to the following reaction [20]:

$$\text{MTB (yellow)} + Gd^{3+} \longrightarrow \text{MTB-Gd complex (blue)}$$

Free MTB exhibits a maximum absorbance wavelength λ_{max}=425 nm. In the presence of free Gd^{3+}, MTB complexes exhibit λ_{max}=605 nm (Fig. 337) [20]. These wavelengths can be used to monitor the presence of free Gd^{3+}.

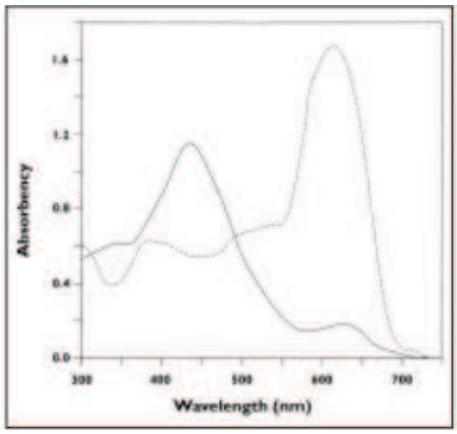

Figure 37: *Absorbance spectra of MTB and MTB-Gd complex [20]*

This enables the quantification of free Gd^{3+} using UV/visible spectroscopy. By preparing different samples containing various amounts of Gd^{3+} in MTB, a calibration curve representing the absorbance as a function of the amount of Gd^{3+} can be drawn. $GdCl_3$ standards in the range of 0-50µM were prepared to obtain the calibration curve of figure 38.

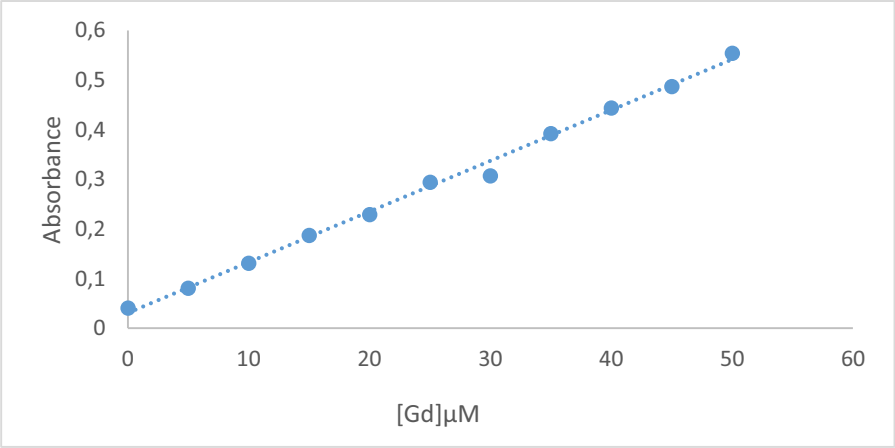

Figure 38: *Variation of absorbance as a function of [Gd^{3+}]*

Hence, by measuring the absorbance of an unknown sample, the amount of Gd^{3+} can be calculated and hence quantified.

A negative test (absence of blue color) ensures the complete complexation of Gd^{3+}, and thus the absence of free Gd^{3+} [19]. It is important to note that ICP-MS analysis is very sensitive and also allows the quantification of the amount of Gd^{3+}. However, it does not give any information concerning the form of Gd^{3+} (free or complexed). Therefore, only after obtaining a negative MTB test and ensuring that all Gd^{3+} is complexed, the amount of complexed Gd^{3+} was measured by ICP-MS.

After complexation, compounds (7) and (8) were subjected to MTB test to ensure the absence of free Gd^{3+}. Sometimes, after the reaction, MTB test revealed a blue color, indicating the presence of free Gd^{3+}. Complexes had to be further treated to get rid of free Gd^{3+}. This was done using a Chelex-100 resin. Chelex-100 is a resin containing paired imin-iodoacetate ions. These ions act as chelators for polyvalent metal ions. Chelex-100 is known for its high selectivity to metal ions and its strong binding affinity. Thus, compounds (7) and (8) were stirred in Chelex-100, until MTB test gave a negative result (yellow color) indicating the absence of free Gd^{3+}. At this point, ICP-MS analysis was performed to determine the amount

of Gd^{3+} incorporated in each of compounds (7) and (8). This also allowed the calculation of the complexation reaction's efficiency.

2.2.2 Complexation Efficiency

Each of compounds (7) and (8) was treated with nitric acid (HNO_3) and then analyzed by ICP-MS as to calculate the amount of Gd^{3+} incorporated in the complex.

Compound (7) has the general molecular formula $C_{17}H_{26}O_{11}N_6Gd$ which has a total molar mass of 647.672 g/moL and the molar mass of Gd is 157.25 g/mol. Thus:

$$\%Gd = \frac{molar\ mass\ of\ Gd}{total\ molar\ mass} x100 \qquad \text{(Equation 3)}$$

By applying the equation 3, compound (7) should theoretically contain 24.2% Gd^{3+} (w/w). ICP-MS analysis of compound (7) revealed the presence of 109.73 µg Gd^{3+} per milligram of compound (7) →100mg of compound (7) contain 10.97mg of Gd^{3+}. Hence, compound (7) turned out to contain 11% by mass Gd^{3+} experimentally.

This allowed the calculation of the reaction efficiency:

$$reaction\ efficiency = \frac{\%Gd\ theo}{\%Gd\ exp} x100 \quad \text{(Equation 4)}$$

By applying equation 4, the complexation reaction efficiency for compound (7) is 45%. Similarly, compound (8) has the general molecular formula $N_7C_{17}H_{27}O_{10}Gd$ and a total molar mass of 646.687 g, which means that it contains theoretically 24.3% by mass Gd^{3+}. ICP-MS revealed the presence of 10% by mass Gd^{3+} in compound (8) and hence the complexation efficiency turned out to be 42%.

Further experiments have been performed to improve the complexation efficiency. Unfortunately, the amount of Gd^{3+} complex did not increase. High temperature and long reaction times are needed to increase the complexation efficiency. This could not be applied in this case due to the thermo-labile azide group. Moreover, it is well-known that commercial DTPA CAs, like Magnevist®, contains non-complexed ligands. Finally, it is interesting to have an excess of ligand to reduce the probability of uncomplexed toxic free gadolinium.

At the same time, MALDI-TOF analysis was performed for compounds (7) and (8).

2.2.3 MALDI-TOF Analysis

MALDI-TOF analysis with dithranol as matrix was performed on compounds (7) and (8).

MALDI-TOF analysis of compound (7) (Fig. 39) revealed a peak at 685.9. Theoretically, $[M+K]^+$ for compound (7) is 686.77 g/mol. Hence, from the MALDI spectrum, the peak representing the molar mass of 685.9 can be attributed to the potassium adduct of compound (7).

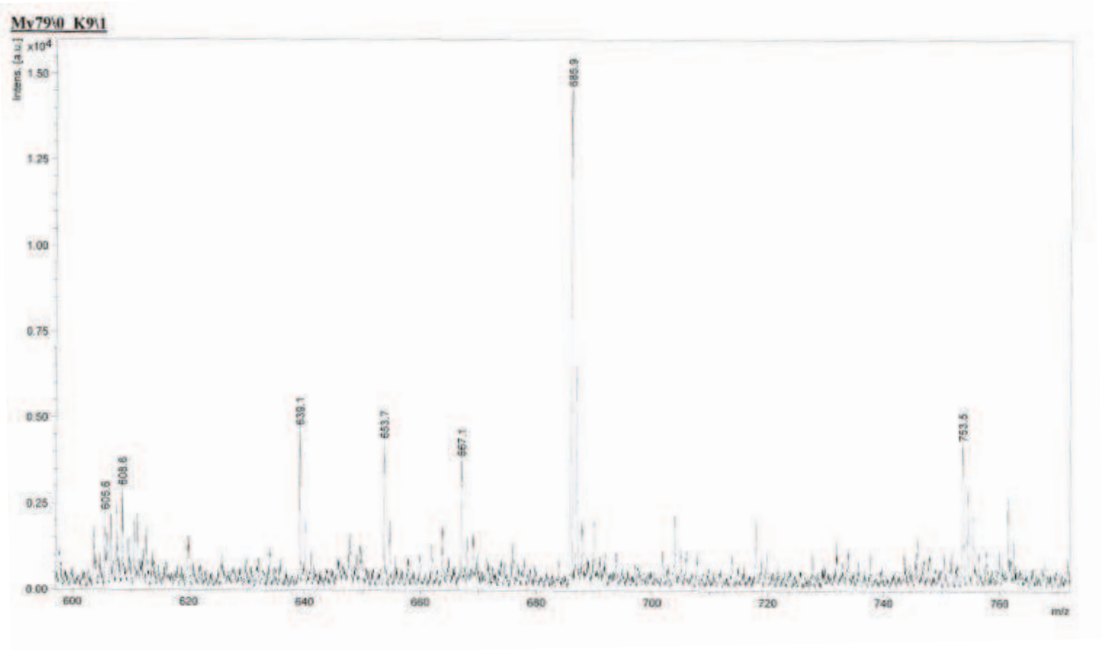

Figure 39: *MALDI-TOF spectrum of azido functionalized mono-ester Gd-DTPA*

For compound (8), $[M+K]^+$ has a molar mass of 685.78 g/mol. A peak appeared on the MALDI spectrum with a molar mass of 685.8 relevant to this adduct (Fig. 40).

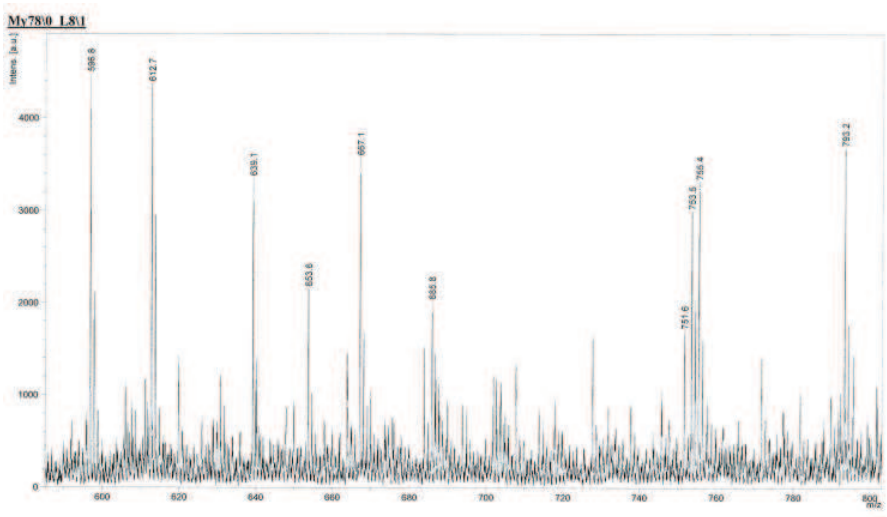

Figure 40: *MALDI-TOF spectrum of azido functionalized mono-amide Gd-DTPA*

Finally, two complexes (7) and (8) bearing an azide group without free Gd^{3+} were prepared.

2.3 Synthesis of poly(methyl methacrylate-*co*-propargyl methacrylate)

PMMA is the polymeric chain of choice which was propargylated and on which the azide based contrast agents (7) and (8) were then fixed by CuAAC to obtain macromolecular contrast agents for long-term MRI visualization. PMMA was chosen because it is non-toxic and has a good safety record in biomedical applications [21]. The polymer is also known for its bio-inertness [22, 23], non-biodegradibility, and good biocompatibility with human tissues [24]. In the literature, few publications are found concerning the use of PMMA in MRI contrast agent. Ratanajanchai *et al*. synthesized PMMA/PEI (polyethylene amine) nanoparticles possessing DTPA chelating high amounts of Gd^{3+}. Although these nanoparticles enhanced MRI intensity more than commercially available hepatic contrast agent, however

Gd^{3+} release occurred after 1 day of incubation, due to the partial chelation of Gd^{3+} by the amine groups of PEI [25]. Martirosyan *et al*. used PMMA with carbon nanotubes as encapsulation materials for Co-based and Gd-based contrast agents for prostate brachytherapy MRI contrast agents. These authors chose PMMA for its MRI transparency [26]. Guillaume *et al.* described the grafting of Gd-DTPA on poly(methyl acrylate). Although the obtained contrast agent rendered a PP mesh visible, yet the amount of Gd^{3+} incorporated could not be controlled [27].

In this work, PMMA containing well defined proportion of propargyl units was synthesized. This allowed a control of the amount of Gd^{3+} in the contrast agent, because the amount of Gd^{3+} incorporated in the macromolecular contrast agent (after click reaction) should be theoretically equal to the amount of propargyl unit.

In the first step, poly(methyl methacrylate-*co*-propargyl methacrylate) (PMMA-*co*-PMA) (11) with a low molar ratio of propargyl methacrylate monomer unit (F< 10 %) was prepared by free or controlled radical copolymerization of methyl methacrylate (9) with propargyl methacrylate (10) (Scheme 7).

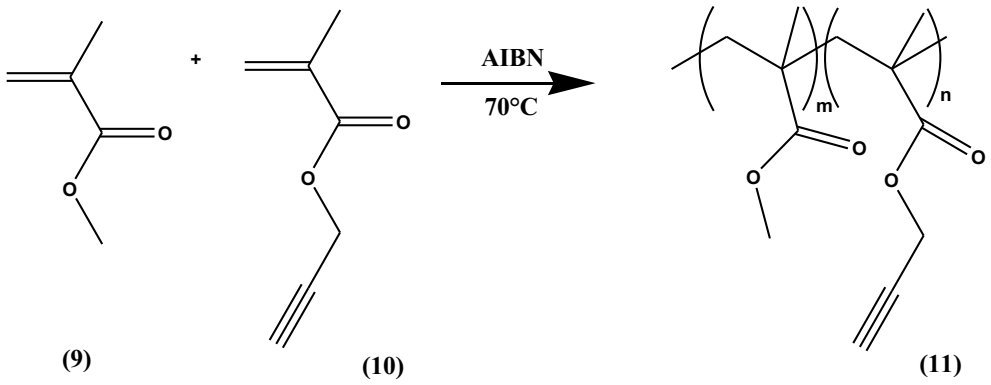

Scheme 7: *Synthesis of PMMA-co-PMA*

The resulting copolymer should contain more than 95% of methyl methacrylate units and less than 5% propargyl methacrylate monomer units. Low proportions of propargyl units were favored to avoid any cross-linking in the acetylenic group, since the propargyl methacrylate was used without any protection of the acetylenic group. The low proportion of acetylenic groups results in a dilution effect thus minimizing side reactions [28]. Schubert *et al*. describe the synthesis of homopolymers of trimethylsilyl propargyl methacrylate in addition to copolymers with MMA by controlled radical polymerization, in which trimethylsilyl propargyl methacrylate had been synthesized using TMS-propargyl alcohol. After polymerization, several steps were needed to remove the protective group [29]. In our case, propargyl methacrylate (10) was synthesized without the protection of the acetylenic group starting from propargyl alcohol and methacryloyl chloride according to the following reaction (Scheme 8).

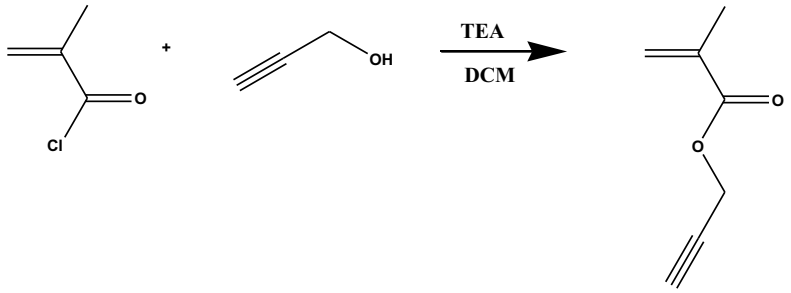

Scheme 8: *Synthesis of unprotected propargyl methacrylate*

^{1}H NMR of the propargyl methacrylate in $CDCl_3$ is presented in Fig. 41.

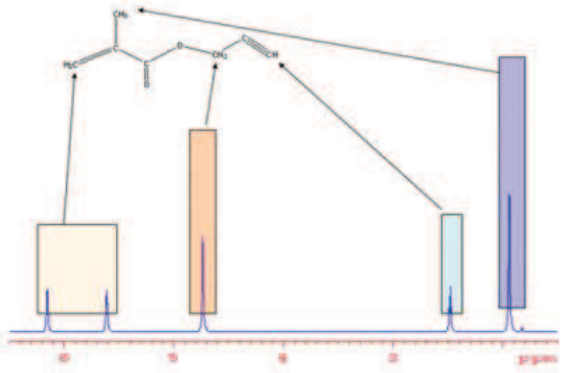

Figure 41: *^{1}H NMR spectrum of propargyl methacrylate*

PMMA-*co*-PMA copolymers with high molar masses were targeted for several reasons. High molar mass results in macromacromolecular contrast agents which have an increased retention time in the body. In addition, a desired property of the macromolecular contrast agent is to be filmogenic on the surface of the commercial polypropylene mesh. The mechanical properties of this coating material strongly depend on the molar mass of the polymer, a higher molar mass resulting in better performance [30]. Therefore, free radical polymerization using AIBN as initiator was used. Free radical polymerization of TMS protected PMA using AIBN as an initiator is reported by Scarpaci *et al* [31].

2.3.1 Synthesis of PMMA-*co*-PMA by free radical polymerization

Various experimental conditions were tried in order to obtain the desired copolymer PMMA-*co*-PMA. Using toluene as a solvent and a reaction temperature of 70°C, various amounts of AIBN and different reaction times were studied. The results are presented in Table 4.

Entry	AIBN *%wt*	Time hours	Conv[a] %	$F_{PMA,exp}$[a]	$M_{n,SEC}$[b] g.mol^{-1}	$Đ$[b]
1	0.5	2	30	1.8	45000	1.6
2	0.5	4	50	1.6	54000	2
3	1	2	40	2.3	40000	1.8
4	1	4	52	2.0	33000	2
5	2	4	74	2	24000	2.2

[a] Determined by ^{1}H NMR. [b]Determined by size exclusion chromatography in THF

Table 4: *Experimental conditions for the synthesis of PMMA-co-PMA by free radical polymerization*

Conversion Calculation:

After quenching the polymerization reaction in liquid nitrogen a few drops of the reaction mixture is tested by ^{1}H NMR for conversion. The calculation is done as follows (Equation 5):

$$\%conversion = \frac{Ipol}{Ipol+Imon} \quad \text{(Equation 5)}$$

Where Ipol is the integration peak of the methoxy peak of the polymer and Imon is the integration of methoxy peak of the monomer from ^{1}H NMR.

% Propargyl methacrylate:

Pure PMMA-*co*-PMA is obtained by precipitation in methanol and heptane. ^{1}H NMR in $CDCl_3$ of the copolymer shown in Fig. 42.

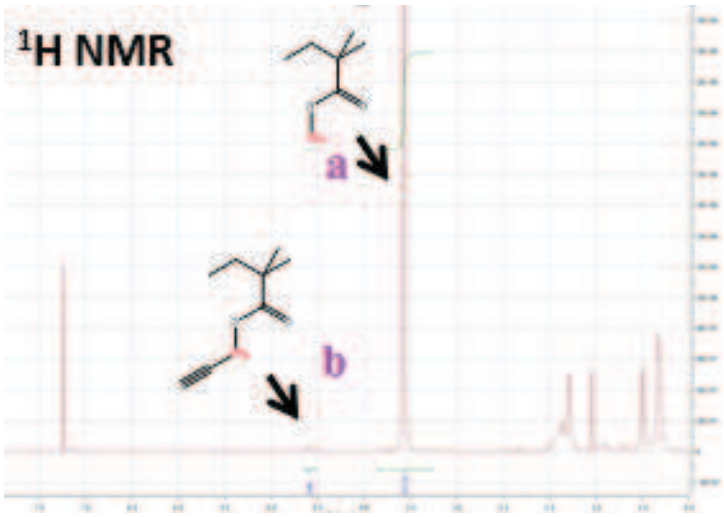

Figure 42: *^{1}H NMR spectrum of PMMA-co-PMA*

Therefore, the % propargyl methacrylate can be calculated from the NMR according to the following equation:

$$\%\ propargyl\ methacrylate = \frac{\frac{Ib}{2}}{\frac{Ib}{2}+\frac{Ia}{3}} \qquad \text{(Equation 6)}$$

Where Ib is the integration of the CH_2 peak in propargyl methacrylate and I a is the integration peak of the methoxy group in PMMA.

Increasing the amount of initiator resulted in an increase in conversion, but a drop in the molar mass. In entry 3, corresponding to 1% by weight AIBN and a reaction time of 2 hours, PMMA-co-PMA with a molar mass of 40000 g/mol, a conversion of 40% and a PDI of 1.8 was obtained. In addition, the PMA ratio calculated from ^{1}H NMR is 2.3% mol/mol as compared to 2.5% theoretical. Since high molar mass rather than high conversion was wished, conditions in Entry 3 were the conditions used for the synthesis of PMMA-*co*-PMA.

2.3.2 Microwave initiated polymerization

This part had been wholly carried in Lebanon. The synthesis of PMMA-*co*-PMA has been realized by microwave radiation. ATRP polymerization and free radical polymerization using benzoyl peroxide (BPO) as initiator have been assessed.

Microwave ATRP polymerization was done with MMA and 1% PMA (mol/mol) in DMF using ethyl 2-bromobutyrate (EBB), copper chloride (CuCl) with N, N, N', N''N'' pentamethyldiethylenetriamine pentaacetic acid at 70°C. The reaction was performed during various durations with the highest molar mass achieved being 21000 g/mol for a duration of 150 minutes. In all cases, experimental Mn (Mn_{exp}) was close to theoretical Mn (Mn_{theo}). Mn_{theo} was calculated according Equation 7.

Mn_{th}= ([monomer]/[EBB]) * M(monomer) (Equation 7)

Results are presented in Table 5.

[EBB]:[CuCl] :[PMDETA]	Time minutes	Conv[a] %	$F_{PMA,exp}$[a]	$M_{nexp,SEC}$[b] g/mol	$M_{ntheo,SEC}$[b] g/mol	Đ
1:1:2	30	38	0.7	12500	15000	1.4
1:1:2	90	40	0.6	15000	16500	1.6
1:1:2	150	50	0.95	20000	21000	1.4

[a]Determined by ^{1}H NMR. [b]Determined by size exclusion chromatography in THF

Table 5: *Experimental conditions for the synthesis of PMMA-co-PMA by microwave ATRP*

Free radical polymerization using microwave radiation and BPO as initiator is also studied. This polymerization is done between MMA and 1% PMA mol/mol using BPO as initiator in DMF at 69°C. The reaction is performed with different amounts of BPO during 15 minutes. Even with this short duration, PMMA-*co*-PMA with molar masses of 32000 have been obtained. The results are presented in Table 6.

%BPO By weight	Time minutes	Conv[a] %	$F_{PMA,exp}{}^{a}$	$M_{n,SEC}{}^{b}$ g.mol^{-1}	$Đ$
0.9	15	81	0.7	5000	2.2
0.7	15	70	0.5	7000	2.1
0.5	15	48	0.9	11000	1.7
0.2	15	21	0.3	20000	1.9
0.1	15	10	0.5	32000	2

[a] Determined by ^{1}H NMR. [b]Determined by size exclusion chromatography in THF

Table 6: *Experimental conditions for the synthesis of PMMA-co-PMA by microwave free radical polymerization*

2.4 Click reaction

Having two types of azido functionalized DTPA ligands, in addition to high molar mass PMMA bearing a known proportion of propargyl group, CuAAC reaction can be applied. CuAAC being a simple and versatile technique is gaining popularity. The triazole moiety formed is also stable to metabolic degradation. Thus compounds (7) and (8) were grafted on PMMA-co-PMA chain by CuAAC reaction.

For CuAAC reaction, azido functionalized Gd-DTPA (complex 7 or 8) was reacted with PMMA-*co*-PMA in THF using CuBr and PMDETA for 48 hours. After that, the product was purified by dialysis against acetone. CuAAC reaction of the two complexes is presented. Reactions of compounds (7) (Scheme 9) and (8) (Scheme 10) are presented.

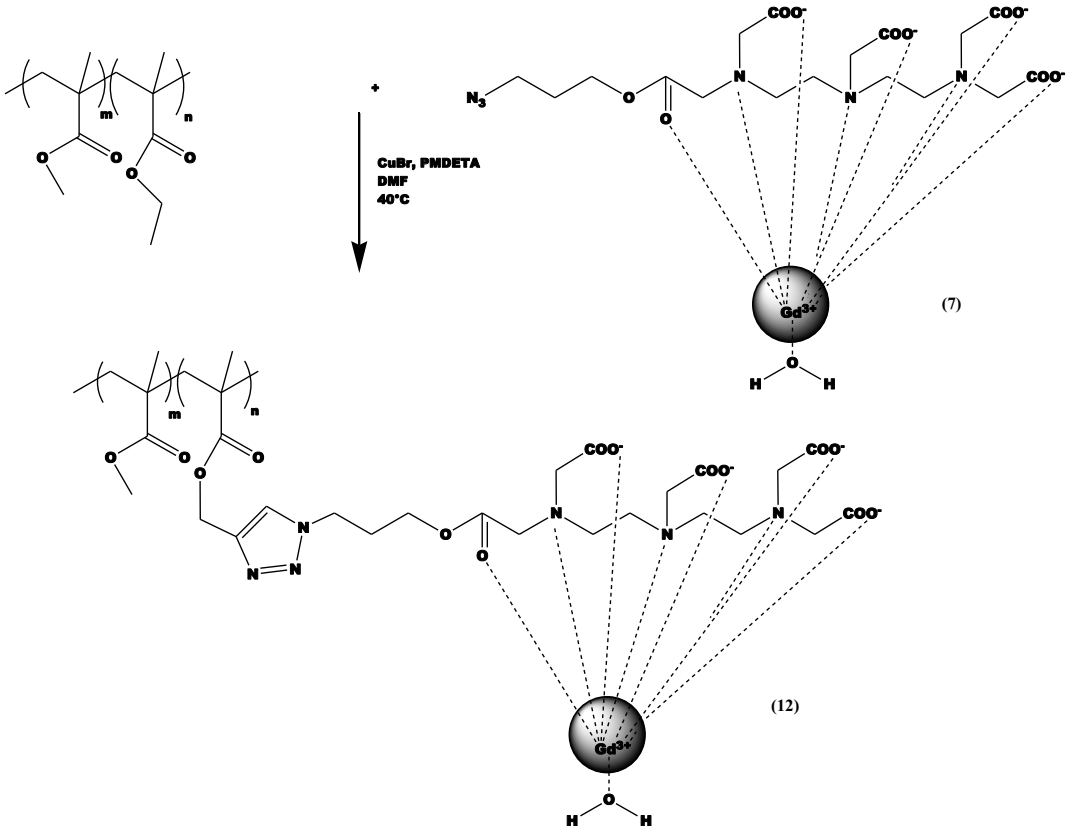

Scheme 9: *CuAAC reaction of azido functionalized mon-ester Gd-DTPA*

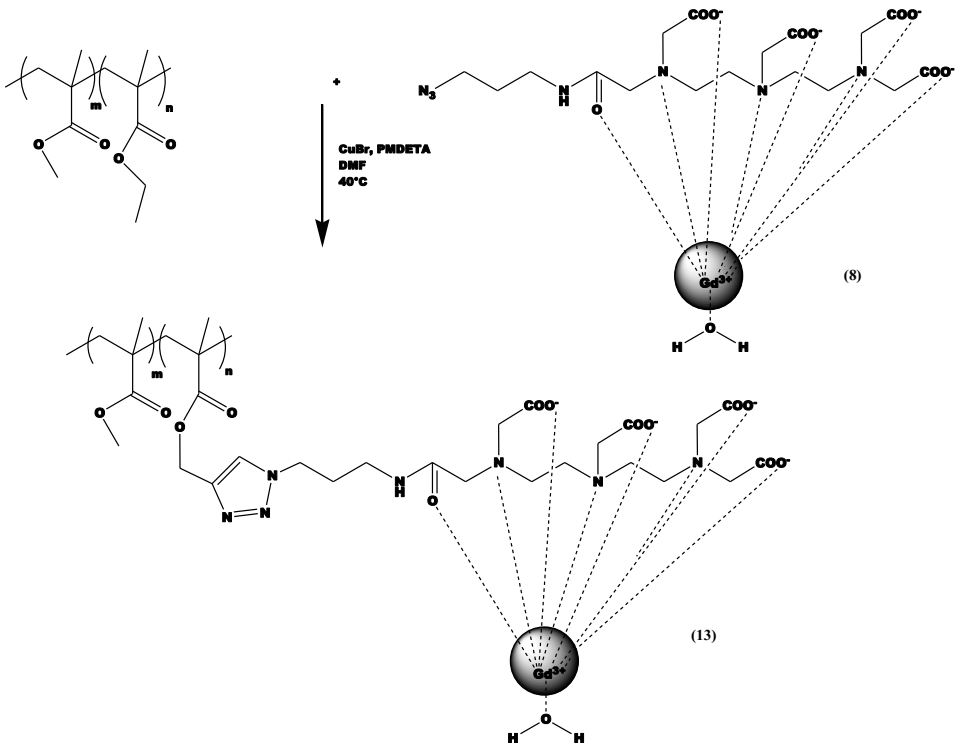

Scheme 10: *CuAAC reaction of azido functionalized mon-amide Gd-DTPA*

The amount of Gd^{3+} incorporated in compounds (12) and (13) was then calculated by ICP-MS. The amount of copper was also measured. Theoretically, and since the polymer contains 2.5% by mol of propargyl units, it should contain 2.5% by mol Gd^{3+} relevant to 2.25% by weight Gd^{3+}.

Ester Based Polymeric Contrast Agent

The amount of Gd^{3+} by weight in compound (12), as calculated by ICP-MS, was 0.4% when CuAAC was performed at room temperature and 1.4% when performed at 40°C. This resulted in an increase in the reaction efficiency from 18 to 62%.

Amide Based Polymeric Contrast Agent

The amount of Gd^{3+} by weight in compound (13), as calculated by ICP-MS, turned out to be 0.5% when CuAAC was performed at room temperature and 1.34% when performed at 40°C. This resulted in an increase in CuAAC efficiency from from 23 to 60%.

The difference between calculated and experimental values is due to the low efficiency of the click reaction, *i.e.* 60 %. However, it is well-know that the efficiency of Huisgen click reaction is not quantitative in macromolecular chemistry, due to the steric hindrance, the poor solubility of the reactant, etc. Nevertheless, the amount of Gd^{3+} into the macromolecular contrast agent was high enough for the next step, the coating of polypropylene mesh. The absence of copper had been checked in both compounds by ICP-MS.

2.5 Conclusion

This chapter described the synthesis of two types of azido-functionalized DTPA ligands: one bearing an ester group and one bearing an amide group. The complexation of these two copounds with gadolinium was also described and MTB test was performed to ensure the

absence of free gadolinium. The synthesis of high molar mass propargylated PMMA by different polymerization techniques was also reported. As a final step, the obtained azido functionalized Gd-DTPAs were grafted on the high molar PMMA with known propargyl proportions by CuAAC. The next chapter will detail the MRI visualization, cytocompatibility and cytotoxicity tests. Tests will be performed on the polymeric contrast agent containing mono-amide Gd-DTPA (compound 13).

References:

[1]: Brase, S. ; Gil, C. ; Knepper, K. ; Zimmermann, V. Organic azides: an exploding diversity of a unique class of compounds. *Angewandte Chemie International Edition* **2005**, 44, 5188 – 5240

[2]: Open chain nitrogen compounds. P.A.S. Smith et al. Vol.2 Benjamin, New York, 1966, 211-256

[3]: Leung, K. Gd-DTPA-Cystine diethyl ester copolymers. *Molecular Imaging and Contrast agent Database (MICAD)*, **2006**

[4]: Quay, SC. Metal Chelates of Diethylenetriamine pentaacetic acid partial esters for NMR imaging. S. US Patent 4687658, **1984.**

[5]: Laurent, S.; Vander Elst, L.; Houze, S.; Guerit, N.; Muller, RN. Synthesis and Characterization of Various Benzyl Diethylenetriaminepentaacetic Acids (dtpa) and Their Paramagnetic Complexes, Potential Contrast Agents for Magnetic Resonance Imaging. *Helvetica Chimica Acta* **2000**, 83, 394-406

[6]: Laurent, S.; Vander Elst, L.; Botteman, F.; Muller, RN. An assessment of the potential relationship between the charge of Gd-DTPA complexes and the exchange rate of the water coordinated to the metal. *European Journal of Inorganic Chemistry* **2008**, 4369-4379

[7]: Baia, P.; Andre, JP.; Geraldes, C.; Martins, JA.; Merbach, AE.; Toth, E. Lanthanide (III) Chelates of DTPA Bis(amide) Glycoconjugates: Potantial Imaging Agents Targeted as Asyaloglycoprotein Receptor. *Journal of Inorganic Chemistry* **2005**, 11, 2110-2119.

[8]: Cheng, TH.; Lin, KT.; Ou, MH.; Shih, HL.; Liu, GC.; Wang, YM. Water exchange and relaxometric studies of Gd(III) Complexes with DTPA-bis(amide) Ligands. *Journal of the Chinese Chemical Society* **2001**, 48, 1099-1105

[9]: Perez-Baena, I.; Loinaz, I.; Padro, D.; Garcia, I.; Grande, HJ. ; Odriozola, I. Single-chain poly(acrylic) nanoparticles with multiple Gd(III) centers as possible MRI contrast agents. *Journal of Materials Chemistry* **2010**, 20, 6916-6922

[10]: El Habnouni, S.; Nottelet, B.; Darcos, V.; Porsio, B.; Lemaire, L.; Franconi, F.; Garric, X.; Coudane, J. MRI visible poly(ε-caprolactone) with controlled contrast agent ratios for enhanced visualization in temporary imaging applications. *Biomacromolecules* **2013**, 14, 3626-3634.

[11]: Arano, Y. ; Uezono, T. ; Akizawa, H. ; Ono, M. ; Wakisaka, K. ; Nakayama, M. ; Sakahara, H. ; Konishi, J. ; Yokoyama, A. Reassessment of diethylenetriamine pentaacetic acid (DTPA) as a chelating agent for indium-111 labeling of polypeptides using a newly synthesized monoreactive DTPA derivative. *Journal of Medicinal Chemistry* **1996**, 39, 3451-3460

[12]: Ardestani, M.S.; Arabzadeh, AJ. ; Heidari, Z. ; Hosseinzadeh, A. ; Ebrahimi, H. ; Hashemi, E. ; Mosaybenia, M. ; Shafee-Alavidgeh, M. ; Alavi, A. ; Babaei, MS. ; Rahmim, A. ; Ebrahimi, SES, Amanlou, M. Novel and facile methods for the synthesis of DTPA-mono-amide: a new completely revised strategy in radiopharmaceutical chemistry. *Journal of Radioanalytical and Nuclear Chemistry* **2010**, 283, 447–455

[13]: Frullano, L.; Caravan, P. Strategies for the preparation of Bifunctional Gd(III) Chelators. *Current Organic Synthesis* **2011**, 8, 535-565

[14]: Vertes, A.; Nagy, S.; Klencsar, Z.; Lovas, RG. ; Rosch, F. Handbook of nuclear chemistry: Radiochemistry and radiopharmaceutical chemistry in life sciences. *Springer,* **2003**, 2167

[15]: Parac-Vogt, TN.; Kimpe, K.; Laurent, S.; Pierart, C.; Elst, LV.; Muller, RN. ; Binnemans, K. Gadolinium DTPA-Monoamide Complexes Incorporated into Mixed Micelles as Possible MRI Contrast Agents. *European Journal of Inorganic Chemistry* **2004**, 3538-3543

[16]: Ferreira, MF. ; Martins, AF. ; Martins, C. ; Toth, E. ; Rodrigues, T. ; Calle, D. ; Cerdan, S. ; Lopez-Larrubia, P. ; Martins, JA. ; Geraldes, C. Amide conjugates of the DO3A-N-(α-amino) propionate ligand: leads for stable, high relaxivity agents for MRI? *Contrast Media Molecular Imaging* **2013**, 8, 40-49

[17]: Platzek, J.; Niedballa, U. Process for the production of monoamides of DTPA. US patent 6677483B2. **2004**

[18]: Khalafi-Nezhad, A.; Mokhtari, B.; Sotnai Rad, MN. Direct preparation of primary amides from carboxylic acids and urea using imidazole under microwave irradiation. *Tetrahedronletters* **2003**, 44, 7325-7328

[19]: Martinelli, J.; Balali-Mood, B.; Panizzo, R.; Lythgoe, MF. ; White, AJ. ; Ferretti, P.; Steinke, JH. ; Vilar, R. Coordination Chemistry of amide functionalized tetraazomacrocycles: structural, relaxometric, and cytotoxicity studies. *Dalton Transactions* **2010**, 39, 10056-10067

[20]: Brown, RR. ; Clarke, DW. ; Daffner, RH. Is a mixture of Gadolinium and Iodinated contrast agents safe during MRI Arthrography? *American Journal of Roentgenology* **2000,** 175, 1087-1090

[21]: Feuser, PE. ; Gaspar, PC. ; Ricci-Junior, E.; da Silva, M.; Nele, M. Sayer, C.; Araujo, P. Synthesis and Characterization of Poly(Methyl Methacrylate) PMMA and Evaluation of Cytotoxicity for Biomedical Application. *Macromolecular Symposia* **2014**, 343, 65–69

[22]: Kumbar, S.; Laurencin, C.; Deng, M. Natural and synthetic biomedical polymers. *Elsevier,* **2014**

[23]: Sugino, A. ; Miyazaki, T. ; Kawachi, G. ; Kikuta, K. ; Ohtsuki, C. Relationship between apatite-forming ability and mechanical properties of bioactive PMMA-based bone cement modified with calcium salts and alkoxysilane. *Journal of materials science. Materials in medicine* **2008,** 19, 1399–1405

[24]: Jessy, RS. ; Ibrahim, MH. Biodegradability and Biocompatibility of Polymers with Emphasis on Bone Scaffolding: a Brief Review. *International Journal of Scientific and Research Publications* 2014**, 4,** 1-3

[25]: Ratanajanchai, M.; Lee, DH. ; Sunintaboon, P.; Yang, SG. Photo-cured PMMA/PEI core/shell nanoparticles surface-modified with Gd–DTPA for T1 MR imaging. *Journal of Colloid and Interface Science* **2014**, 415, 70–76

[26]: Martirosyan, K.; Stafford, RJ. ; Elliott, AM. ; Frank, SJ. PMMA/SWCNTs nanocomposites for prostate brachytherapy MRI contrast agent markers. *Nanoscience and technology Institue-Nanotech* **2009,** 2, 44-47.

[27]: Guillaume, O. ; Blanquer, S. ; Letouzey, V. ; Cornille, A. ; Huberlant, S. ; Lemaire, L. ; Franconi, F. ; de Tayrac, R. ; Coudane, J. ; Garric, X. Permanent Polymer Coating for in vivo MRI Visualization of Tissue Reinforcement Prostheses. O. Guillaume et al. *Macromolecular Bioscience* **2012**, 12, 1364–1374

[28]: Sanchez-Sanchez, A. ; Asenjo-Sanz, I. ; Buruaga, L. ; Pomposo, JA. Naked and Self-Clickable Propargylic-Decorated Single-Chain Nanoparticle Precursors via Redox Initiated RAFT Polymerizationa. *Macromolecular Rapid Communications* **2012**, 33, 1262-12367

[29]: Krieg, A.; Becer, CR.; Hoogenboom, R.; Schubert, US. Tailor maid side-chain functionalized macromolecules by combination of Controlled Radical Polymerization and Click Chemistry. *Macromolecular Symposia* **2009**, 275-276, 73-81

[30]: Brouwer, JAM. ; Van ES, JJGS. ; German, AL. The molar mass dependence of latex particle deformation. *Macromolecular Sympoisia* **2000**, 151, 459-464

[31]: Scarpaci, A. ; Cabanetos, C. ; Blart, E. ; Montembault, V. ; Fontaine, L. ; Rodriguez, V. ; Odobel, F. Post funcytionalization of poly(propargyl methacrylate) using copper catalyzed 1,3 dipolar Huisgen cycloaddition: an easy route to electro-optic materials. *Journal of Polymer Science Part A: Polymer Chemistry* **2009**, 47, 5652-5660

Chapter 3
MRI, Stability, and Cytocompatibilty Evaluation

Using the combination of free radical polymerization and click chemistry, an azido-functionalized mono-amide Gd-DTPA contrast agent has been grafted on a propargylated PMMA chain. For simplicity, the compound will be referred to as PMMA CA. The obtained macromolecular contrast agent contains 1.34% by weight Gd^{3+} as detected by ICP-MS. The aim of the synthesis of this polymeric contrast agent was to test its capability to render a PP mesh visible by MRI. The effect of the variation of the amount of Gd^{3+} present in PMMA CA on the MRI visualization of the PP mesh was assessed. In addition, and since this contrast agent is intended to be used for long periods of time and in biomedical applications, it was assessed for its stability and cytocompatibility.

3.1 MRI Visualization

A solution of PMMA CA was sprayed on a commercial PP mesh, in order to assess the agent's ability on rendering the PP mesh MRI visible. MRI visualization was performed on a Bruker Biospec 70/20 operating at 7T magnetic field. In order to study the effect of the amount of Gd^{3+} present in the contrast agent on the MRI visualization, meshes were sprayed with MRI contrast agent having different % by weight of Gd^{3+}. They were prepared by dilution of PMMA CA in commercial PMMA to obtain 0.14, 0.23 and 0.79% w/w of Gd^{3+} in the mixture. Each polymeric contrast agent was then sprayed on the PP mesh using the airbrushing technique. The airbrushing technique was chosen to deposit the PMMA contrast agent on the PP mesh for the following reasons.

3.1.1 Airbrushing technique

The aim was to coat the PP mesh with a film of the PMMA based contrast agent. The process of coating in the pharmaceutical industry goes back in date to the mid 1800s with the

introduction of sugar coated tablets [1]. In general, a method for the formation of a polymeric film coating is the dissolution of a polymer in an appropriate solution and then spraying it as a fine mist. Droplets of the solution containing the polymer strike the surface of the substrate (in this case the PP mesh), spread on it, and upon the evaporation of the solvent a film is formed (Fig. 43). The choice of the solvent is essential because if the solvent evaporates rapidly the solvent-containing polymer may dry before striking the surface, and if the solvent dries too slowly the polymeric solution may dry before striking or spreading on the mesh [2]. In addition to that, high molar mass polymer is needed because reducing molecular weight affects critically the film strength [3].

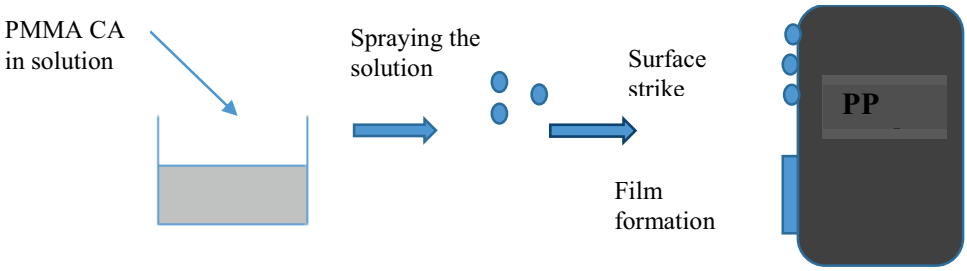

Figure 43: *Mechanism of the formation of the polymeric film by the spraying technique*

The spraying technique allows the indirect deposition of the PMMA contrast agent (high molar mass, 40 000 g) on the PP mesh.

For this, the polymeric solution was prepared by dissolving PMMA contrast agents (containing different % by weight Gd^{3+}) in dichloromethane. Each contrast agent was then spread on a commercial PP mesh using the airbrushing technique with an "Infinity Airbrush System" supplied by Harder & Steenbeck (Osteinbeck, Germany) under 3 bars argon pressure at a distance of 5 cm (Fig. 44). We prepared three meshes that were dried overnight under vacuum until a constant weight is obtained.

The airbrushing technique is a versatile method that allows the preparation of regular and homogeneous films without altering the mesh's shape and mechanical properties [4]. It allows the direct deposition of the polymeric solution on the PP mesh [5].

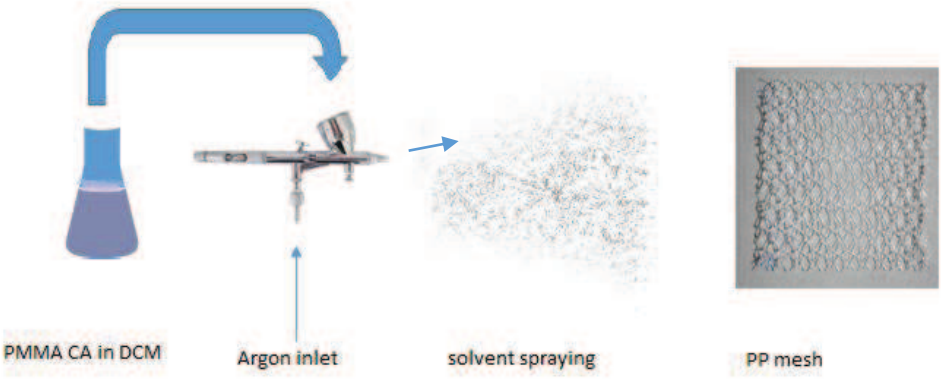

Figure 44: *Spraying of PMMA CA on PP mesh by airbrushing technique*

3.1.2 MRI Results

The effect of the proportion of Gd^{3+} in the polymer on MRI visualization is shown in Fig. 45 . Polypropylene meshes covered with PMMA CA were visualized using 7T MRI. In the absence of CA, the polypropylene mesh was not visible (Fig. 45).

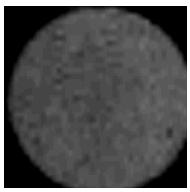

Figure 45: *7T MR image of PP mesh without PMMA CA*

Polypropylene meshes were coated with MRI-visible PMMAs at differentGd^{3+} concentrations of 0.14, 0.24 and 0.79 % by weight (Fig. 46). The amounts of Gd^{3+} present on each mesh were respectively 1.4, 2.3 and 8 µg per mg of polymeric contrast agent sprayed on

a mesh having a mass of around 10 mg. Results revealed that regardless the amount of Gd^{3+}, the meshes turned out to be MRI visible even with concentrations of Gd^{3+} as low as 1.4 µg per mg (0.14% w: w) of polymeric contrast agent. Thus the presence of only 0.14% by weight of Gd^{3+} in the PMMA CA was sufficient to make the PP mesh visible by MRI.

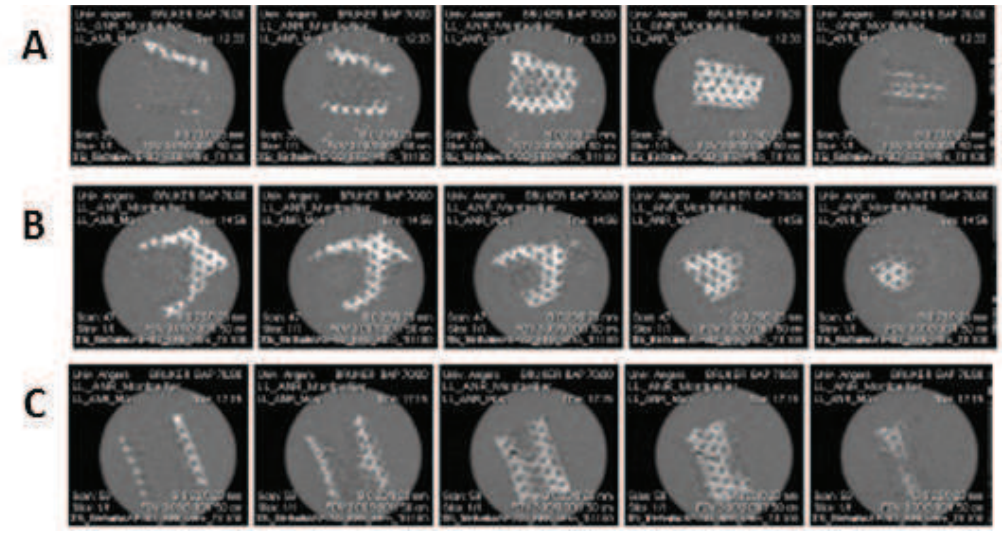

Figure 46:*7T MR images of PP meshes coated with PMMA CA containing (A) 0.14% (B) 0.23%, and (C) 0.79% by weight Gd^{3+}*

3.2 Stability Studies in PBS

The ability of the PMMA contrast agent to render the PP mesh visible is not enough for medical applications, stability is another feature this CA should possess. In other words, Gd^{3+} should remain incorporated in the PMMA CA and should not be released over time. The stability of Gd-complexes is gaining more attention because of nephrogenic systemic fibrosis (NSF) occurring in patients with severe renal failure. NSF is a disorder that mainly affects the skin (but other tissues can be targeted) resulting in disability or, in severe cases, death. The primary cause leading to NSF is the transmetallation between Gd^{3+} released from the Gd-chelate, and endogenous metals (zinc, copper, and calcium) thus releasing free Gd^{3+}. This is mainly observed in patients with severe renal problems [6]. Hence, transmetallation is directly

related to the chelate's thermodynamic stability. For this, stable contrast agents are a necessity to eliminate any risks associated with free Gd^{3+} and to prevent the precipitation of gadolinium salts.

Our PMMA contrast agent will be assessed for stability in PBS buffer solution at 37°C to detect the release of free Gd^{3+} over time and to assess its suitability for application as long-term MRI contrast agent. PMMA CA films containing 0.1 and 0.43% Gd^{3+} by weight were prepared and placed in PBS solution. The release was monitored over a 30 days period.

3.2.1 PMMA contrast agent film preparation

Films containing different % by weight of Gd^{3+} were prepared by diluting the PMMA contrast agent (containing 1.34% by weight Gd^{3+}) with commercial PMMA and dissolving it in dichloromethane. 1 mL of the solution was placed in a circular mold. After solvent evaporation, films containing 0.10% and 0.43% by weight of Gd^{3+} were obtained (Fig. 47).

Figure 47: *PMMA CA films for stability and cytocompatibility studies*

3.2.2 Stability Test Results

Each film (0.1 and 0.43% of Gd^{3+}) was placed separately in a PBS solution at 37˚C under stirring at 130 rpm. At scheduled time points (1, 7, 30 and 90 days) 1 mL of PBS buffer was withdrawn (then replaced by 1 mL fresh buffer) and analyzed by ICP-MS for Gd^{3+} release study.

Films containing 0.1% Gd^{3+} w/w showed no detectable release of Gd^{3+} in PBS over a period of 90 days. Films containing 0.43% Gd^{3+} w/w (79 µg of Gd^{3+}) showed a release of 0.4% Gd^{3+} (corresponding to 0.231 µg Gd^{3+}) throughout the 90 days (Fig. 48). In both cases this represents a very low release of Gd^{3+} showing the stability of the CA during this period of time.

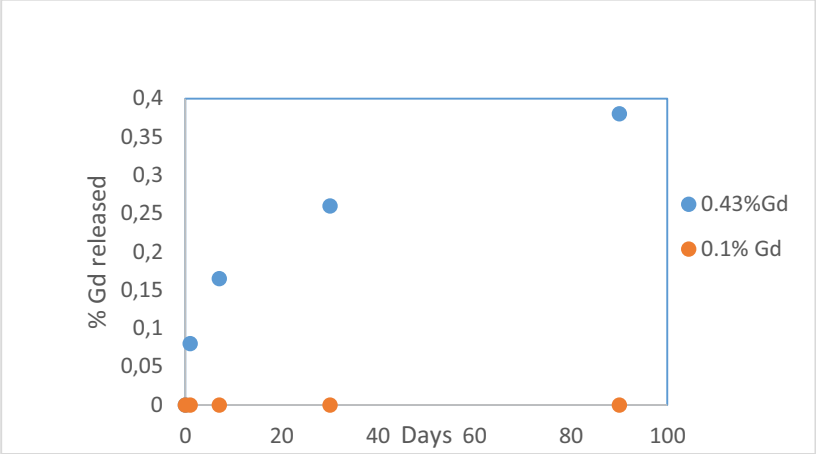

Figure 48: *Gd release from 0.1 and 0.43% containing films in PBS*

Moreover, it is important to note that only a few µgrams of gadolinium were released, while the gram scale is used for the amount of Gd^{3+} administered in conventional MR scans. The FDA's recommended dose of Magnevist in the US is 0.2 mL/kg corresponding to 0.1 mmol Gd/kg of body weight. Hence, for a 60 kg person, 6 mmol of Gd are administered, corresponding to around 1g of Gd^{3+}. In some other countries, up to 0.6 mL/kg Magnevist can be injected corresponding to 0.6 mmol Gd^{3+}/kg of body weight, corresponding to 6g of Gd^{3+} [7].

3.3 Cytocompatibility Test

The obtained PMMA contrast agent should also be cytocompatible, hence a cytocompatibility test is essential to evaluate its effect on cells. For this, films containing various amounts of Gd^{3+} were prepared from PMMA CA as described in the section above. Cytocompatibility tests were performed on films containing 0.23, 0.5, and 1.34% Gd^{3+} by weight. These films were placed in direct contact with murine fibroblast cells.

3.3.1 Cytotoxicity Test

Cytocompatibility tests were performed on L-929 murine fibroblast cells (as recommended by the International and European standards ISO 10993-5:2009).

3.3.2 Cytotoxicity Results

Fig. 49 shows that PMMA CA with 0.23 and 0.5% Gd^{3+} were cytocompatible and did not have any effect on cell growth after 24 hours, whereas those containing 1.34% Gd^{3+} were detrimental for the cells. The LDH direct contact cytotoxicity test used to assess cytocompatibility works as follows: LDH or lactate dehydrogenase is an enzyme liberated in culture media once cells are dead. The presence of LDH reduces tetrazolium salt in LDH mixture to formazan dye having a red colour and a maximum absorbance at 490 nm. Thus, the presence of dead cells is indicated by both a red colour and high UV absorbance at this wavelength. This is the case with the TCPS negative control which contained the cells lysis, and in the case of the direct contact of PMMA MRI films containing 1.34% Gd^{3+} as revealed in Figure 48. The graph also shows that MRI PMMA films containing 0.23 and 0.5% Gd^{3+}(w/w) had almost no UV absorbance, and thus no cytotoxicity was observed. The result is not surprising because a study performed by Porsio *et al*. [8] revealed that MRI visible PCL

nanoparticles with 1% Gd^{3+}(w/w) caused a lower cell proliferation as compared to the same nanoparticles with lower Gd^{3+} amounts. Hence, polymeric contrast agents with the lowest amounts of Gd^{3+} are recommended in order to assure cytocompatibility by keeping a good MRI visibility.

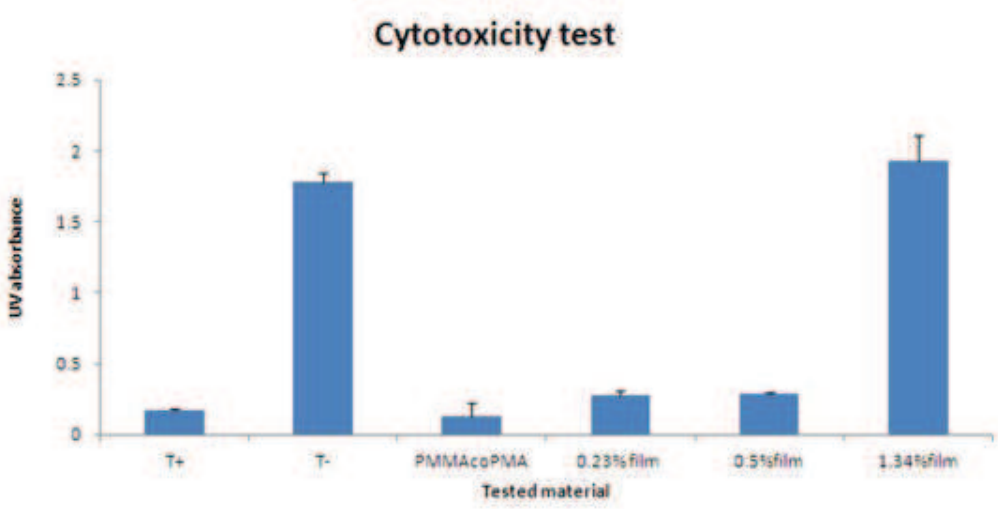

Figure 49: *Cytocompatibility results of 0.23 and 0.5% Gd containing films*

3.4 Conclusion

The coating of the polypropylene mesh with the PMMA CA rendered it visble by MRI. Even if the CA agent contained only 0.1% by weight gadolinium, it was still able to render the PP mesh visible at 7T. PMMA CA with up to 0.5% Gd, turned out to be stable and cytocompatible.The next chapter will describe the synthesis of polymeric fluorophores. Three of these fluorophores are organic and the last fluorophore involves the complexation of europium in the azido-functionalized mono-amide DTPA ligand.

References

[1]: Porter, SC. Coating of pharmaceutical dosage forms. In: Allen, L.V.E.A. (Ed.), Remington the Science and Practice of Pharmacy. *Pharmaceutical Press, London,* **2012**, 977–987.

[2]: Felton, LA. Mechanisms of polymeric formation. *International Journal of Pharmaceuticals* **2013**, 457, 423-427

[3]: Goddard, E.; Gruber, JV. Principles of Polymer Science and Technology in Cosmetics and Personal Care. *Marcel Dekker Inc.***1999,** 22, 254.

[4]: Guillaume, O. ; Blanquer, S. ; Letouzey, V. ; Cornille, A. ; Huberlant, S. ; Lemaire, L. ; Franconi, F. ; de Tayrac, R. ; Coudane, J. ; Garric, X. Permanent Polymer Coating for in vivo MRI Visualization of Tissue Reinforcement Prostheses. O. Guillaume et al. *Macromolecular Bioscience* **2012**, 12, 1364–1374

[5]: Behrens, AM.; Casey, BJ.; Sikorski, MJ.; Wu, KL.; Tutak, W.; Sandlers, AD.; Kofinas, P. In-situ Deposition of PLGA nanofibers via solution blow spinning. *ACS Macroletters* **2014**, 3, 249-254

[6]: Broome, DR. Nephrogenic systemic fibrosis associated with gadolinium based contrast agents: A summary of the medical reporting literature. *European Journal of Radiolgy* **2008**, 66, 230-234

[7]:http://www.fda.gov/downloads/AdvisoryCommittees/CommitteesMeetingMaterials/Drugs/DrugSafetyandRiskManagementAdvisoryCommittee/UCM192006.pdf

[8]: Porsio, B. ; Lemaire, L.; El Habnouni, S. ; Darcos, V.; Franconi, F.; Garric, X.; Coudane, J. ; Nottelet, B. MRI-visible nanoparticles from hydrophobic gadolinium poly(ε-caprolactone) conjugates. *Polymer* **2015,** 56, 135-140

Chapter 4

Fluorescent poly(methyl methacrylate)

The previous part of the thesis described the synthesis of a PMMA derivative for long-term MRI visualization. During the last decade, fluorescence imaging was gaining attention. A sensitive camera is now used *in vivo* to detect the fluorescence of fluorophores [1]. The fluorophore allows the molecule to absorb energy at a specific wavelength and emit energy at a different but specific wavelength [2]. For this, the alkyne functionalized PMMA will be attached by click chemistry to four different fluorophores: anthracene, fluorescein, rhodamine, and europium complex.

4.1 Poly(methyl methacrylate) derivative functionalized with anthracene

Numerous publications describe the synthesis of anthracenic fluorophore derivatives [3,4]. Although organic fluorophores, as anthracene, have desirable UV absorption and visible emission, yet different types of interactions may occur between the fluorophores themselves resulting in aggregates which can decrease the emission intensity. In order to reduce the interactions between the fluorophores, polymers can be used as separators between organic fluorophores thus reducing their interactions. For this, Su *et al*. describe the chemical linking of the anthracenic fluorophore to PMMA which inhibited the associations between central anthracene rings. This phenomenon increased the quantum yield, which is the number of emitted photons per absorbed photons [5]. In fact, the presence of the azide on the anthracene group also quenches the fluorescence due to a photo-induced electron transfer effect. The formation of triazole compounds via CuAAC reduced the electron donating effect of nitrogen, thus reducing this effect and restoring the fluorescence [6]. This fluorogenic CuAAC reaction has broad applications in the medical field due to its high efficiency, mild reaction conditions and distinct fluorescence properties of the product. A very strong fluorescent signal is obtained from weakly or even non-fluorescent starting materials [6,7].

In our case, to form the triazole moiety and to obtain a fluorescent compound, propargylated PMMA was reacted with azido anthracene under mild CuAAC conditions (Scheme 11).

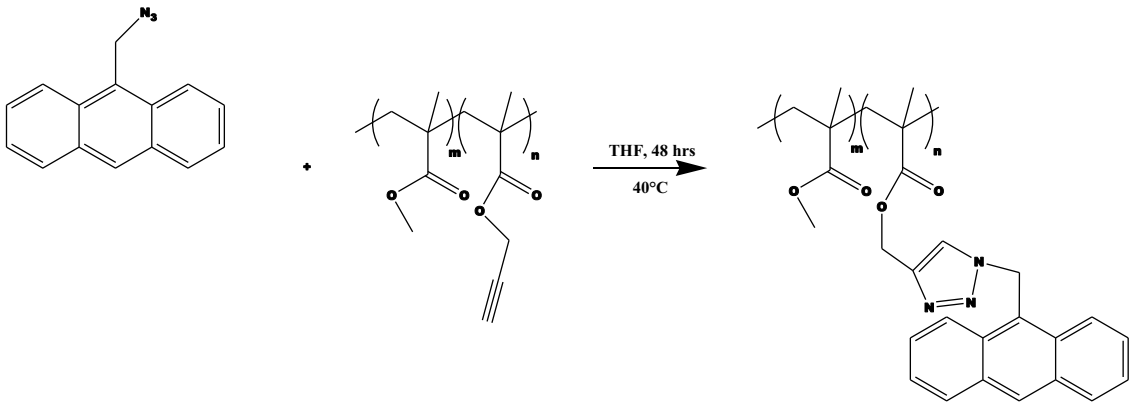

Scheme 11: *Synthesis of anthracene functionalized PMMA*

In a first step, 9-azido methyl anthracene was synthesized.

4.1.1 Synthesis of 9-azido methyl anthracene

9-azido methyl anthracene was synthesized by reaction of 9-chloro methyl anthracene on sodium azide in acetonitrile (Scheme 12). The pure product was obtained by recrystallization in ethanol followed by passing it on a chromatography column.

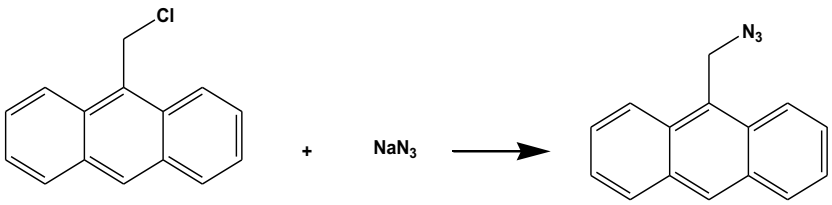

Scheme 12: *Synthesis of 9-azido methyl anthracene*

The purity of the compound was verified by ^{1}H NMR and the presence of the azide peak appeared at 2100 cm^{-1} in FT-IR (Fig. 50).

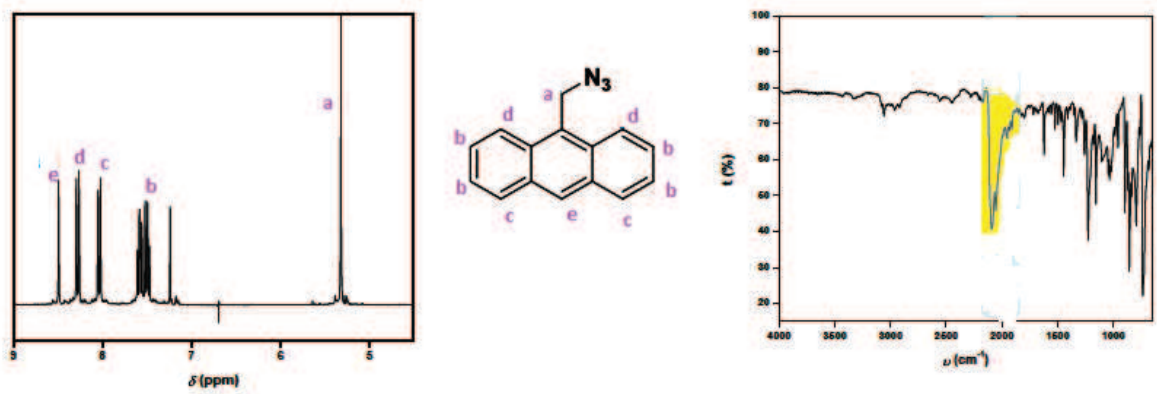

Figure 50: *^{1}H NMR and FT-IR of 9-azido methyl anthracene*

4.1.2 Synthesis of anthracene-functionalized poly(methyl methacrylate) by click chemistry

In order to obtain the fluorescence of the anthracene which was quenched due to the presence of the azide group, the formation of the triazole moiety was a necessity. CuAAC reaction took place between PMMA containing propargyl groups (2.5% mol/mol) and 9-azido methyl anthracene in THF for 48 hours at 40°C. The mixture was then precipitated in ethanol to get rid of free azido-anthracene [8].

The GPC trace using UV detector revealed the absence of UV absorbance of the polymer (Fig. 51) and a molar mass of around 20000 g/mol.

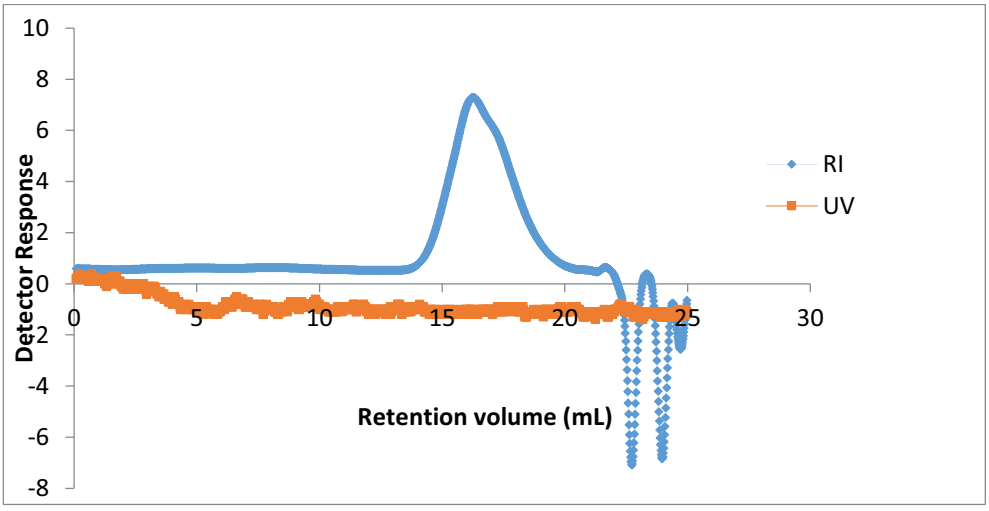

Figure 51: *GPC-UV of PMMA-co-PMA*

After CuAAC, and using 290nm wavelength, GPC revealed a UV signal at the same retention volume as the one of the polymer, revealing the presence of a fluorescent polymer without any free 3-azido anthracene (Figure 52).

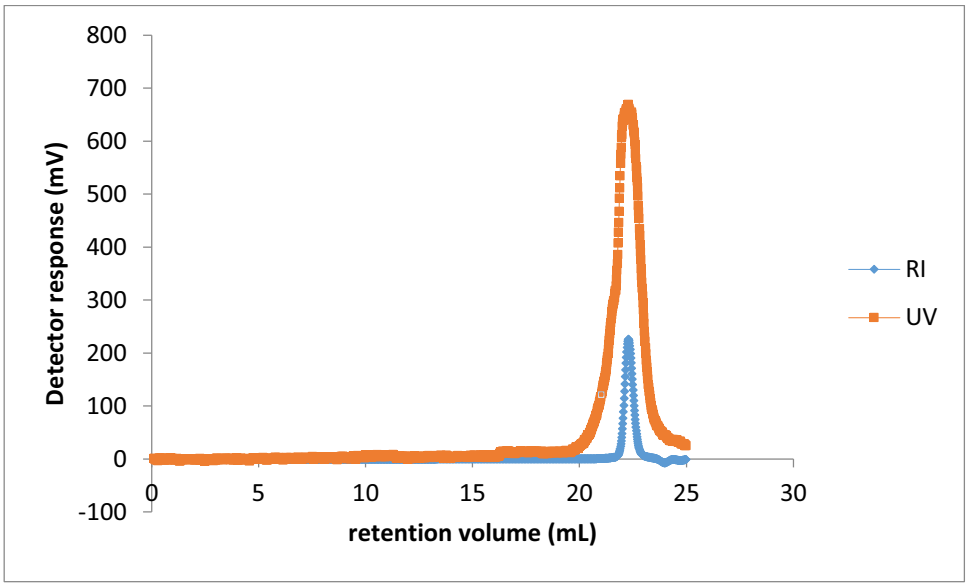

Figure 52: *GPC-UV of anthracene fluorecent PMMA*

Theoretically, the anthracene functionalized PMMA should contain 4.2% by weight anthracene (relevant to the 2.5% by mol propargyl units the PMMA contains). The amount of anthracene in the anthracene fluorescent PMMA was determined by UV-visible spectroscopy. Working at a wavelength of 358 nm, a calibration curve of anthracene was drawn (Figure 53).

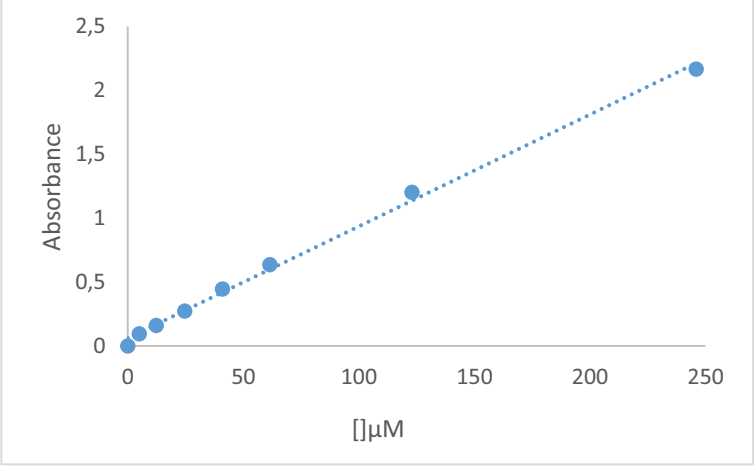

Figure 53: *Variation of absorbance as function of [anthracene]*

The calibration curve was obtained with a statistically acceptable fit of 0.9954. Using this calibration curve, the amount of anthracene in the anthracene fluorescent PMMA turned out to be 1.8% by weight as compared to theoretically 4.2% by weight. This is due to the low efficiency of the CuAAC reaction which maybe improved by increasing the temperature. However, the temperature in our case is a limitation due to the presence of the azide group.

4.2 PMMA derivative functionalized with Fluorescein Isothiocyanate (FITC)

The use of FITC as a fluorophore in bioassays is well known. Pinheiro *et al*. described the synthesis of Fe_3O_4 functionalized nanoparticles with FITC, mediated by polyethyleneimine (PEI) and these particles were preliminary evaluated as fluorescent [9]. This fluorophore is extensively used in cell biological studies [10]. In our case, FITC was modified with 3-azido propylamine so that it contained an azide group and the azido modified FITC was then conjugated to propargylated PMMA. The obtained PMMA-FITC was then sprayed on a PP mesh and evaluated by fluorescence microscopy for the emission of green color characteristic of FITC.

As a first step, azido modified fluorescein was obtained by the reaction between FITC and 3-azido propylamine in DMF in the presence of triethylamine. The reaction mixture was stirred for 2 hours at room temperature (Scheme 13) [11].

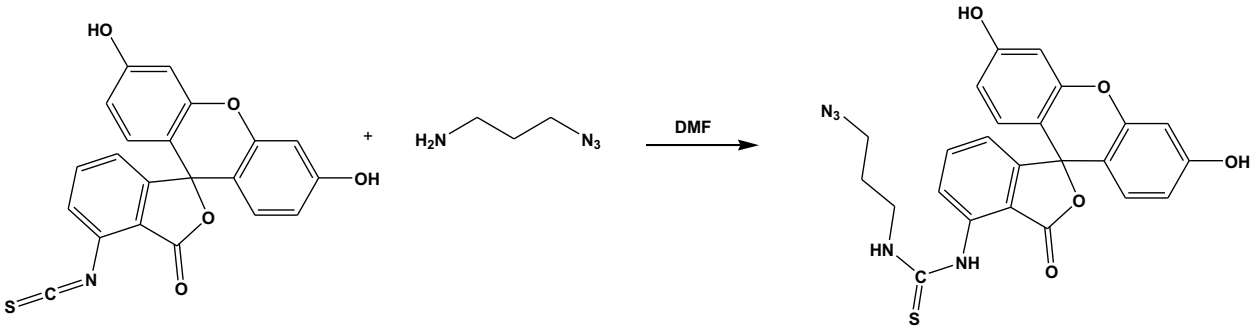

Scheme 13: *Synthesis of azido modified fluorescein*

The presence of the azide was verified by FT-IR by the appearance of the peak at 2100 cm^{-1}. The azido functionalized FITC was further attached to the propargylated PMMA by CuAAC using CuBr and PMDETA. The reaction took place in DMSO for 48 hours at 40°C. The PMMA-FITC was obtained by precipitation in ethanol (Scheme 14).

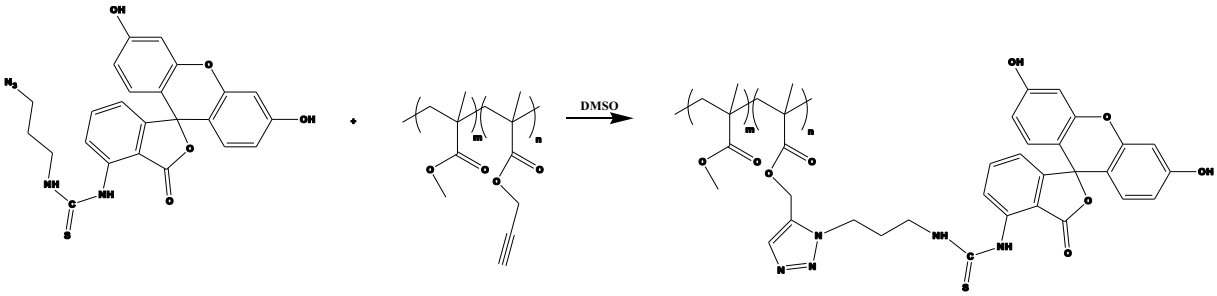

Scheme 14: *Synthesis of PMMA-FITC*

GPC trace using UV detector-UV in DMF at 450 nm revealed the absence of free FITC. GPC was performed in DMF because the product was not soluble in THF. Fig. 54 and 55 represent the GPC-UV traces of FITC and PMMA-FITC.

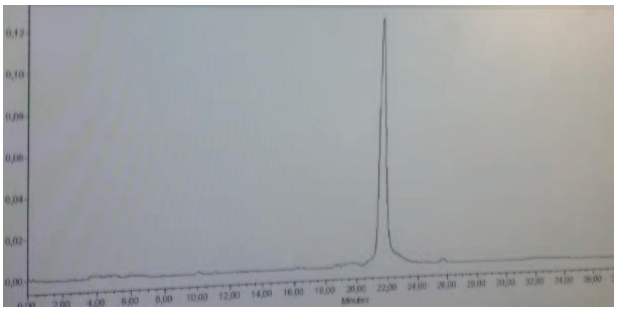

Figure 54 : *GPC-UV of FITC*

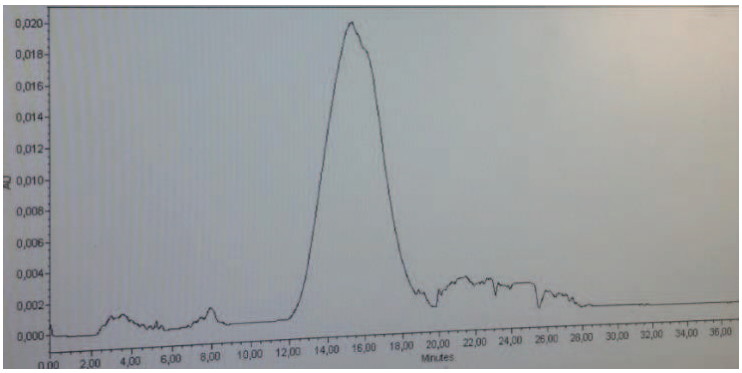

Figure 55: *GPC-UV of PMMA-FITC*

In order to depose PMMA-FITC on the PP mesh, the airbrushing technique was used. PMMA-FITC was solubilized in DCM and the solution was sprayed on the PP mesh. The mesh was then observed by fluorescent microscopy. In the presence of white light, the mesh revealed the presence of only a small amount of PMMA-FITC due to the low solubility of the compound in DCM (Fig.56).

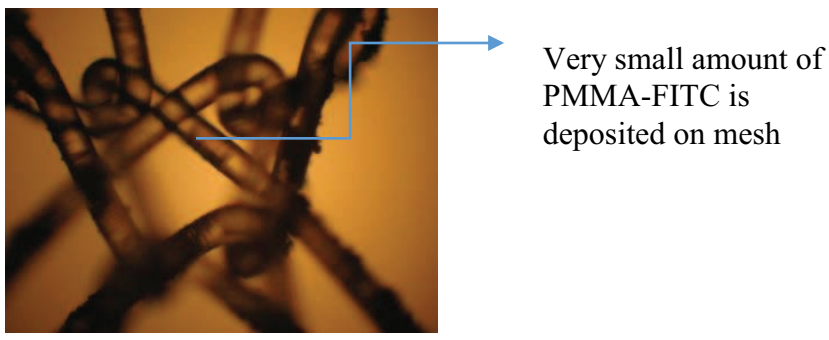

Figure 56: *White light visualization of PMMA-FITC on PP mesh*

By placing a green light filter, only green light can pass and excite the PMMA-FITC on the mesh. FITC has an excitation wavelength of around 495 nm (green light) and an emission of around 518 nm also corresponding to green light. Hence, the excitation of PMMA-FITC at the correct wavelength should reveal a green color. However, in this case no green fluorescence was observed probably due to the insufficient amount of PMMA-FITC present on the mesh (Fig. 57).

Figure 57: *no green light visualization of PMMA-FITC on PP mesh*

NB: Under a red light filter, only red light can pass and excite PMMA-FITC. The wavelength of red light does not allow the excitation of PMMA-FITC, and that is why no emission occurred and no fluorescence was observed.

4.3 PMMA derivative functionalized with rhodamine B isothiocyanate (RITC)

Rhodamine B is one of the rhodamines known for its red fluorescence and photostability [12]. Rhodamine dyes are widely used as fluorescent probes due to their broad fluorescence in the visible region of the electromagnetic spectrum. In many cases, rhodamine dye is modified and linked to biomolecules [13]. In this work, rhodamine B isothiocyanate was modified to give a RITC azide. Rhodamine B isothiocyanate was then reacted with 3-azido propylamine for 2 hours in DMF with triethyl amine (Scheme 15). After solvent evaporation, the pure product was obtained. The FT-IR spectrum shows a peak at 2100 cm^{-1} corresponding to the azide peak.

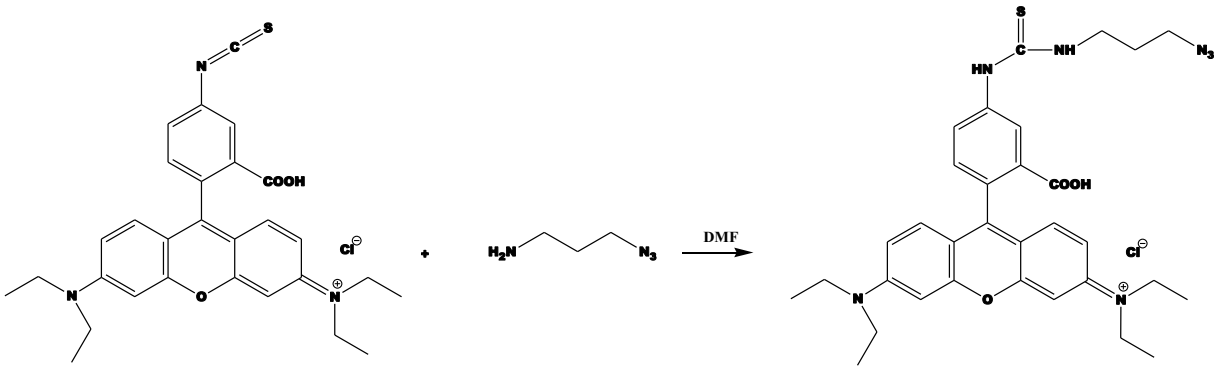

Scheme 15: *Synthesis of azido functionalized rhodamine B isothiocyanate*

RITC-azide was further attached to the propargylated PMMA by CuAAC using CuBr and PMDETA. The reaction took place in DMSO for 48 hours at 40°C (Scheme 16). The PMMA-RITC was obtained by precipitation in ethanol.

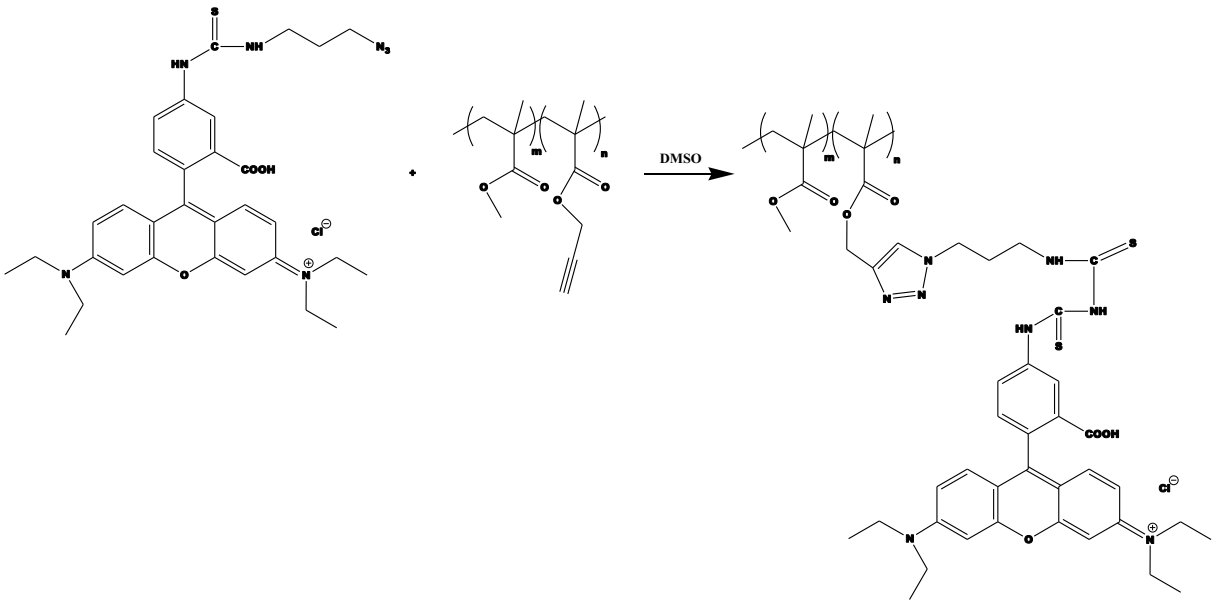

Scheme 16: *Synthesis of PMMA RITC*

The GPC trace in DMF using an UV detector revealed the absence of free RITC and the conjugation of RITC to the PMMA.PMMA-RITC was then dissolved in DCM and sprayed on PP mesh by the air-brushing technique. Visualization of the mesh by white light revealed the presence of PMMA-RITC on the mesh (Fig. 58).

Figure 58: *White light visualization of PMMA-RITC on PP mesh*

By placing a green filter and upon excitation of this mesh by green light, a light fluorescence could be observed (Fig.59).

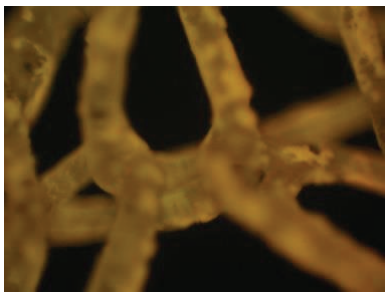

Figure 59: *Green light visualization of PMMA-RITC on PP mesh*

Excitation with red light of the PP mesh with PMMA-RITC gave a highly fluorescent red color due to the emission wavelength of RITC (≅ 650nm).

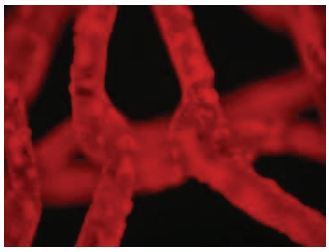

Figure 60: *Red light visualization of PMMA-RITC on PP mesh*

As preliminary studies, these results indicate that the obtained PMMA-RITC can generate red light if excited at the correct wavelength, which can be useful *in vivo* fluorescence after further studies.

4.4 PMMA derivative with europium complex

Lanthanides, especially Terbium and Europium, are gaining attention for replacement of organic fluorophores. [14]. Complexes of europium are especially gaining much interest for several reasons [15]:

- They have large Stokes shifts (i.e. the difference in wavelength between excitation's maximum and emission's maximum)
- They have a Long-lived fluorescence

Europium has to be complexed because the ligand absorbs the excitation radiation and transfers it to the europium which then emits the light thus acting as an antenna. For example, the creation of the triazole group acts as an antenna for the lanthanide energy transfer process [16]. In this case, azido-functionalized DTPA monoamide was reacted with Eu(III) triflate in pyridine at 70°C for 3 hours (Scheme 17). After solvent evaporation, the product was refluxed in ethanol for 1 hour, centrifuged and filtrated to obtain the pure product.

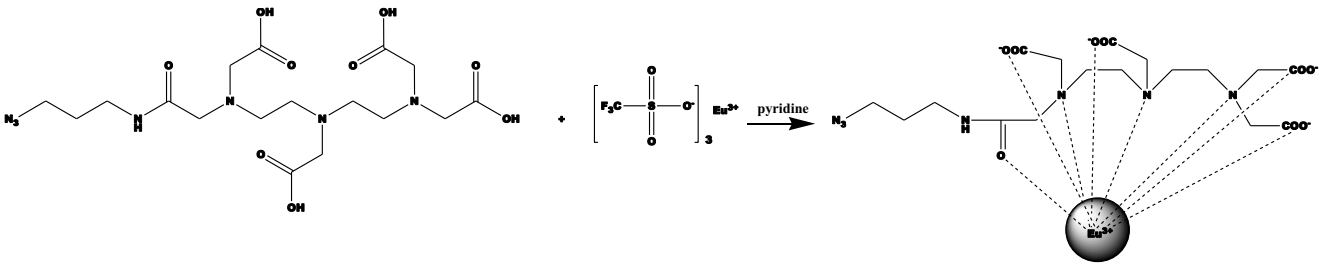

Scheme 17: *Synthesis of azido functionalized mono-amide Eu DTPA*

The product has a molar mass of 624.39 g/mol. MALDI-TOF revealed the presence of a peak at 1249.2 ($2M^{+)}$ as compared to 1248.78 theoretical. The spectrum also showed the presence of free europium triflate, which unlike gadolinium is not toxic (Fig. 61).

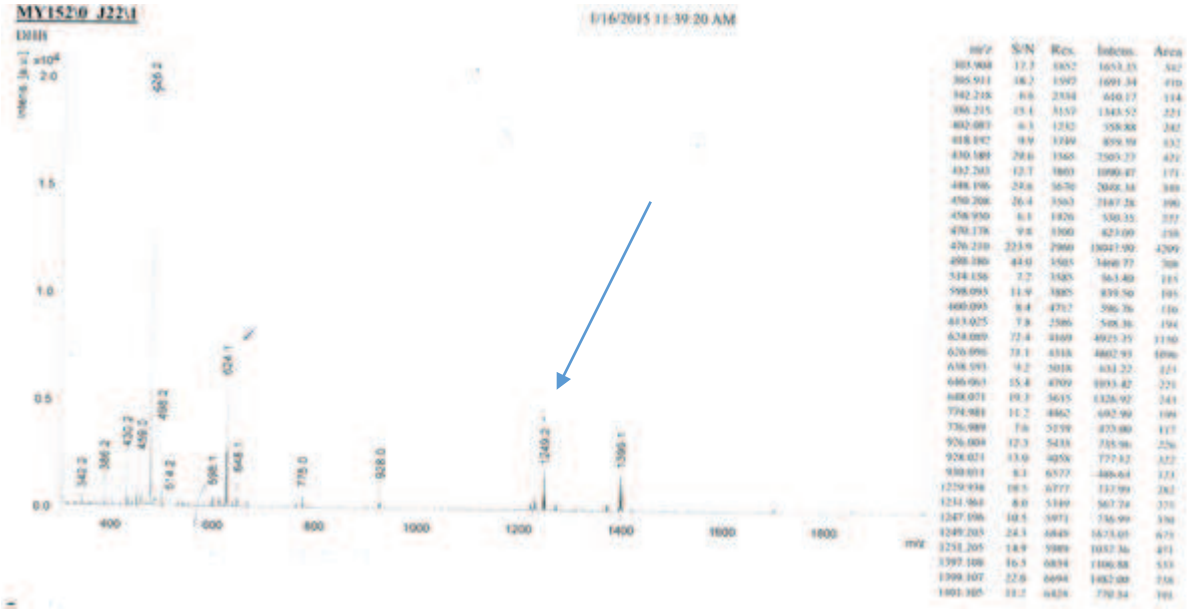

Figure 61: *MALDI-TOF spectrum of Eu-DTPA complex*

The Eu-DTPA complex bearing an azido group was then attached to propargylated PMMA by CuAAC reaction in DMF at 40°C for 48 hours. The Eu-PMMA was obtained by precipitation in ethanol (Scheme 18).

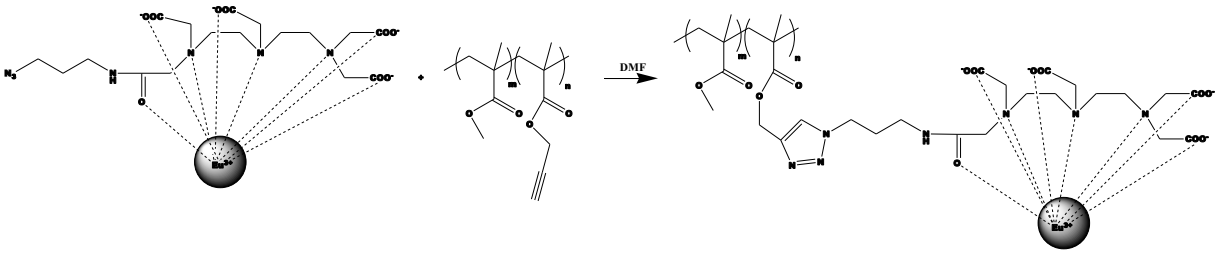

Scheme 18 : *Synthesis of PMMA-Eu*

Eu-PMMA was then dissolved in DCM and sprayed on a PP mesh. Red emission of Eu^{3+} is at 630 nm [14]. Under a red light, the PP mesh revealed a red fluorescence (Fig. 62) indicating the ability of the triazole to act as antenna.

Figure 62: *Red fluorescence of PMMA-Eu on PP mesh*

4.5 Conclusion

The synthesis of polymeric fluorophores was reported. PMMA-FITC needs furher improvement in solubility. PMMA-RITC and PMMA with Eu-DTPA gave red fluorescence when excited at the right wavelength, thus showing possibility to be used in the medical fluorescence field upon further studies.

References:

[1]: Rao, J.; Dragulescu-Andrasi, A.; Yao, H. Fluorescence imaging in vivo: Recent Advances. *Current opinion in biotechnology* **2007**, 18, 17-25

[2]: Sauer, M.; Hofkens, J.; Enderlein, J. Handbook of fluorescence spectroscopy and Imaging. *WILEY-VCH Weinheim*, **2011**

[3]: Calero, P.; Martinez-Manez, R.; Sancenon, F.; Soto, J. Synthesis, characterization and optical properties of silica nanoparticles coated with anthracene fluorophore and thiourea hydrogen-bonding subunits. *European Journal of Inorganic Chemistry* **2008**, 36, 5649-5658.

[4]: de Miejere, A.; Zhao, L.; Belov, VN.; Bossi, M.; Noltemeyer, M.; Hell, SW. 1, 3-Bicyclo [1.1.1]pentanediyl : The shortest rigid linear connector of phenylated photocromic units and a 1,5-dimethoxy-9,10-di(phenylethynyl) anthracene fluorophore. *Chemistry* **2007**, 13, 2503-2516

[5]: Su, FK.; Hong, JL.; Lin, LL. Restraining the Associations of Anthracene Fluorophore by chemically linking to poly(methyl methacrylate). *Journal of Applied Polymer Science* **2008**, 107, 124-131

[6]: Le Droumaguet, C. ; Wang, C. ; Wang, Q. Fluorogenic click reaction. *Chemical Society Reviews* 2010, 39, 1233-1239

[7]: Xie, F.; Sivakumar, K.; Zeng, Q.; Bruckman, MA.; Hodges, B.; Wang, Q. A fluorogenic click reaction of azido-anthracene derivatives. *Tetrahedron* **2008**, 64, 2906-2914

[8]: Evanoff, D.; Hayes, SE.; Ying, Y.; Shim, GH.; Lawrence, JR.; Carroll, JB.; Roeder, RD.; Houchins, JM.; Huebner, CF.; Foulger, SH. Functionalization of crystalline colloidal arrays through click chemistry. *Advanced Materials* **2007**, 19, 3507-3512

[9]: Pinheiro, PC.; Daniel-Da-Silva, A.; Tavares, DS.; Calatayud, MP.; Goya, GF.; Trindade, T. Fluorescent Magnetic Bioprobes by Surface Modification of Magnetite Nanoparticles. *Materials* **2013**, 6, 3213-3225

[10]: Cole, L.; Coleman, J.; Evans, D.; Hawes, C. Internalization of fluorescein isothiocyanate and dluorescein isothiocyanate-dextran by suspension-cultured cell plants. *Journal of Cell Science* **1990**, 96, 721-730

[11]: Huang, B.; Kukowska-Latallo, JF.; Tang, S.; Zong, H.; Johnson, KB.; Desai, A.; Gordon, CL.; Leroueil, PR.; Baker JR Jr. The facile synthesis of multifunctional PAMAM dendrimer conjugates through copper-free click chemistry. *Supplementary Data Biorganic and Medicinal Chemistry Letters* **2012**, 22, 3152-3156

[12]: Mottram, LF.; Forbes, S.; Ackley, BD.; Peterson, BR. Hydrophobic analogues of rhodamine B and rhodamine 101: potent fluorescent probes of mitochondria in living C. elegans. *Beilstein Journal of Organic Chemistry* **2012**, 8, 2156-2165

[13]: Beija, M.; Afonso, CAM.; Martinho, JMG. Synthesis and application of Rhodamine derivatives as fluorescent probes. *Chemical Society Reviews* **2009**, 38, 2410-2433

[14]: Reifernberger, JG.; Ge, P.; Selvin, PR. Progress in Lanthanides as Luminescent Probe. *Published in reviews in fluorescence*, **2005**, 2. Springer.

[15]: Evangelista, RA.; Pollak, A.; Allore, B.; Templeton, EF.; Morton, RC.; Diamandis, EP. A new Europium chelate for protein labelling and time-resolved fluorometric applications. *Clinical Biochemistry* **1988**, 21, 173-178

[16]: http://prod.sandia.gov/techlib/access-control.cgi/2013/137827.pdf

Conclusion & Perspectives

Progress realized in medical imaging modalities, in particular in magnetic resonance imaging, has given clinicians a very efficient method for diagnosis and post-operation follow-up. At the same time, the majority of prosthetic implants (especially those intended to be used for moderate or long durations) are invisible by MRI, fluorescence or radiography and their visualization is a necessity to obtain informations concerning their fixation and their fate in the body after implantation. Contrast agents can be employed to enhance signals.

The main aim of this thesis was to synthesize a MRI-visible polymer by grafting a contrast agent, i.e. a gadolinium complex, on the polymeric chain. This MRI-visible polymer should then be coated on a polypropylene mesh to make the device visible by MRI. The polymer should be non-degradable to allow a long-time visualization of the implanted medical device. Among the different contrast agents available, we chose azido-functionalized Gd-DTPA ligands which were grafted by click chemistry on a preformed propargylated PMMA.

To obtain a long term visualization of implanted meshes we synthesized a new monoazido functionalized DTPA ligand, using a simple pathway. Complexation of this DTPA ligand with Gd^{3+} led to a Gd-DTPA contrast agent. Macromolecular contrast agents based on PMMA were then prepared by click chemistry of azido-functionalized Gd-DTPA ligand onto propargylated PMMA. This new MRI-visible polymer was characterized by ICP-MS analysis in order to determine the amount of gadolinium. Results revealed that an important increase in the amount of grafted Gd^{3+} did not improve visualization of the mesh. Thus amounts of Gd^{3+} as low as 0.1% by weight rendered polypropylene meshes visible on a 7T MRI apparatus. These low amounts of Gd^{3+} made the MRI-visible polymer also cytocompatible and stable during a few months. This should allow a long-term use in the body for biomedical applications after further *in vivo* stability studies.

Besides MRI, fluorescence imaging is gaining a lot of attention. For this, we reported the synthesis of fluorescent PMMAs. PMMA was linked to three different fluorophores based on

azido anthracene, fluorescein, and rhodamine. The synthesis of fluorescent PMMA based on europium was also reported in which the triazole moiety acted as the antenna. Preliminary results for the four fluorophores are interesting, especially in the case of europium derivatives. However, advanced fluorescent microscopy should be applied, in addition to stability studies of the europium complex.

This work holds several future perspectives. The synthesized PMMA CA has to be tested for stability for longer periods of time, followed by total degradation in nitric acid, as to measure the amount of Gd^{3+} by ICP-MS. The ability of this CA to render PP mesh visible should be tested on 1.5T MRI. As a further stage, this CA should be tested in vivo in mice for cytotoxicity studies.

The synthesized fluorophores, mainly the europium based fluorophore should be tested using in vivo-fluorescence, to test its ability to render PP mesh visible by fluorescence.

The synthesis of the mono-amide DTPA ligand bearing both Gd and Eu is also gaining interest. This allows the synthesis of a dual function DTPA ligand: an MRI contrast agent when needed, and a red fluorophore when excited at the right wavelength.

Experimental Part

1. Materials

Dimethylfornamide (DMF, Aldrich) and toluene (Aldrich) were dried over calcium hydride overnight and distilled under reduced pressure. Pyridine (Aldrich) was dried over KOH and distilled. Tetrahydrofuran (THF, Aldrich) was dried by refluxing over a benzophenone-sodium mixture until a deep blue colour appeared and distilled. Methyl methacrylate (MMA, Aldrich) was purified through a basic aluminum oxide column in order to remove the inhibitor. AIBN was recrystallized in ethanol. All other materials were obtained from Aldrich and were used without any further purification.

2. Characterization

NMR Spectroscopy: AMX300 Bruker spectrophotometer operating at 300MHz was used to record the NMR spectra. AMX400 Bruker spectrophotometer was used to obtain the ^{1}H spectra. Deuterated chloroform and water were used as solvent, and chemical shifts were expressed in ppm with respect to tetramethylsilane (TMS).

FT-IR: FT-IR spectra were obtained on a Perkin Elmer spectrum 100 FT-IR spectrophotometer with an attenuated total reflectance (ATR) method.

LC-MS and MALDI analyses: A Q-TOF (Waters) spectrometer with an electrospray interface was used to obtain LC-MS spectra. An Ultra-FlexIII spectrometer (Bruker) was used to obtain MALDI-TOF spectra. All solvents were HPLC grade.

Preparative HPLC: HPLC separation was performed at SYNBIO3, Montpellier, on HPLC (Waters) with HD-C18 column using HPLC acetonitrile with 0.1% trifluoroacetic acid as eluent.

Size Exclusion Chromatography: Size exclusion chromatography (SEC) was performed at room temperature using a Viscotek GPCmax system equipped with a Viscotek guard column (10×4.6 mm) and two Viscotek columns LT 5000L mixed medium (300×7.8 mm), a Viscotek VE 3580 refractometric detector and a Viscotek VE 3210 UV/Vis detector. Calibration was

established with polystyrene standards from Polymer Laboratories. THF was used as solvent with a flow rate of 1 $mL.min^{-1}$.

ICP-MS Analyses: Quantification of Gd^{3+} and Cu^{+} was performed on an Element XR sector field ICP-MS (inductively coupled plasma) with an indium enriched ultrapure solution as an internal standard. The analyses were performed in the GeoSciences laboratory at the University of Montpellier.

MR imaging experiments: these were performed on a Bruker Biospec 70/20 system operating at a magnetic field of 7T (Bruker, Wissembourg, France). The resonant circuit of the NMR probe was a 35-mm diameter birdcage resonator. Meshes (around 1 cm^2) were embedded in degassed 1% by weight agar gel prior to imaging. Gadolinium-free samples corresponded to a polypropylene mesh without Gd contrast agent. To test signal enhancement, T1 weighting was introduced into the MR images using an inversion pulse in rapid three-dimensional (3-D) acquisition with relaxation enhancement (RARE) sequence (TR = 3000 ms; mean echo time (TEm) = 8 ms; RARE factor = 8; FOV = 3 × 3 × 1.5 cm; matrix 128 × 128 × 64). Inversion time was set at 1100 ms, sufficient to allow canceling of the embedding gel.

Fluorescence microscopy: Nikon 150231 microscope was used.

3. Synthesis of azido-functionalized mono-ester DTPA ligand

Synthesis of 3-azido propanol

3-chloropropanol (5.1mL, 5.77g, 61mmol) with sodium azide (7.94g, 122mmol) and tetrabutyl ammonium hydrogen sulfate (40mg) were dissolved in 5 mL water and heated at 80˚C for 24 hours, then left under stirring for 12 hours at room temperature. The obtained product was extracted with diethyl ether (3×50ml). The organic phase was then dried over $MgSO_4$ and evaporated by rotary evaporation. 4.7g of the pure colorless liquid were obtained by distillation under reduced pressure (yield 75 %).

Characterization by ^{1}H NMR (300MHz, $CDCl_3$): δ(ppm)= 3.69 (t,2H,CH_2O); 3.40 (t,2H, CH_2N_3), 1.78 (m,2H, $CH_2CH_2CH_2$)

Synthesis of azido-functionalized mono-ester DTPA ligand

3-azido propanol (0.28g, 2.8 mmol) and DTPA bis-anhydride (1g, 2.8 mmol) were dissolved in 20mL dry DMF. The reaction mixture was stirred under argon for 24 hours. After removal of DMF under vacuum, the product was dissolved in water and subjected to freeze drying. The LC-MS spectrum revealed the presence of two products: azido-functionalized bis-ester DTPA ligand (*M*=559.24 g/mol) and azido-functionalized mono-ester DTPA ligand (*M*=476.44 g/mol). Starting from 2g of this mixture, preparative HPLC separation gave 0.75g of the mono-ester ligand as a white powder (yield=38%).

Characterization by ^{1}H NMR (400MHz, D_2O): δ(ppm)= 1.9(m, 2H, $CH_2CH_2N_3$), 3.4(t, 10H, NCH_2 and CH_2N_3), 3.7(s, 2H, NCH_2CO_2H), 4(s, 3H, NCH_2CO_2H), 4.3 (s, 1H, OCH_2).

LC-MS (ES+, m/z):477.2 g/mol $[M+H]^+$.

FT-IR(ATR, cm^{-1}) 2100 (N_3).

4. Synthesis of azido-functionalized mono-amide DTPA ligand

Synthesis of 3-azido propylamine

3-azido-1-propylamine was synthesized according to a known procedure. 3-chloropropylamine hydrochloride (4 g, 30.8 mmol), sodium azide (6 g, 92.3 mmol), and water (30 mL) were added in a round bottom flask. The solution was heated overnight at 80˚C. After cooling in an ice bath, KOH (4 g) and diethyl ether (50 mL) were added. After separation of the organic phase, the aqueous phase was further extracted with diethyl ether (3×50 mL). The organic phase was then dried over magnesium sulfate and evaporated under reduced pressure. Purification of the crude product by distillation yielded 2.46 g of the pure product as coloress oil with a yield of 80 %.

Characterization: ^{1}H NMR (300MHz, $CDCl_3$): δ(ppm)= 3.3 (t,2H,CH_2N_3); 2.8 (t,2H, CH_2NH_2), 1.6 (m,2H, $CH_2CH_2CH_2$), 1.4 (s, NH_2). FT-IR (ATR, cm^{-1}): 2100(N_3)

Synthesis of azido-functionalized mono-amide DTPA ligand

DTPA bis-anhydride (1.9 g, 5.3 mmol, 1 equiv.) and imidazole (3.04 g, 44.2 mmol) were solubilized in DMF at 80 ˚C. The solution was then cooled to 50 ˚C, and a mixture of azidopropylamine (0.53g, 5.3mmol, 1equiv.) and pyridine (0.22 mL) was added dropwise. The mixture was left at 50 ˚C for 5 hours, then precipitated in acetone, filtered and freeze-dried. The LC-MS spectrum revealed the presence of bis-amide (*M*=557.75 g/mol) and mono-amide DTPA ligands (*M*=475.45 g/mol).The monofunctional DTPA was purified by preparative HPLC separation (0.555 g, yield 30 %).

Characterization: ^{1}H NMR (400MHz, D_2O) δ ppm: 1.8 (2H, m, $CH_2CH_2N_3$), 3.4 (12H, t, $N(CH_2)_2N$ and CH_2N_3), 3.7(2H, s, NCH_2CO_2H), 4 (8H, s, NCH_2CO_2H).

FT-IR (ATR, cm^{-1}): 2100 (N_3).

LC-MS (ES+, m/z): 476.2 Da [$M+H^+$]

5. Synthesis of Gadolinium Complexes

MTB protocol

2.6 ml of glacial acetic acid were added to 800 mL ultra-pure water. The pH was then adjusted to 5.8 by addition of 1M NaOH solution. This buffer was then used to prepare 50µM of MTB solution. $GdCl_3$ standards in the range of 0-50µM were prepared in the buffered MTB to obtain the calibration curve.

Gadolinium Complexation with azido-functionalized mono-ester DTPA

Pyridine (2.1 mmol, 0.16 mL) was added to azido-functionalized mono-ester DTPA (100 mg, 0.21 mmol) dissolved in a minimum of H_2O and stirred for 10 minutes at room temperature. $GdCl_3.6H_2O$ (0.15g, 0.42 mmol) was then added, and the mixture was left at 40 ˚C for 24 hours. Solvents were removed under vacuum, and an aqueous solution of the complex was

stirred in Chelex 100 resin overnight to remove free Gd^{3+}. The product was then filtered, freeze-dried to give 70 mg of white solid (yield=52%). 7mg of the prepared complex were dissolved in 3mL MTB solution and analyzed by UV spectroscopy. A yellow color was observed indicating the absence of free gadolinium.

Characterization: ICP-MS revealed the presence of 11% by weight of Gd^{3+} in the complex.

MALDI-TOF (dithranol, m/z): $[M+K^+]$=685.9 Da versus 686.77 calculated.

FT-IR (ATR, cm^{-1}): 2100 (N_3).

Gadolinium Complexation with azido-functionalized mono-amide DTPA

Pyridine (2 mmol, 0.16 mL) was added to azido-functionalized DTPA **1** (100 mg, 0.2 mmol) dissolved in few mL of H_2O and stirred for 10 minutes at room temperature. $GdCl_3.6H_2O$ (0.15g, 0.4 mmol) was then added, and the mixture was left at 40 ˚C for 24 hours. Solvents were removed under vacuum, and an aqueous solution of the complex was stirred overnight in Chelex 100 resin to remove free Gd^{3+}. The product was then filtered, freeze-dried to give 64mg of white solid (yield=50%). The absence of free gadolinium was verified by methyl thymol blue (MTB) colorimetric test.

Characterization: The amount of complexed $Gd^{3+}$was calculated by ICP-MS, revealing 10% Gd by weight.

MALDI-TOF (dithranol, m/z): $[M+K^+]$=685.8 Da versus 685.78 calculated.

FT-IR (ATR, cm^{-1}): 2100 (N_3).

6. Synthesis of Poly(methyl methacrylate-*co*-propargyl methacrylate)

Synthesis of propargyl methacrylate

Methacryloyl chloride (13.95 g, 133 mmol) in 50 mL dichloromethane was added dropwise at 0 ˚C during 30 minutes to propargyl alcohol (5 g, 89 mmol) and triethyl amine (13.51 g, 133 mmol) in 50 mL dichloromethane. The reaction was then left overnight at room temperature. After removal of ammonium salts by filtration over celite, the product was washed with

3×50mL of saturated $NaHCO_3$ and 3×50mL H_2O. The product was dried over $MgSO_4$ and solvents were removed under reduced pressure. The final product was obtained as colorless oil by vacuum distillation. (4g, yield=36%)

Characterization: ^{1}H NMR (300 MHz, $CDCl_3$) δ (ppm): 1.97 (3H, s, CH_3-C=CH_2), 2.48(1H, s, C≡CH), 4.76(2H, s, OCH_2), 5.63(1H, s, C=CHH), 6.18(1H,s,C=CHH).

Synthesis of (PMMA-co-PMA) by free radical polymerization initiated by AIBN

Polymerization was carried out in toluene solution using a standard Schlenk technique under inert atmosphere of argon. Typically, methyl methacrylate (5 g, 49.9 mmol, 97.5 equiv.), propargyl methacrylate (0.158 g, 1.279 mmol, 2.5 equiv.), AIBN (0.05 g, 0.3 mmol, 1% w/w), and toluene (20 mL) were placed in an oven-dried Schlenk tube. The tube was fitted with a rubber septum. The solution was further degassed by three freeze-thaw-pump cycles. The resulting mixture was placed in a thermostatically controlled oil bath at 70˚C for 2 hours. The reaction was stopped with liquid nitrogen. The polymer was precipitated in cold methanol then in cold heptane, and finally collected by filtration and dried under vacum. **Characterization:** ^{1}H NMR (300MHz, $CDCl_3$) δ(ppm): 3.5(s,3H, OCH_3) and 4.2 (s,2H,CH_2-C≡CH).

$M_{n,SEC}$ = 40000 g.mol^{-1}, $Đ$=1.8

Synthesis of (PMMA-co-PMA) by microwave initiated ATRP

Polymerization was carried out in DMF using a microwave vessel in an ETHOS 1 microwave apparatus. Typically, methyl methacrylate (5 g, 49.9 mmol, 97.5 equiv.) and propargyl methacrylate (0.063 g, 0.51 mmol, 1 equiv.), EBB (0.024 g, 0.12 mmol), CuCl (0.012g, 0.09 mmol), PMDETA (0.038g, 0.22 mmol), and DMF (10 mL) were placed in an oven-dried microwave tube which was then fitted in a closed microwave vessel. The mixture was placed in a microwave oven at 70˚C at different time intervals (30 min, 90 min, and 150 min). The reaction was stopped with liquid nitrogen. The polymer was precipitated in 7/3

methanol/water mixture with 0.1% hydrochloric acid. The product was collected by filtration and dried *in vacum*.

Characterization: ^{1}H NMR (300MHz, $CDCl_3$) δ(ppm): 3.5(s,3H, OCH_3) and 4.2 (s,2H,CH_2-C≡CH).

$M_{n,SEC}$ and $Đ$ varied according to time intervals.

Synthesis of (PMMA-co-PMA) by microwave initiated free radical polymerization

Polymerization was carried out in a DMF solution using a microwave vessel in an ETHOS 1 microwave apparatus. Methyl methacrylate (5 g, 49.9 mmol, 97.5 equiv.) and propargyl methacrylate (0.063 g, 0.51 mmol, 1 equiv.) were initiated by various amounts of BPO (0.1, 0.2, 0.5, 0.7 and 0.9% by weight) in DMF (10 mL). The different mixtures were placed in separate oven-dried microwave tubes which were then fitted in a closed microwave vessel. The mixtures were placed in a microwave oven at 70˚C for 15 minutes. The reaction was stopped with liquid nitrogen. The polymer was precipitated in 7/3 methanol/water mixture with 0.1% hydrochloric acid. The product was collected by filtration and dried *in vacum*.

Characterization: ^{1}H NMR (300MHz, $CDCl_3$) δ(ppm): 3.5(s,3H, OCH_3) and 4.2 (s,2H,CH_2-C≡CH).

$M_{n,SEC}$ and $Đ$ varied according to amounts of BPO used.

7. CuAAC Experimental Conditions

Synthesis of Ester Based Polymeric Contrast Agent

In a Schlenk tube were placed poly(methyl methacrylate-*co*-propargyl methacrylate) (100 mg, 2.5% mol propargyl unit), Gd-DTPA mono-ester complex (13.54 mg, 22 μmol, 1.2 equiv.), CuBr (3 mg, 22 μmol, 1.2 equiv.), and the least amount of DMF to solubilize the components. The tube was fitted with a rubber septum. The solution was further degassed by three freeze-pump-thaw cycles, stirred under argon, and PMDETA (7.44 mg, 43 μmol, 2.4 equiv.) was added. The reaction was left at 40 ˚C for 48 hours. The crude material was purified by dialysis

(6000-8000 MWCO) against acetone which was renewed regularly. After 3 days, acetone was evaporated to yield pure gadolinated PMMA (40 mg, yield 80%) with 1.4% by weight Gd^{3+} as measured by ICP-MS.

Synthesis of Amide Based Polymeric Contrast Agent

In a Schlenk tube were placed poly(methyl methacrylate-*co*-propargyl methacrylate) (50 mg, 2.5% mol propargyl unit), Gd-DTPA mono-amide complex (7 mg, 10 μmol, 1.2 equiv.), CuBr (1.5 mg, 10 μmol, 1.2 equiv.), and the minimum amount of DMF to solubilize the components. The tube was fitted with a rubber septum. The solution was further degassed by three freeze-pump-thaw cycles, stirred under argon, and PMDETA (3.7 mg, 22 μmol, 2.4 equiv.) was added. The reaction was left at 40 ˚C for 48 hours. The crude material was purified by dialysis (6000-8000 MWCO) against acetone which was renewed regularly. After 3 days, acetone was evaporated to yield pure gadolinated PMMA (40 mg, yield 80%) with 1.34% by weight Gd^{3+} as obtained by ICP-MS.

8. Meshes Preparation for MRI Visualization

Meshes were sprayed with PMMA MRI contrast agent having different Gd^{3+} percentages prepared as follows: the synthesized polymeric contrast agent has been diluted by commercial PMMA and dissolved in DCM to obtain 0.14, 0.23 and 0.79% w/w of Gd^{3+}. Each polymeric solution was sprayed on commercial polypropylene mesh ($3\times3cm^2$) using Infinity Airbrush system supplied by Harder & Steenbeck (Osteinbeck, Germany) under a pressure of argon of 3 bars and at a distance of 5 cm. Meshes were dried overnight under vacuum until a constant weight was obtained.

9. Film formation

Films containing various % of Gd^{3+} have been prepared by diluting the MRI-visible polymer with commercial PMMA and dissolution in DCM. After solvent evaporation, films containing various amounts of Gd^{3+} were then obtained.

10. Stability

Films containing 0.10% and 0.43% by weight of Gd^{3+} were placed in PBS solution at 37˚C under stirring at 130 rpm. At scheduled time points (1, 7, 30 and 90 days) 1 mL of PBS buffer was withdrawn (then replaced by 1 mL fresh buffer) and analyzed by ICP-MS for Gd^{3+} release study.

11. Cytocompatibility

Cells were cultured in MEM culture media by adding horse serum (10% v/v), penicillin, streptomycin and 1% GLUTAMAX. Cells were grown in a 5% CO_2 incubator at 37 ˚C for around 24 hours till a confluence of around 80%, in which cells had covered the totality of the wells as observed by an electron microscope. At this point, the culture medium was sucked out and thrown. The different films were then gently placed on these cells. Films of gadolinium-free poly(methyl methacrylate-*co*-propargyl methacrylate) were also placed in addition to blank samples, negative control (the cells with cell lysis) and positive control (the cells). To each of the wells 1000 µL of LDH reaction mixture was added and samples were incubated for 24 hours. Each sample was repeated 3 times. After 24 hours, 10 µL of each sample were transferred to UV wells to which 100 µL of LDH were added. Sample was tested for UV absorbance at 490 nm by Victor V3 Perkin Elmer UV spectrophotometer.

12. Synthesis of fluorescent markers

Synthesis of 9-azido methyl anthracene

9-chloro methyl anthracene (1g, 4.4 mmol) and sodium azide (0.43 g, 6.6 mmol) were heated in 30 mL acetonitrile at 50°C for 5 hours. The mixture was recrystallized in methanol/dichloromethane and the product was further purified by passing it over a silica column using 4:1 heptane:ethyl acetate as eluent. A yellow product was obtained (0.93g, yield=90%).

Characterization: ^{1}H NMR (400 MHz, $CDCl_3$) δ (ppm): 5.32 (2H, s, CH_2), 7.24-7.60 (4H, m, anthracene), 8.02 (2H, m, anthracene), 8.26 (2H,m,anthracene), 8.5 (1H, S, anthracene). FT-IR (ATR, cm^{-1}): 2100(N_3)

Synthesis of anthracene-functionalized poly(methyl methacrylate)

In a Schlenk tube were placed poly(methyl methacrylate-*co*-propargyl methacrylate) (300 mg, 2.5% mol propargyl unit), 9-azido methylanthracene (21 mg, 90 μmol, 1.2 equiv.), CuBr (13 mg, 90 μmol, 1.2 equiv.), and the minimum amount of THF to solubilize the components. The tube was fitted with a rubber septum. The solution was further degassed by three freeze-pump-thaw cycles. The mixture was stirred under argon, and PMDETA (31 mg, 180 μmol, 2.4 equiv.) was added. The reaction was left at 40 ˚C for 48 hours. The crude material was purified by precipitation in ethanol

Synthesis of azido-functionalized fluorescein

Fluorescein isothiocyanate (48.5 mg, 0.124 mmol) was dissolved in dry DMF. 400μL triethyl amine and 3-azido propylamine (11.8 mg, 0.118 mmol) in 200μL DMF were added. The reaction was stirred at room temperature for two hours. The product was obtained after DMF evaporation under vacuum (37mg, yield=65%).

Characterization: FT-IR(ATR, cm^{-1}) 2100 (N_3).

Synthesis of PMMA functionalized with FITC

In a Schlenk tube were placed poly(methyl methacrylate-*co*-propargyl methacrylate) (150 mg, 2.5% mol propargyl unit), azido functionalized fluorescein (21.7 mg, 44.4 μmol, 1.2 equiv.), CuBr (6.4 mg, 44.4 μmol, 1.2 equiv.), and the minimum amount of DMSO to solubilize the components. The tube was fitted with a rubber septum. The solution was further degassed by three freeze-pump-thaw cycles. The mixture was stirred under argon, and PMDETA (15 mg, 88 μmol, 2.4 equiv.) was added. The reaction was left at 40 ˚C for 48 hours. The crude material was purified by precipitation in ethanol.

Synthesis of azido-functionalized Rhodamine

Rhodamine B isothiocyanate (49.8mg, 0.093 mmol) was dissolved in dry DMF. 400µL triethyl amine and 3-azido propylamine (9.77 mg, 0.097 mmol) in 200µL DMF were added. The reaction was stirred at room temperature for two hours. The product was obtained after DMF evaporation under vacuum (40.1mg, yield=65%).

Characterization: FT-IR(ATR, cm^{-1}) 2100 (N_3).

Synthesis of PMMA functionalized with Rhodamine

In a Schlenk tube were placed poly(methyl methacrylate-*co*-propargyl methacrylate) (150 mg, 2.5% mol propargyl unit), azido functionalized rhodamine (28.5 mg, 44.7 µmol, 1.2 equiv.), CuBr (6.4 mg, 44.4 µmol, 1.2 equiv.), and the minimum amount of DMSO to solubilize the components. The tube was fitted with a rubber septum. The solution was further degassed by three freeze-pump-thaw cycles. The mixture was stirred under argon, and PMDETA (15 mg, 88 µmol, 2.4 equiv.) was added. The reaction was left at 40 ˚C for 48 hours. The crude material was purified precipitation in ethanol

Synthesis of azido functionalized mono-amide Eu DTPA

Azido-functionalized mono-amide DTPA ligand (100mg, 0.21 mmol) was dissolved in a few mL pyridine. Europium triflate (0.138g, 0.231 mmol) in 1mL water was added. The reaction was heated at 70°C for 3 hours. After solvent evaporation, the product was refluxed in ethanol for one hour, centrifuged, and filtrated to obtain the pure complex (62mg, yield=50%). **Characterization:** MALDI-TOF (2,5 dihydroxybenzoic acid as matrix): 1249.2 [$2M^+$] experimental as compared to 1248.78 theoretical.

Synthesis of Eu-PMMA

In a Schlenk tube were placed poly(methyl methacrylate-*co*-propargyl methacrylate) (100 mg, 2.5% mol propargyl unit), azido functionalized Eu-DTPA ligand (18.58 mg, 29.7 µmol, 1.2 equiv.), CuBr (4.27 mg, 29.7 µmol, 1.2 equiv.), and the minimum amount of DMF to

solubilize the components. The tube was fitted with a rubber septum. The solution was further degassed by three freeze-pump-thaw cycles. The mixture was stirred under argon, and PMDETA (10.3 mg, 59.5 μmol, 2.4 equiv.) was added. The reaction was left at 40 ˚C for 48 hours. The crude material was purified precipitation in ethanol.